

## Introduction to Magneto-Chemistry of Mono, di and Trinuclear complexes

Tulika Gupta

Dept. of Chemistry, IIT Bombay, Mumbai-400076

**Abstract:** “Molecular Magnets are single molecules consisting of a magnetic core and shielding organic ligands. In everyday life, “magnetism” phrase refers to solid materials, metals, alloys, oxides. As per our normal notion, molecules are considered to be isolated, non-magnetic objects. The available magnets can be classified in two categories: “hard” magnets and “soft” magnets. “Hard” magnets remain magnetized permanently; they are magnetic even when there is no applied magnetic field. They have an important remnant magnetization in a zero applied magnetic field. Magnetite, whose chemical formula is written  $\text{Fe}_3\text{O}_4$ , is a hard magnet known for a long time. “Soft” magnets are not permanent magnets; they are attracted to hard magnets but lose their magnetization rapidly when the hard magnet is removed (their remnant magnetization is weak or zero). Metallic iron is a soft magnet. Hard magnets (neodymium-iron-boron alloy, for example) create around them a magnetic field, which can be visualized by soft magnets (iron powder for example). The magnetic field is not visible and magnetic interactions manifest themselves at a distance, without direct contact. One of the oldest, best known and most useful applications of magnetism is the compass. It was an important navigation tool, enabling the great discoveries of the XV-XVIth centuries, from C. Columbus, Vasco de Gama, J. Cartier or Zhong He in Spain, Portugal, France and China. The needle orients in the earth magnetic field, due to the huge metallic masses of the earth nucleus. “

**Motivation and Basic Knowledge:** Magnets” adorn fridge doors and display boards. More seriously, in a world often dominated by the market, hard and soft magnets play crucial roles in motors, transformers, etc and magnet industry is a very important one. Hence, understanding of basics of magnetism and detailed analysis of magneto-chemistry would lead to exploration of various innovative fields. Magnets and magnetism always provide source of inspiration and excitement and can be executed towards the transformation of solar energy into mechanical energy.

**Acknowledgement:** This review is written partly based on Diamond Jubilee celebration lecture at the department Chemistry, St. Xavier's College, Tirunelveli, Tamilnadu by Prof. Gopalan Rajaraman, Department of Chemistry, IIT Bombay and also based on his lecture notes on Advances in Molecular magnetism at the department of Chemistry, IIT Bombay. We would like to express our gratitude to all the eminent scientists across the world working in the area of molecular magnetism since past two decades, i.e. Prof. O. Kahn, Prof. D.Gatteschi, Prof. R. Sessoli, Prof. A. Caneschi, Prof. A.K.Powell, Prof. J. Long, Dr. J. V. Slageren, Prof. M. Murugesu, Prof. R.E.P.Winpenny, Prof. L. Chibotaru, Prof. J. Tang, Dr. L. Ungur, Prof. W. Wernsdorfer, Prof. G. Christou, Prof. E. K. Brechin, Prof. L. Jones, Prof. E. Coronado, Prof. E. Colacio, Prof. E. Ruiz, Prof. K. S. Murray, Prof. N. Ishikawa, Prof. Helene Bolvin, Prof. E. J. McInnes, Prof. D. Collison, Prof. R. Clerac, Prof. C. Coulon, Prof. A. Bencini, Prof. L. Bogani, Prof. S. Piligkos, Prof. M. Evangelisti, Prof. M. Affronte, Prof. G. Aromin, Prof. K. Bernot, Prof. V. Chandrasekhar, Prof. A. Duncan, Prof. F. Neese, Prof. H. Miyasaka, Dr. S. Langley, J. Friedman, Prof. K. Dietrich and Prof. S. Maheswaran. Most importantly, we are indebted to Prof. M. Verdaguer whose lectures on molecular magnetism have been used for our summarised write-up on molecular magnetism. We have also taken suggestions from books written by Prof. O. Kahn, Prof. E. J. Miller and M. Drillon, Prof. E. K. Itoh and M. Kinoshita, Prof. M. Verdaguer and Prof. E. Linrt proved to be extremely beneficial for our summary. We have performed thorough study on all of their published materials on molecular magnets and procured ideas have been used to write this journal and perform calculations for our research project. Eventually, GR would like to acknowledge financial support from the Government of India through the Department of Science and Technology (EMR/2014/000247; SR/NM/NS-1119/2011) and Indian Institute of Technology, Bombay to access the high performance computing facility. TG would like to thank UGC New Delhi for SRF fellowship.

## **§1. Introduction:**

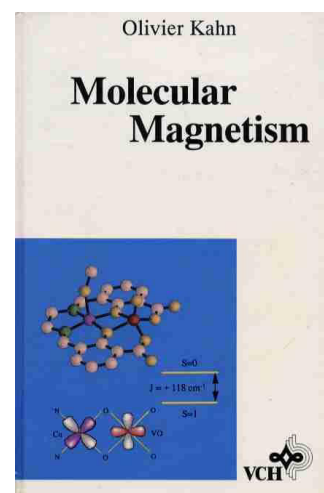
‘Molecular Magnetism’ can be introduced as “The study of magnetic properties of isolated molecules and assemblies of molecules” as quoted by eminent scientist Prof. Olivier Kahn. According to him, it is an interdisciplinary field, where chemists design and synthesize materials of increasing complexity based on a feedback interaction with physicists who develop sophisticated experimental measurements to model the novel properties associated with molecular materials. Molecules may contain one or more magnetic centres. It is a scientific discipline which conceives designs, synthesises



studies and uses new molecular magnetic materials in an interdisciplinary way. Assemblies can be molecular crystals (weak inter-molecular interactions) or extended systems built from molecular precursors (bulk molecular properties). The magnetism word was originated from Greece due to its possession of several magnetic ores while long back at 625 B.C discovery of magnetite stonewalled the concept of considering magnetism from innovative perspective.

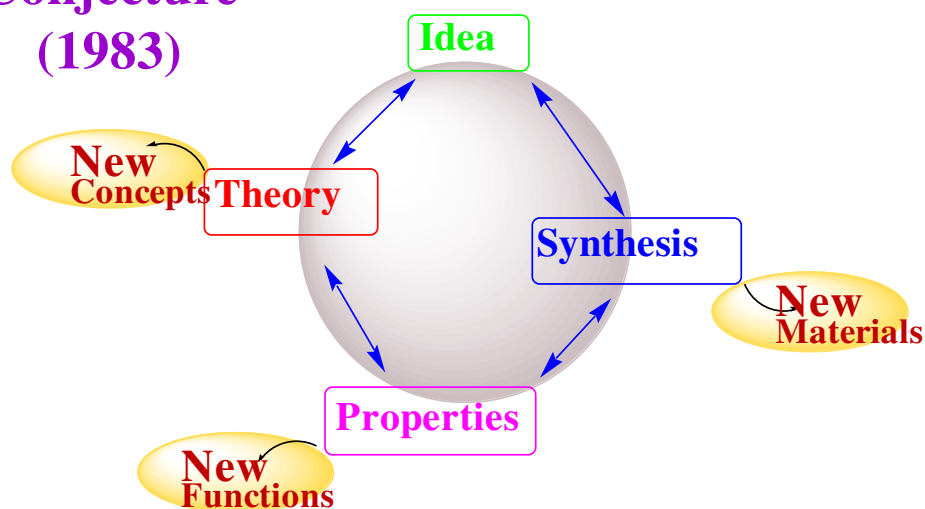
“The instrument shown beside resembles a spoon, and when it is placed on a plate on the ground, the handle points to the south”. (280 BC. Magnetic materials have tremendous potential applications in multi-billion pound industry, medicine (as MRI agents), Telecommunication/IT industry (magnetic disks/data storage), acoustic devices, motors, generators etc. Unequivocally, their role towards unravelling the theory of solid state chemistry and physics, understanding magnetic interaction in Human Biology [Cu(II)-Fe(III)] interaction in cytochrome c oxidase, or the iron storage protein ferritin which displays superparamagnetic like behaviour) as well as in Animal Biology (magnetite magnets in birds heads used for navigation) is fundamental).

Consistent effort by physicists and chemists led to the coalition of molecules to magnetic materials at the end of the twentieth century. Magnets emerging out from molecular assemblies (Molecular Magnets or Molecule Based Magnets) are fabrications cordial; paving the way of synthesising new generation magnetic, electronic and photonic devices. Additionally, these magnets have the advantage of combining magnetic properties with mechanical, electrical and optical ones and also amply potent to alter magnetic properties with simple chemical methodologies. According to Carlin in 1986, “Magnetochemistry is essentially the use of magnetic techniques for obtaining structural information on simple paramagnetic systems, and it is a branch of chemistry which uses physical measurements”. On the other hand, Prof. Kahn has defined molecular magnetism as “an interdisciplinary field, where chemists design and synthesize materials of increasing complexity based on a feedback interaction with physicists who develop sophisticated experimental measurements to model the novel properties associated with molecular materials”.



Sir Olivier Kahn<sup>2</sup> was one of those who allowed switching from magnetochemistry to molecular magnetism. Additionally, eminent scientists across the world i.e. D. Gatteschi, R. Sessoli, A. Caneschi, W. Wernsdorfer, M. A. Novak, G. Christou, have done extensive studies towards the fast development of magnetism.

## Conjecture (1983)



The successful and strange story of Haldane gap arose in the quest of answering questions of physicist which predicted dynamic mass generation by the Néel magnon.

## §2. Definition and Units:

‘Magnetic behaviour’ is intrinsic response of a material to an applied or external magnetic field. This is triggered by the electronic spin and mutual alignment of them as well as with respect to the adjacent

atoms/molecules. Each electron has concomitant magnetic moment associated with its angular momentum (spin and orbital). [Classically, electrons are moving charged particles: this imparts a magnetic moment]

In presence of external homogeneous magnetic field (H), field within the body will be deviated from the free space value to induce magnetization within the body. Magnetization intensity is expressed as energy (E) variation rate in the magnetic field i.e.:

$$M = -\frac{\partial E}{\partial H}$$

In H field, for one mole of compound the sample attains molar magnetization M i.e.

$$\frac{\partial M}{\partial H} = \chi$$

$\chi$  = molar magnetic susceptibility

In weak magnetic field, magnetic susceptibility becomes independent of magnetic field, i.e.  $M = \chi H$ . Magnetic susceptibility is fundamental property of magnetic materials.

Because magnetic susceptibilities are often highly temperature dependent (see later), chemists often quote the effective magnetic moment. When orbital angular momentum is quenched we often use the “spin-only” formula to give  $\mu_{so}$  (Bohr Magneton units).

$$\mu_{so} = \sqrt{g^2 S(S+1)} \approx \sqrt{n(n+2)}$$

The relationship between  $\mu_{so}$  and  $\chi$  is given by:

$$\mu_{so} = \sqrt{\frac{3k}{N\beta^2}} \sqrt{\chi T} = 2.828 \sqrt{\chi T}$$

where  $k$  = Boltzmann constant

$\beta$  = Bohr Magneton

$N$  = Avogadro's number

**Units:** Very confusing. Most people use the cgs (cm grams seconds) emu (electromagnetic unit) system, rather than SI units.

Quantity(Symbol)	Units
Magnetic field(H)	G(Gauss)
Molar magnetisation ( $M$ ) [a.k.a. molar magnetic moment]	$\text{cm}^3 \cdot \text{G} \cdot \text{mol}^{-1}$ , but sometimes see reported in $N\beta$ units ( $1 N\beta = 5585 \text{ cm}^3 \cdot \text{G} \cdot \text{mol}^{-1}$ )
Gram magnetic susceptibility ( $\chi_g$ )	$\text{emu} \cdot \text{g}^{-1}$ or $\text{cm}^3 \cdot \text{g}^{-1}$

Molar magnetic susceptibility ( $\chi$ )	emu.mol <sup>-1</sup> or cm <sup>3</sup> .mol <sup>-1</sup>
$\chi.T$	cm <sup>3</sup> .K.mol <sup>-1</sup>

### **§3. Measurement of $\chi$ :**

Magnetic susceptibility ( $\chi$ ) is being determined based on two principles (i) force and (ii) induction methods which two are dependent on application of external magnetic field.

#### **§3.1 Force Methods: The Gouy Method:**

In presence of inhomogeneous magnetic field, imposed displacement force supposedly leads to apparent variation in weight. In this method, the finely ground sample is packed into a silica tube followed by suspension from balance. The uppermost part of the sample lies in zero field while the bottom part is within the region of high field(H). Determination of the force on the sample ( $\chi$ ) is being undertaken from the weight variation in zero and applied field(H).

The sample can be loaded in a cryostat to measure the temperature dependence of magnetic susceptibility.

Advantage: good sensitivity,  $\sim 10^{-6} - 10^{-8}$  emu.

Disadvantage: Requires large amount of sample (a few 100 mg). Results are dependent on packing of sample in tube (i.e. uniform sample packing is required).

#### **§3.2 Induction Methods:**

This methodology is dependent on the induction of electric current arising from magnetic field variation. In this technique, magnetization the sample in an applied field induces a voltage/current in a sensing coil when moved through the coil. The sensing coil is an electric current looped around the sample. The strength of the induced voltage  $\propto \chi$ .

#### **Vibrating Sample Magnetometer:**

The sample is mounted on the end of a rigid rod which oscillates vertically at a fixed frequency in a uniform magnetic field. The oscillation of the magnetised sample induces a voltage in the sensing coil.

Advantages: a) robustness of the equipment b) amicable to high magnetic materials (requires small amount if sample).

Disadvantages: poor sensitivity ( $\sim 10^{-5}$  emu) entails usage of small amount of sample.

### **SQUID (Super Conducting QUantum Interference Device) magnetometer:**

Utility lies in modern magnetochemical studies. The magnetising field is provided by a superconducting (Sc) electromagnet. Sample is surrounded by Sc sensing coil coupled to a second Sc loop which enters the SQUID itself.

SQUID operates via a mechanism similar to that of VSM. The magnetised sample is moved through the coil, inducing a current in the double-loop circuit, which being Sc (*i.e.* zero resistance) causes no damping or loss of the original signal. This induces a field in the second loop inside the SQUID, directly related to the field produced by the sample. The SQUID itself amplifies very small changes in magnetic fields into large electrical signals.

Advantages: a) High sensitivity ( $>10^{-12}$  emu) b) used to study single crystal samples, powders ,i.e. easy variable temperature control.

Disadvantages: complex and expensive equipment.

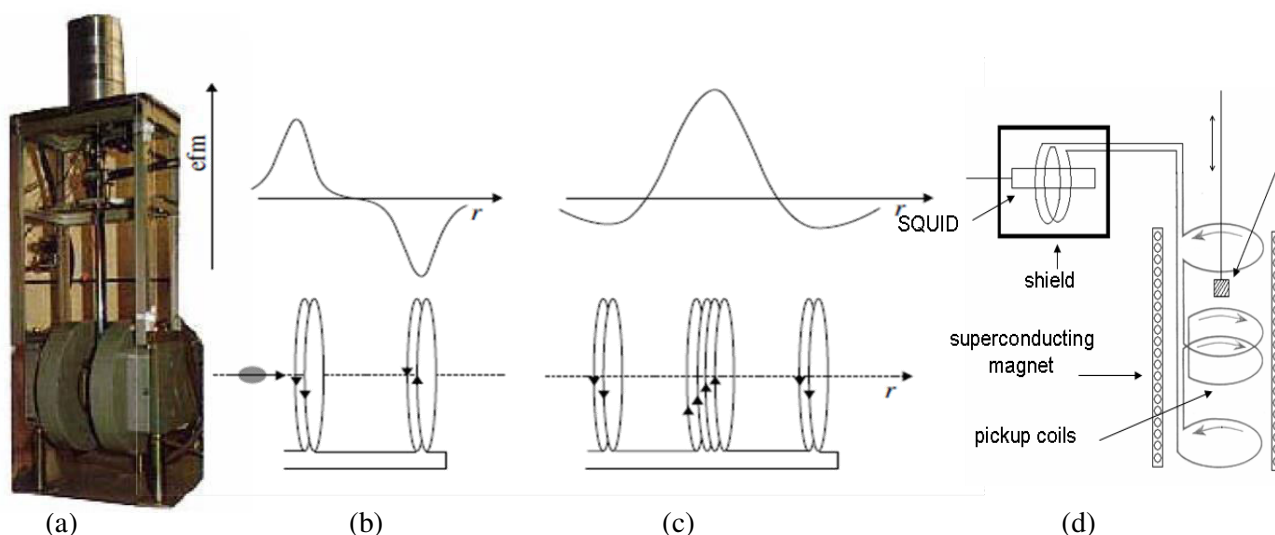


Figure1. Schematic picture of (a) VSM (b) First order gradiometer (c) Second order gradiometer (d) SQUID magnetometer.

### **High magnetic field experiments:**



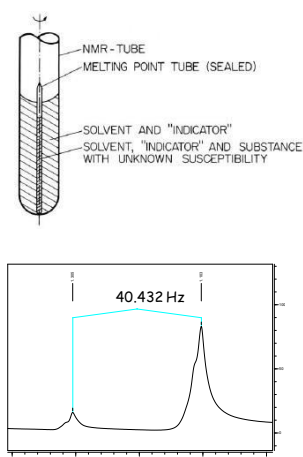
Figure2. NHML, Florida, 45T DC field.<sup>3</sup>

(a)



(b)

Figure3. (a) June 2011: Helmholtz-Zentrum Dresden- Rossendorf set a new world record for magnetic fields with 91.4 T---a few milliseconds (b) 35 Tesla DC field [Grenoble High Magnetic Field Laboratory](#))



### Evans method: for liquid samples:

The adjacent Figure 4 demonstrates Evans method. Evans method is used for measuring liquid samples and used to measure difference in NMR chemical shift in a solvent by the presence of paramagnetic species. Here, a small capillary with the solution of the paramagnetic compound in e.g. water together with an indicator like e.g. tert-butyl-alcohol inside an NMR tube filled with the same mixture without paramagnetic compound is used. The resonance position of a line in NMR spectrum depends on the bulk magnetic susceptibility of the

medium and the shift in resonance position due to paramagnetic impurities. In this method, susceptibility can be estimated from the distance in Hz of the two signals.

## §4. Classification in Magnetism:

The measured susceptibility ( $\chi$ ) can be expressed as summation of two components

$$\chi = \chi^D + \chi^P$$

$\chi^D$  and  $\chi^P$  denotes diamagnetic and paramagnetic susceptibilities respectively.

$\chi$  positive value implies paramagnetic material while negative magnitude indicates diamagnetic materials.

### §4.1 Diamagnetism:

Diamagnetic materials are weakly repelled by weak magnetic field; appear to weigh slightly less in an applied field. It is an underlying property of matter and present even when it is masked by paramagnetism.  $\chi$  has negative value;  $\sim 10^{-6}$  to  $10^{-4}$  cm<sup>3</sup> mol<sup>-1</sup>, importantly independent of temperature



and applied magnetic field. It is an inherent property of all matter, including paramagnets and arises from the interaction between paired electrons (motion of electrons in their orbits) and applied magnetic field(H). Diamagnetic susceptibilities are additive in nature. Rather, they can be roughly calculated either from atomic susceptibilities( so called ‘‘Pascal’s Constants’’) and constitutive corrections or group(ligand /counterion) susceptibilities. The corrections are generally positive which accounts for the fact that a molecule with multiple/conjugate bonds is less diamagnetic compared to the similar molecule with only single bonds. Diamagnetism is a property of all matter which arises from the interaction of electron pairs with H, generating a field opposing H .i.e., M is negative.  $\frac{\delta E}{\delta H}$  is positive. Diamagnetic materials tend to move to regions of lowest field strength,i.e. repelled by H.

Example: Calculate diamagnetic contribution to magnetic susceptibility of  $K_3[Fe(CN)_6]$ .

$$\begin{aligned} 4K^+ &\rightarrow 3 \times -14.9 = -44.7 \times 10^{-6} \\ 6CN^- &\rightarrow 6 \times -13.0 = -78.0 \times 10^{-6} \\ Fe^{3+} &\rightarrow = \underline{-10.0 \times 10^{-6}} \\ \chi^D &= -132.7 \times 10^{-6} \text{ cm}^3 \cdot \text{mol}^{-1} \end{aligned}$$

The theory of this phenomenon has been understood explicitly since several decades, and *ab initio* calculations have been proved to yield reasonably relevant results for small molecules Eg: Molecules are frequently considered as isolated non-magnetic creatures.  $N_2$  or  $H_2$ .

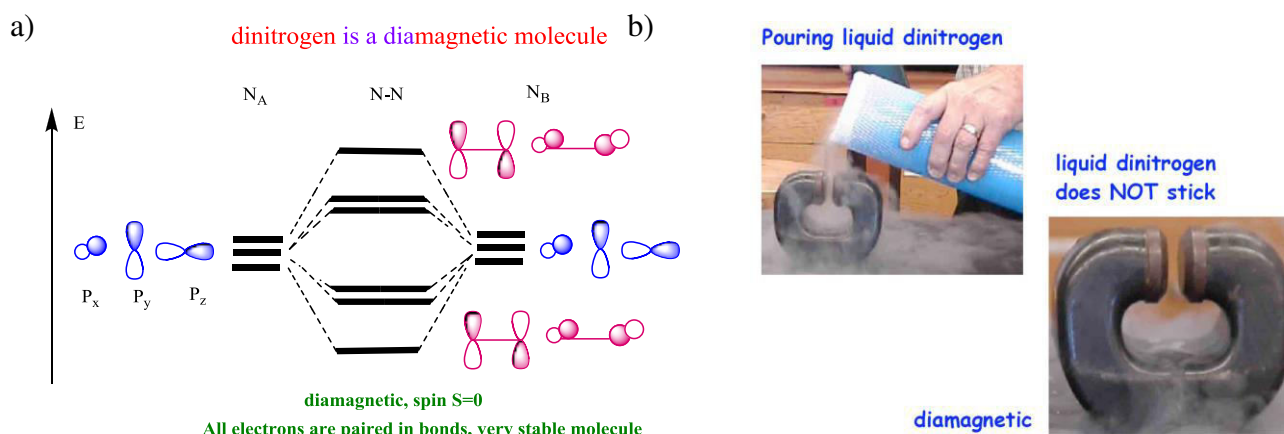


Figure 5. (a) Representation of the involved molecular orbitals in diamagnetic  $N_2$  molecule which lacks any magnetic properties as shown in (b)

#### §4.2 Paramagnetism:

These materials are attracted by an applied magnetic field i.e. appear to gain in weight in applied field. For paramagnetic compounds of low molecular weight the additive methods may be sufficient to estimate the  $\chi^D$  due to their negligible magnitude at low temperature. However, the complexity of

this magnitude determination arises for compounds possessing high molecular weight (eg: biomagnetism) with few paramagnetic centres. Studying  $\chi^D$  independently or extracting mathematically temperature independent contribution can remedy the aforementioned issues. This property arises from the interaction between unpaired electrons and applied magnetic field, strongly effective as compared to diamagnetism.  $\chi$  has positive value;  $\sim +10^{-4}$  to  $10^{+1} \text{ cm}^3 \text{ mol}^{-1}$ ; independent of H while depends on temperature. T dependence provides information on the electronic structure of the paramagnet. Afterwards, we will assume that experimentally determined susceptibilities have been corrected for the diamagnetic contribution and for simplicity, we will use  $\chi$  instead of  $\chi^P$ .  $M$  and  $\chi$  are positive,  $\frac{\delta E}{\delta H}$  is negative. This arises from the interaction of H with the magnetic field of the unpaired electrons due to its spin and orbital angular momentum. An electron has a negative charge, and whenever charge moves, a magnetic field is generated. There are two plausible sources of a magnetic field (i.e. a magnetic moment) for an electron.

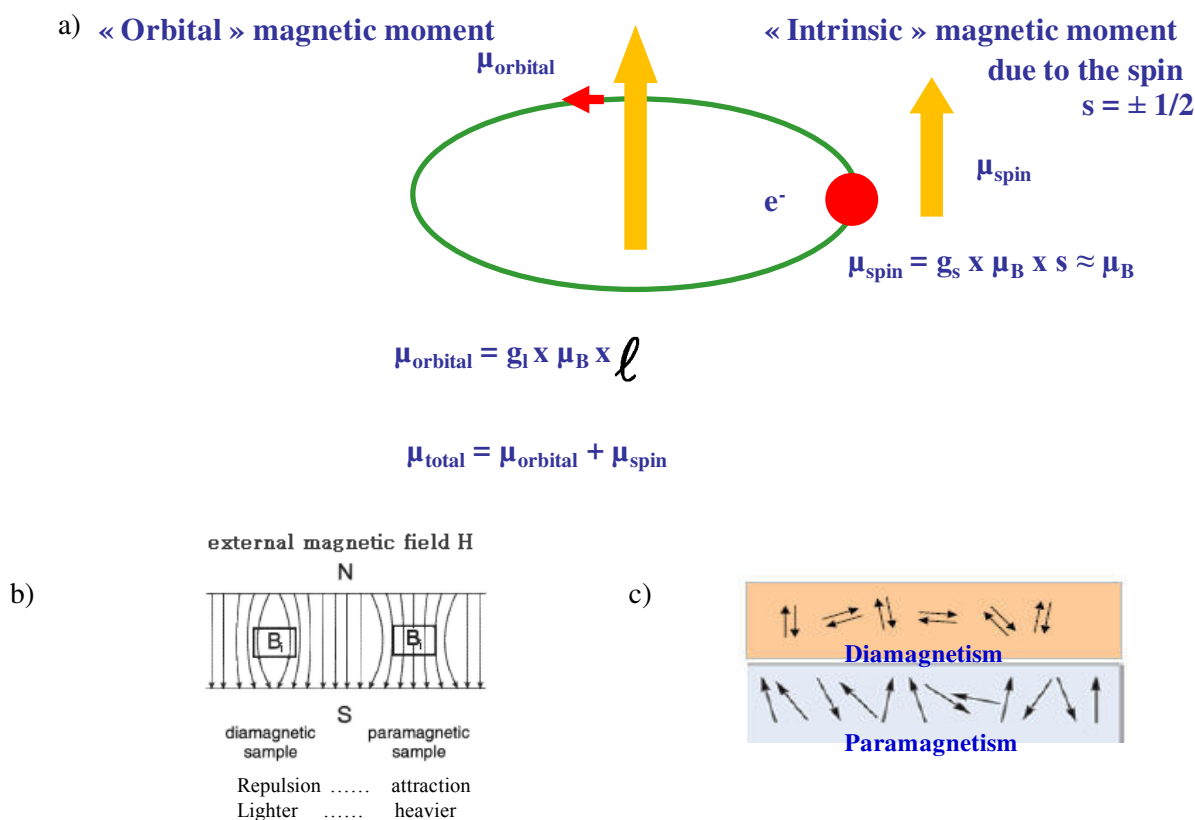


Figure 6. (a) Pictorial representation of determining factors behind orbital angular momentum (b) dependence of diamagnetic and paramagnetic materials on magnetic field (c) Electronic spin orientation within the diamagnetic and paramagnetic molecule.

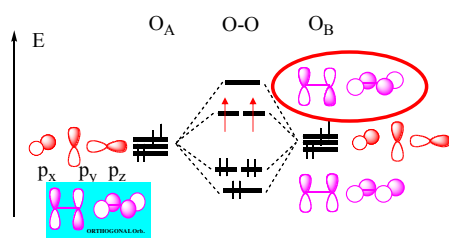


Figure 7. Molecular orbital diagram for  $O_2$  paramagnetic molecule.

The adjacent figure 7 implies the molecular orbital explanation for  $O_2$  paramagnetic molecule,  $O_2$  is paramagnetic, spin  $S = 1$ . Two of its electrons have parallel magnetic moments that shapes aerobic life and allows our existence as human beings. When dioxygen is in an excited state; it can become a singlet (spin  $S=0$ ) and strange reactivity appears ; sometimes useful (glow-worm ...)

### §4.3 Classes of Paramagnetism: Magnetic Interactions

Magnetically Dilute Compounds: Focussed primarily towards describing the properties of single-ion magnets and discrete molecular clusters which has no long range magnetic order. Compounds possessing such properties are known as magnetically dilute.

Magnetically non-Dilute Compounds: Complexes may possess long range magnetic order given the neighbouring paramagnetic centres interact which leads to the predominant governing nature of the interaction.

We have implicitly assumed that the magnetic behaviour of a paramagnetic atom (or ion) is independent of its neighbours (the system is said to be magnetically dilute). If the neighbouring paramagnetic centres do interact (the system is magnetically concentrated) then the magnetic behaviour is governed by the nature of the interaction. Three types of behaviour exists:

(i) Ferromagnetic: neighbouring spins tend to align parallel to each other.

(ii) Antiferromagnetic: neighbouring spins tend to align antiparallel.

(iii) Ferrimagnetic: antiferromagnetic interaction between unequal spins.

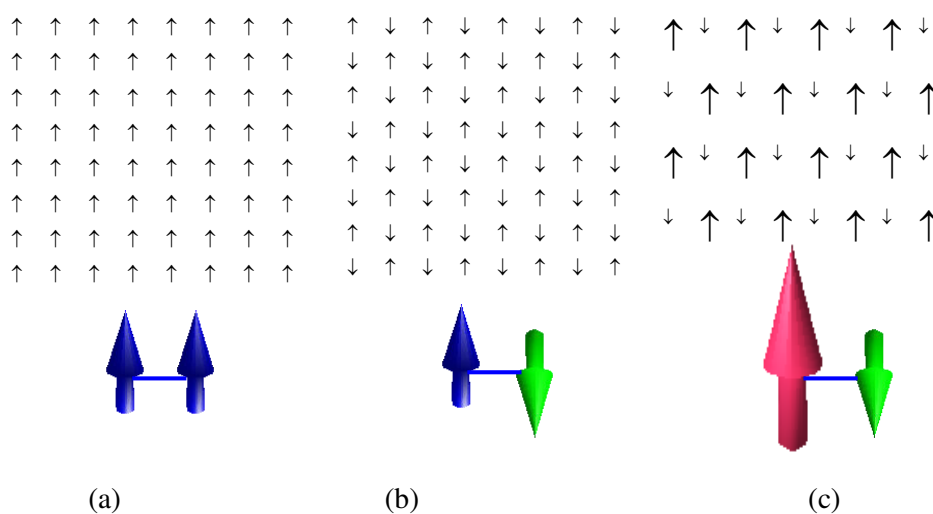


Figure 8. Schematic representation of (a) Ferromagnetic (b) Antiferromagnetic and (c) Ferrimagnetic exchange interactions.

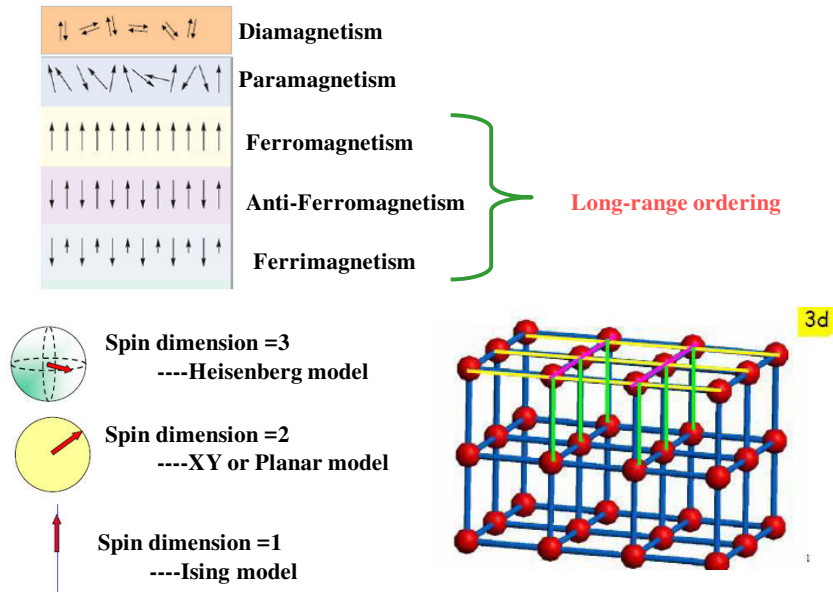


Figure 9. Electron spin alignment for Diamagnetism, Paramagnetism, Ferromagnetism, Antiferromagnetism and Ferrimagnetism and Representation for Heisenberg model, Ising model.

Introduction to Domains:

Magnetic domain is a magnetic region within the magnetic material where magnetization lies in a uniform direction. The magnetization of a piece of ferromagnetic material spontaneously divides into small regions i.e. magnetic domains in order to minimise magnetostatic energy. Domain formation induces areas of space within which the elementary magnets are all parallel.

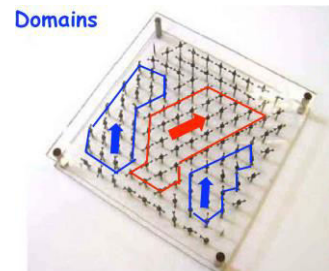
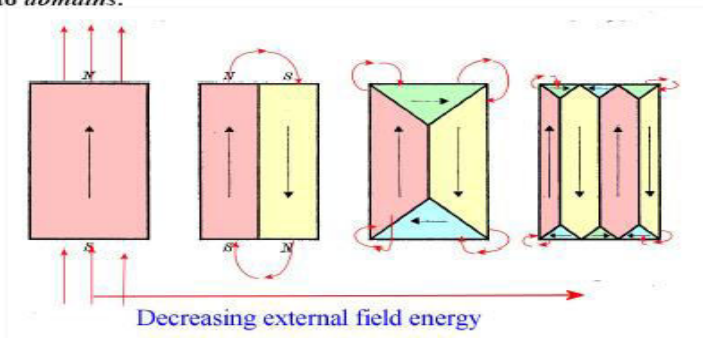
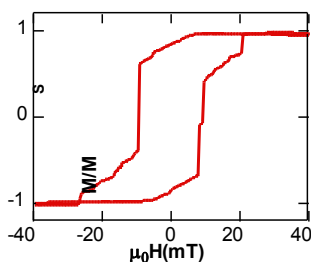


Figure 10. Diagram of a magnetic domain

The external field energy can be decreased by dividing the material into domains.



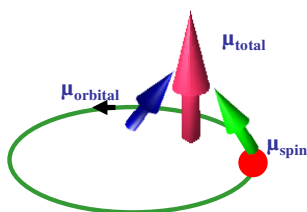
The internal energy is increased because not all the spins are now aligned parallel to one another.



multi-domain nucleation, propagation and annihilation of domain walls

Figure 11. Representative benefits of creating boundaries between domains i.e. domain walls with the aim to minimise magnetostriction energy.

#### §4.3 Derivation of $M$ and $\chi$ : Paramagnetism has two contributions:



(a) Spin Angular Momentum: intrinsic spin of an electron.

(b) Orbital Angular Momentum: if an electron can move around the nucleus.

The total momentum depends on the way these two momenta couple. For further proceedings, we need to link the aforementioned parameter to  $M$  or  $\chi$  of paramagnets.

Figure 12. Contributory factors of magnetic moment

### §5. Temperature dependence of $\chi$ :

#### §5.1 Curie Law:

For magnetically dilute systems, the temperature dependence of  $\chi$  is often found experimentally to be inversely proportional to  $T$ . This is known as Curie Law behaviour.

$$\chi_m = \frac{M}{H} = \frac{Ng^2\beta^2}{4kT} \longrightarrow \text{This is the Curie Law for } S=1/2$$

$$\chi_m = \frac{C}{T} \longrightarrow \text{where } C = \text{Curie constant (cm}^3 \cdot \text{K} \cdot \text{mol}^{-1}\text{), characteristic of a given system.}$$

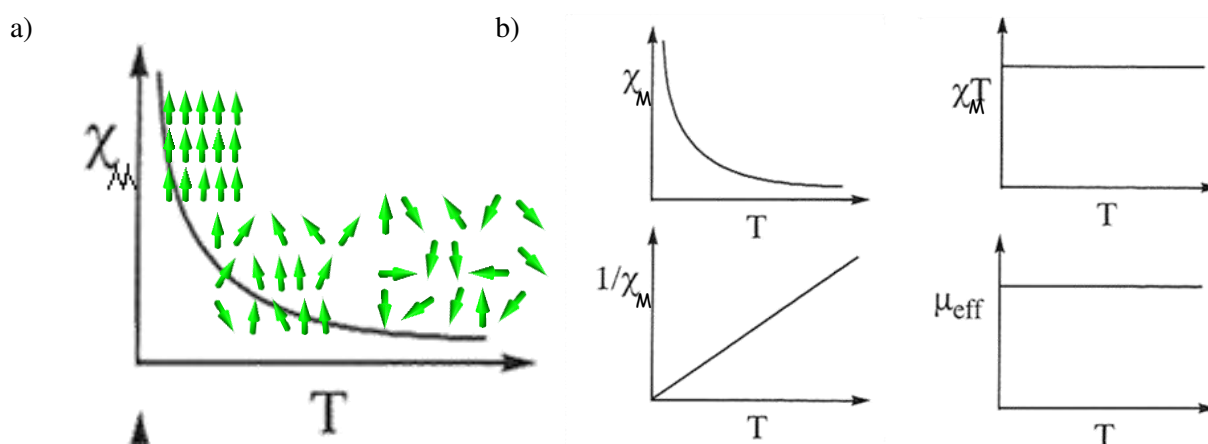
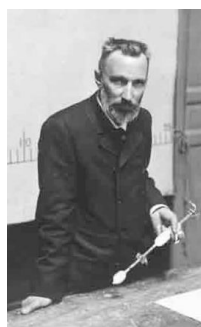


Figure 13. a) For  $\chi$  vs  $T$  plot representation for orientation of electronic spins at step-wise portions in the plot and b)  $\chi$  vs.  $T$ ;  $\chi$  vs.  $1/T$ ;  $\chi T$  vs.  $T$ ;  $\mu_{eff}$  vs  $T$  plots.

Temperature dependence of the magnetic behaviour can be explained by any of the following equations:  $\chi$  vs.  $T$ ;  $\chi$  vs.  $1/T$ ;  $\chi T$  vs.  $T$ . From the above plots, we can infer that,  $\chi$  vs.  $T$  increases as  $T$  decreases.  $1/\chi$  vs.  $T$  is a straight line through the origin, with gradient  $C^{-1}$ . In practice often plot  $\chi T$  vs.  $T \rightarrow$  horizontal line ( $\chi T = C$ ). effective magnetic moment ( $\mu_{eff}$ ) remains independent of temperature.

The aforementioned plots are used to show masked features and play vital role in complicated, non-Curie law behaviour.

Proposal of Curie Law was discovered 100 years ago, from experimental data even before the introduction of quantum mechanics.



**Pierre Curie, France**  
Nobel Prize in 1903



Figure 14. Discovered of Curie Temperature Sir Pierre Curie who won Nobel Prize alongwith glimpse of his work on magnetism from his notebook and final dissertation.

Curie constant comprises of various constants. Given the quenching of orbital angular momentum:

$$C = \chi T = \frac{N\beta^2}{3k} g^2 S(S+1) \approx \frac{g^2}{8} S(S+1)$$

$$\Rightarrow \frac{4}{g^2} \chi T = \frac{S(S+1)}{2}$$

$g$  = Landé  $g$ -factor (characteristic of sample, often  $\approx 2$ )

$S$  = spin quantum number ( $= \frac{1}{2} \times$  number of unpaired electrons)

Hence, can use  $C$  to determine  $S$  of system (and therefore oxidation state, H.S. vs. L.S., coordination geometry, etc)

Important aspects to be considered:

(i)  $\mu_{so} = \sqrt{\frac{3k}{N\beta^2}} \sqrt{\chi T} = \sqrt{g^2 S(S+1)}$

(ii) In magnetically dilute systems,  $\mu_{so}$  is independent of temperature.  $\chi$  is strongly temperature dependent.

(iii) Curie Law is only valid when  $H/kT$  is small (low  $H$ , high  $T$ ), *i.e.* when  $M = \chi H$  holds true.

(iv) At large  $H/kT$  (large  $H$ , low  $T$ ) the magnetisation ( $M$ ) reaches a limiting or saturation value,  $M_{sat}$ , given by

$$M_{sat} = Ng\beta S$$

$$M_{sat} = gS \text{ in B.M. (N}\beta\text{) units}$$

Therefore, can also determine  $S$  from saturation limit (again, only valid when orbital angular momentum is quenched).

$$\mu_n = \frac{-\delta E_n}{\delta H_0} = -m_s g \beta$$

(v)  $\mu_n$  = magnetic moment (magnetization) contribution in the  $z(H)$  direction of a molecule in a given  $m_s$  state where  $E_n$  = energy of that state.

(vi) To calculate total magnetization/magnetic moment ( $M$ ) of the sample, we must sum the  $\mu_n$ 's of each possible  $m_s$  weighted by their Boltzmann's populations.

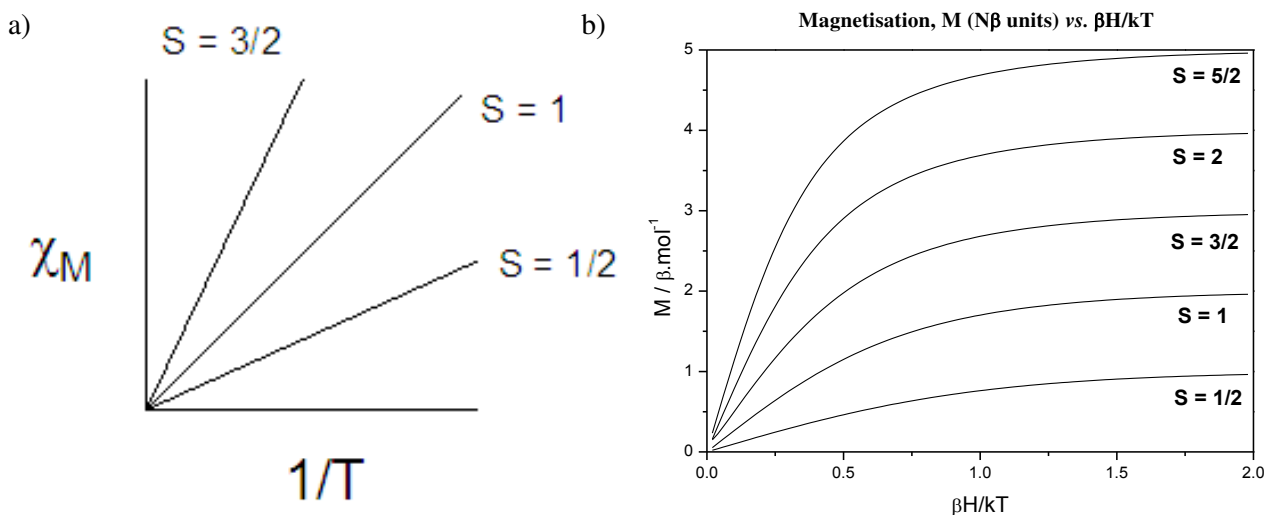


Figure 15. (a) Magnetic susceptibility vs  $T$  plot varies alongwith the change of molecule i.e. change of overall spin ( $S$ ) of the molecule (b) Change of magnetization on variation of  $S$  with respect to the magnetic field.

If available thermal energy,  $kT \gg \Delta E$  then MS levels have almost the same population, governed by Boltzmann distribution. The resultant net magnetisation (or magnetic polarisation),  $M$ , is small. As  $H$  is increased the spins tend to align with  $H$ , subsequent rise in  $M$  according to  $M = \chi H$ . When  $\Delta E \gg kT$  (i.e. at high  $H$ , low  $T$ ) only MS =  $-S$  is significantly populated. This is further followed by full alignment of spins with field and  $M = M_{\text{sat}}$ . We can think of the following example: Thermal energy (KT) :  $\Delta E = g\beta H$ , assume  $g=2$ .  $KT = 210 \text{ cm}^{-1}$  at 300K;  $KT = 3 \text{ cm}^{-1}$  at 4.2K.  $g\beta H = 0.1 \text{ cm}^{-1}$  at  $H=0.1T(1000G)$   $g\beta H = 2.0 \text{ cm}^{-1}$  at  $H=2T(20000G)$

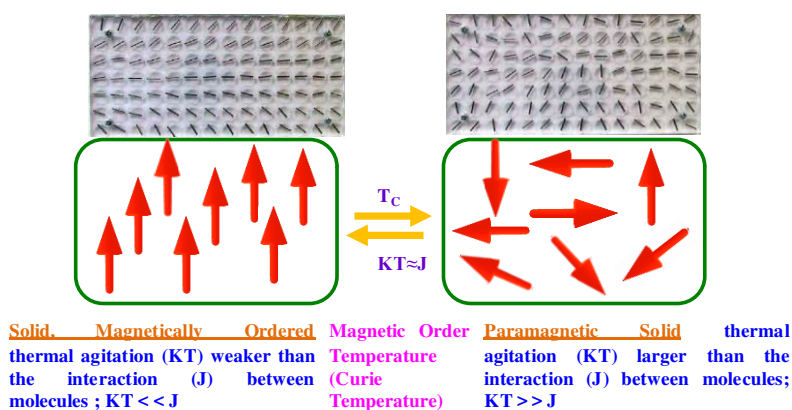


Figure 16. Pictorial representation of electronic spin transition between electronic spins being influenced by thermal agitation and exchange interaction.

### **§5.2 The Curie-Weiss Law:**

In practice, often find deviations from the Curie Law. Experimental data can sometimes be fitted to a Curie-Weiss Law.

$$\chi = \frac{C}{T - \theta} \qquad \theta = \frac{zJS(S+1)}{3k}$$

where  $\theta$  = Curie-Weiss constant (units of K), given by intercept of  $1/\chi$  vs.  $T$  plot with abscissa.  $\theta$  can be positive or negative in sign;  $\theta$  arises due to the weak intermolecular interactions.

$z$  = number of nearest neighbour interactions.

$J$  = interaction between nearest neighbour.

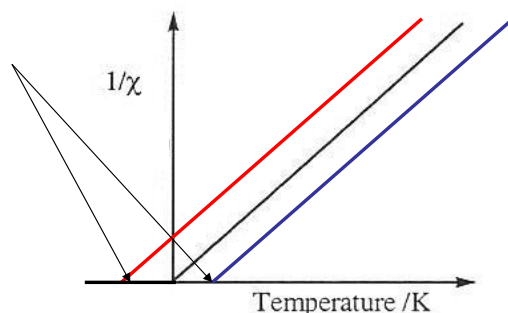


Figure 17. Implication of Curie-Weiss Law

Curie-Weiss behaviour (i.e. non-zero  $\theta$ ) is sometimes indicative of weak intermolecular interactions (i.e. weak magnetic interactions between neighbouring paramagnetic centres), in which case: positive  $\theta \Rightarrow$  ferromagnetic (FM) interaction and negative  $\theta \Rightarrow$  antiferromagnetic (AFM) interaction. However, Curie-Weiss behaviour can also arise from e.g. low lying excited states, or zero-field splitting effects.

## **§6. Experimental protocols in magnetism :**

### **§6.1 Zero-Field-Cooled(ZFC) measurements:**

In this method, first sample is cooled to about 2 K, then the outer magnetic field is switched on and the sample is heated to about 300 K. It freezes the randomly contribution of the sample. It gives information about the temperature dependence of the susceptibility  $\chi$ . This is the most often used method.

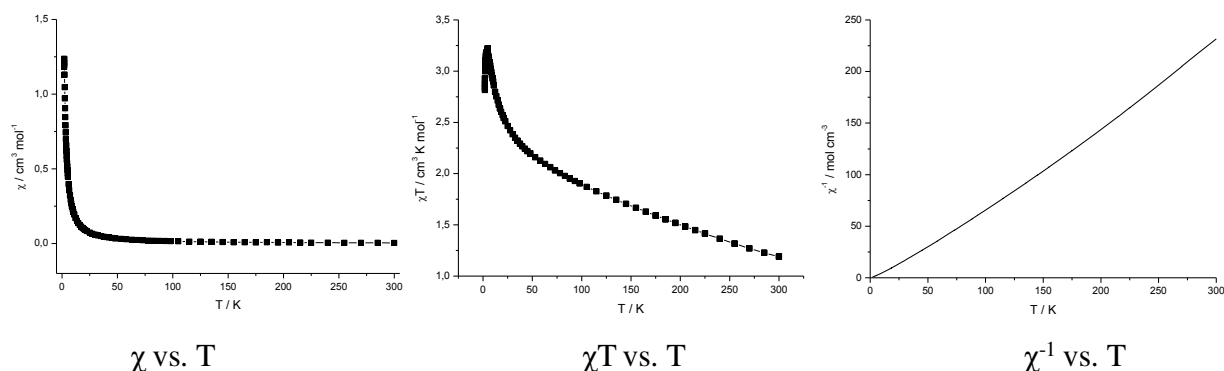




Figure 18. Different contributions from susceptibility with respect to temperature as performed using zero-field cooled measurements.

### §6.2 Field-Cooled(FC) measurements:

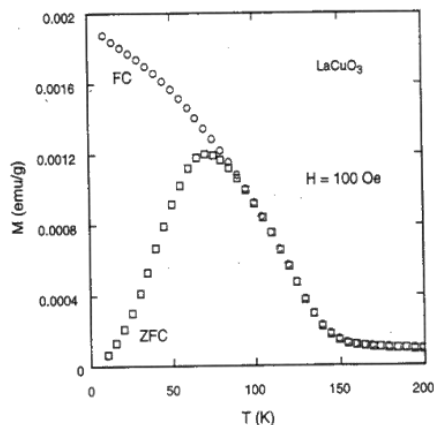


Figure 19. Representation of Blocking Temperature-incident to estimate Single Molecule Magnet (SMM) characteristics

In this method, sample is cooled with an applied magnetic field. It shows the history dependence of the magnetization. Together with the ZFC it gives information about the dynamics of the system. The curve of the ZFC magnetization data shows a maximum  $\rightarrow$  blocking or freezing temperature  $T_B$ . The curve in the adjacent Figure 19 of the FC magnetization data coincides above the blocking temperature with that of the ZFC  $\rightarrow$  system is at the equilibrium. But the measurement is strongly affected by the sweeping rate of the temperature. This method is used to preliminary screen for the presence of irreversibility and  $T_B$ .

### §6.3 Field Scan:

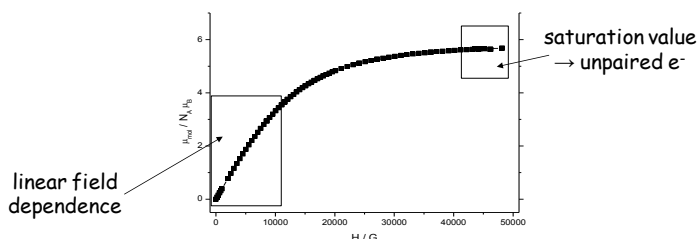


Figure 20. Figure elucidating field scan experimental tool vital for magnetism.

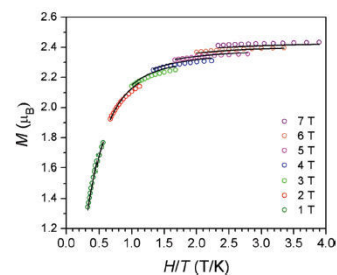


Figure 21. Low temperature magnetization data collected under various dc magnetic field exemplifying zero-field splitting

The field is swept at a low temperature (part of the hysteresis loop). The equations are only valid for  $H/kT$  small  $\rightarrow$  linear behaviour of the curve. The magnetic field for FC and ZFC must lie in the linear area. Saturation is achieved beyond a certain field which provides the number of unpaired electrons directly.

### §6.4 Reduced Magnetization:

In this method, several field scans were collected at different temperatures followed by the collection of  $M$  vs.  $H/T$  diagram. This method offers information about Zero-Field-Splitting. Adjacent figure 21

implies the presence of series of nonsuperimposable isofield curves which fall dramatically short of reaching the magnetization underlining zero-field splitting as well as magnetic anisotropy.

### §6.5 Magnetic hysteresis:

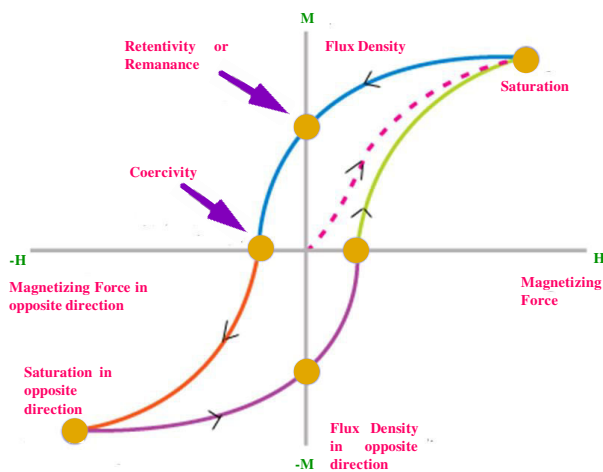


Figure 22. Schematic representation of magnetic hysteresis in a magnetic material

On application of magnetic field, the atomic dipoles of a ferromagnet are expected to align themselves with respect to the applied magnetic field. Sometimes, even after removal of magnetic field aligned spins will not relax back to zero magnetization, instead it retains the alignment giving rise to the magnetized material. In order to promote the bringing back of magnetization to zero, an alternating magnetic field in the opposite direction needs to be applied whose magnetization would trace out a loop known as hysteresis loop. Absence of retraceability of the magnetization curve

is a characteristic known as hysteresis which can be correlated to the presence of magnetic domains in the material. Linear correlation lacks between field strength  $H$  and magnetization  $M$ . In presence of demagnetization ( $H=M=0$ ),  $M$  will exhibit initial magnetization curve in  $M$ - $H$  plot upon increasing level of field strength. This curve moves rapidly upwards followed by subsequent approach towards an asymptote known as magnetic saturation. Upon monotonic decrease of the magnetic field, magnetization is supposed to follow completely different curve. At zero magnetic field, the stipulated magnetization is counterbalanced from the origin resulting the term remanence. The aforementioned,  $M$ - $H$  plot can be regarded as hysteresis loop and main loop given the plot is being considered at all strengths of magnetic field. The width of the middle section of this loop is equal to the twice of the coercivity of the material. Coercivity can be defined as measure of the reverse magnetic field required to drive back the magnetization to zero after becoming saturated. Smaller, random jumps (Barkhausen jumps) in the magnetization curve (only in closer look) arise due to the crystallographic defects such as dislocations. It is worth mentioning that, hysteresis loop begins at a starting point ( $H=0$ ) when the intrinsic magnetic dipole moments are randomly oriented and the material is expected to show Paramagnetism property. On application of magnetic field ( $H$ ), it proceeds upto the saturation point (as mentioned by saturation symbolisation in figure 23) which leads to the alignment of all the magnetic dipole moments towards the direction of the magnetizing force and no such increment of magnetic flux occurs. When  $H$  is brought back to zero, retentivity point as mentioned in figure 23 arises owing to its possession of remanent magnetization. The equilibrium state of zero magnetization (random orientation of magnetic dipoles) can be retrieved by the application of magnetic field in the opposite

direction. This remanent magnetization is to be eradicated coercive magnetizing force has to be applied in the reverse direction. The point which lacks magnetic flux/magnetization ( $M=0$ ) due to the revocation of dipole moments active in the opposing direction is termed as the coercivity as mentioned in figure 23. On enhancement of the magnetizing force in the negative direction, similar saturation is expected to be observed even in the reverse direction. This renders the loop which continues with an equal but opposite retentivity and coercivity until the achievement of original saturation point. In order to get back to the origin ( $M=H=0$ ) the material has to be demagnetized (regains its paramagnetic characteristics) by either reversing the direction of the magnetic field or colliding the material with a surface or heating it in a way it crosses its corresponding Neel temperature. At this specified temperature, a ferromagnetic material is supposed to make transition to Paramagnetism owing to the thermal fluctuations in the magnetic dipole moment that randomize the spins.

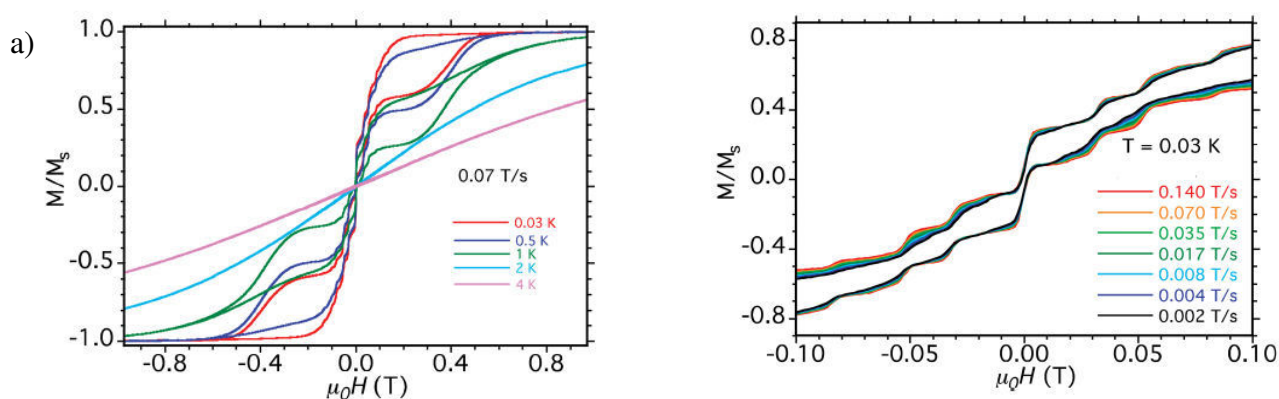


Figure 23. Magnetization vs field plot for a single crystal (a) with the field at different temperatures and constant field sweep rate/field scanning rates and (b) for different sweep rates of the magnetic field where temperature remains constant. (It is important to notify that the above two diagrams have been published and meticulously explained).<sup>4</sup>

Magnetization vs magnetic field plot performed at various sweep rates and temperatures keeping the other parameter constant have been shown in figure 23. The magnetic field is being sweep from -1T to +1T which has been brought back to -1T. Figure 23a implies magnetization vs field plot for different temperatures but at constant field scanning rate of 0.07 T/s. From this figure we can infer that, coercivity/opening of the hysteresis loop increases with the decrease of temperature (as vindicated by wider plateau region for red/lower temperature as compared to sky/higher temperature). This can be explained on the basis of reduced number of molecules which may relax via thermal process resulting increased relaxation via tunnelling. Figure 23b indicates the magnetization vs field curve carried out at different field sweep rates but at constant temperature. Coercivity is found to

rise with the increase in sweep rate owing to the less importance of the number of molecules that undergo relaxation via tunnelling.

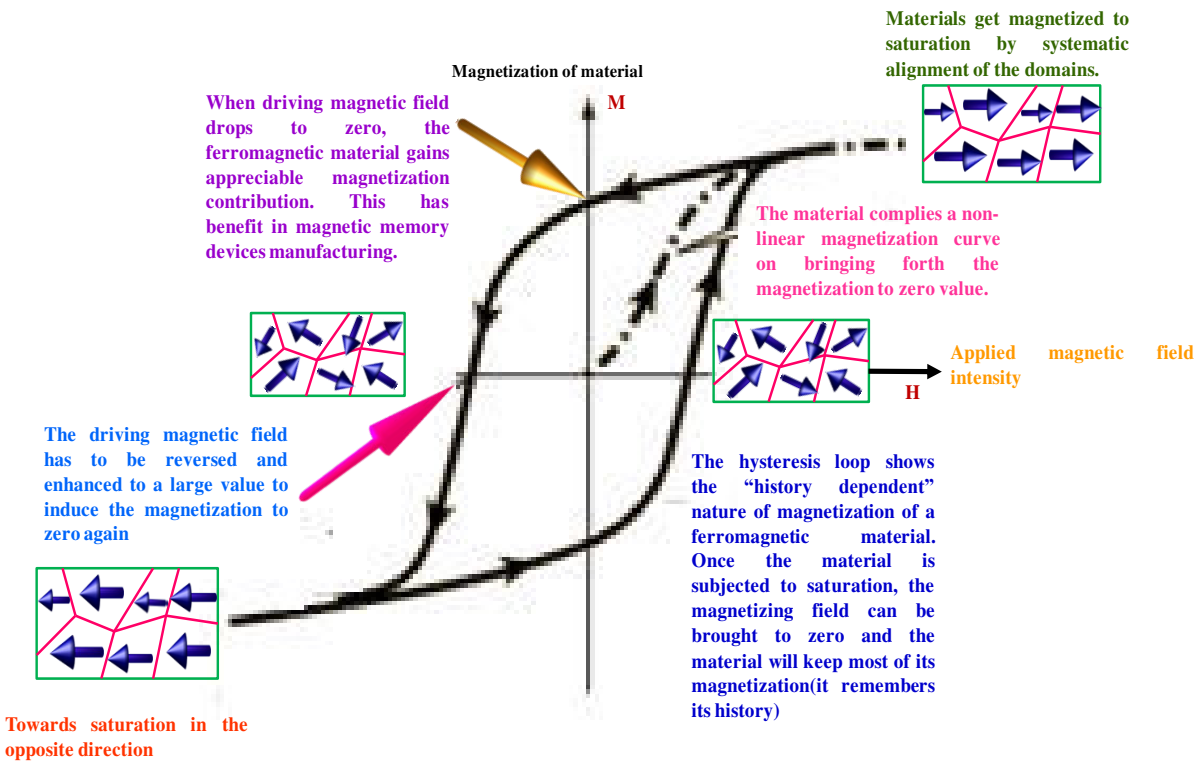


Figure 24. Underlying steps in the magnetic hysteresis

Sample is cooled and the field is swept .An opening of the curve is called a hysteresis loop. Due to slow relaxation of the molecule compared with the time to sweep the field. The width of the loop is directly related to the dynamics of the molecule. Adjacent figure depicts the underlying steps in hysteresis.

**§6.6 AC susceptibility measurements:**

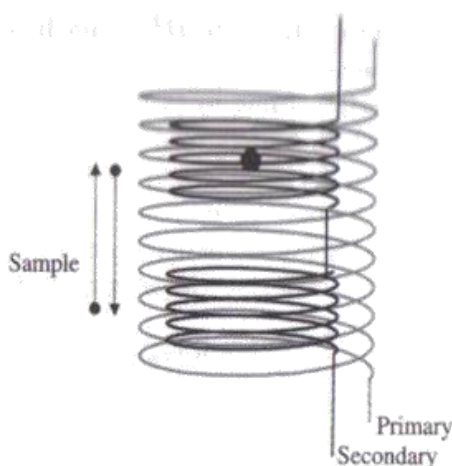


Figure 25. Illustration of AC susceptibility measurements

Setup: first-order gradient coil (adjacent figure) inside a primary coil, which induces an alternating magnetic field. The dynamics of magnetization can be investigated by varying the frequency  $\omega$ . The establishment of the thermal equilibrium requires a time  $\tau$ . If the frequency of the ac field is low  $\rightarrow \omega \tau \ll 1$ , the isothermal susceptibility  $\chi = \chi_T$  is measured. If the frequency of the ac field is high  $\rightarrow \omega \tau \gg 1$ , the adiabatic susceptibility  $\chi = \chi_S$  is measured. Employing the tool when we measure the magnetic susceptibility in response to an AC magnetic field (field varies sinusoidally) , AC susceptibility

contribution comes. It has additional advantages of explaining many complex phenomena which cannot be elucidated in terms of constant-field DC magnetic susceptibility measurements.

## **§7. Detailed analysis of various magnetic interactions:**

### **§7.1 Ferromagnetism:**

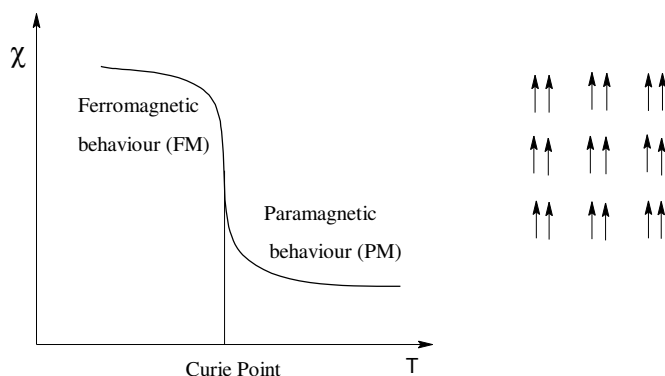


Figure 26. Dependence of magnetic susceptibility on temperature in a ferromagnetic material with the intrinsic electronic spin alignment.

J positive with spins aligned in parallel direction below Curie Temperature ( $T_C$ ).

### **§7.2 Anti-Ferromagnetism:**

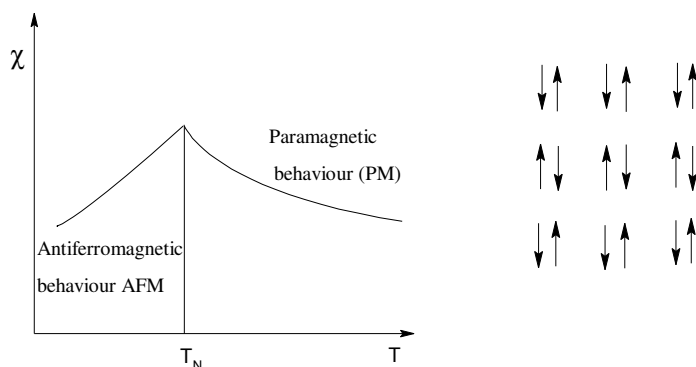


Figure 27. Dependence of magnetic susceptibility on temperature in a anti-ferromagnetic material with the intrinsic electronic spin alignment.

J negative with spins aligned in antiparallel direction below Neel Temperature ( $T_N$ ).

### **§7.3 Ferrimagnetism:**

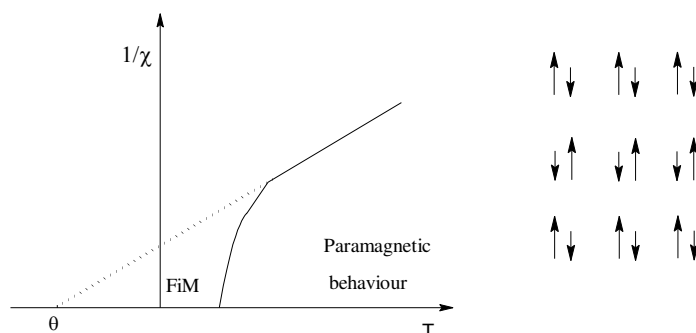


Figure 28. Dependence of magnetic susceptibility on temperature in a ferrimagnetic material with the intrinsic electronic spin alignment.

J negative with spins of unequal magnitude antiparallel direction below Critical Temperature.

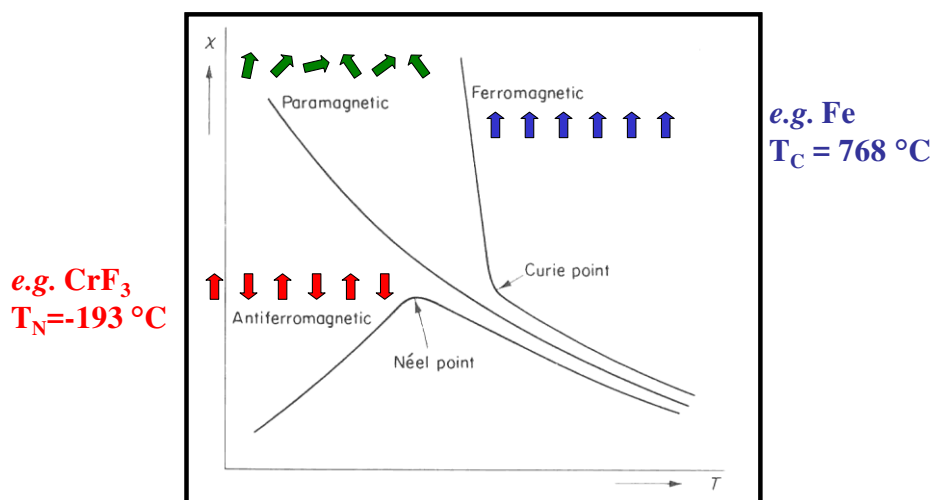


Figure 29. The above figure illustrates ferromagnetic and antiferromagnetic behaviour of Fe and CrF<sub>3</sub> respectively with their respective temperature beyond which Ferro/Antiferro magnetism will be destroyed and paramagnetic property will be regained.

The above diagram indicates  $\chi$  vs T plot for magnetically dilute and non-dilute compounds. It is to mention that, interaction of ferro- and antiferromagnets with magnetic fields is many order of magnitude stronger than paramagnets.

### §8. Single-Ion magnetic properties:

s Elements										p Elements																																			
H																	He																												
Li	Be	d Elements : transition														B	C	N	O	F	Ne																								
Na	Mg	Al	Si	P	S	Cl	Ar																																						
K	Ca	Sc	Ti	V	Cr	Mn	Fe	Co	Ni	Cu	Zn	Ga	Ge	As	Se	Br	Kr																												
Rb	Sr	Y	Zr	Nb	Mo	Tc	Ru	Rh	Pd	Ag	Cd	In	Sn	Sb	Te	I	Xe																												
Cs	Ba	La	Hf	Ta	W	Re	Os	Ir	Pt	Au	Hg	Tl	Pb	Bi	Po	At	Rn																												
Fr	Ra	Ac	f Elements																																										
<table border="1"> <tr> <td>Ce</td><td>Pr</td><td>Nd</td><td>Pm</td><td>Sm</td><td>Eu</td><td>Gd</td><td>Tb</td><td>Dy</td><td>Ho</td><td>Er</td><td>Tm</td><td>Yb</td><td>Lu</td> </tr> <tr> <td>Th</td><td>Pa</td><td>U</td><td>Np</td><td>Pu</td><td>Am</td><td>Cm</td><td>Bk</td><td>Cf</td><td>Es</td><td>Fm</td><td>Md</td><td>No</td><td>Lr</td> </tr> </table>																		Ce	Pr	Nd	Pm	Sm	Eu	Gd	Tb	Dy	Ho	Er	Tm	Yb	Lu	Th	Pa	U	Np	Pu	Am	Cm	Bk	Cf	Es	Fm	Md	No	Lr
Ce	Pr	Nd	Pm	Sm	Eu	Gd	Tb	Dy	Ho	Er	Tm	Yb	Lu																																
Th	Pa	U	Np	Pu	Am	Cm	Bk	Cf	Es	Fm	Md	No	Lr																																
44,956	47,867	50,942	51,996	54,938	55,845	58,933	58,693	63,546	65,39																																				
Sc	Ti	V	Cr	Mn	Fe	Co	Ni	Cu	Zn																																				
21	22	23	24	25	26	27	28	29	30																																				
88,906	91,224	92,906	95,94	98,906	101,07	102,91	106,42	107,87	112,41																																				
Y	Zr	Nb	Mo	Tc	Ru	Rh	Pd	Ag	Cd																																				
39	40	41	42	43	44	45	46	47	48																																				
138,91	178,49	180,95	183,84	186,21	190,23	192,22	195,08	196,97	200,59																																				
La	Hf	Ta	W	Re	Os	Ir	Pt	Au	Hg																																				
57	72	73	74	75	76	77	78	79	80																																				

Figure 30. Periodic table depicting the position of transition metal ions and lanthanide ions.

Energy level splitting in mononuclear hexa-coordinated complexes:

## Splitting of the energy levels

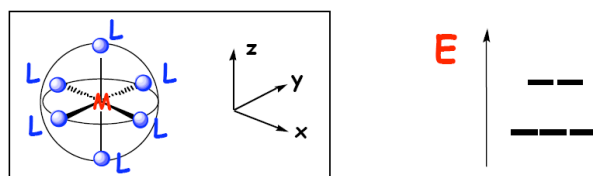


Figure 31. Splitting of the energy levels of a transition metal ion in presence of octahedral ligand field.

Analysing extent of energy levels splitting:

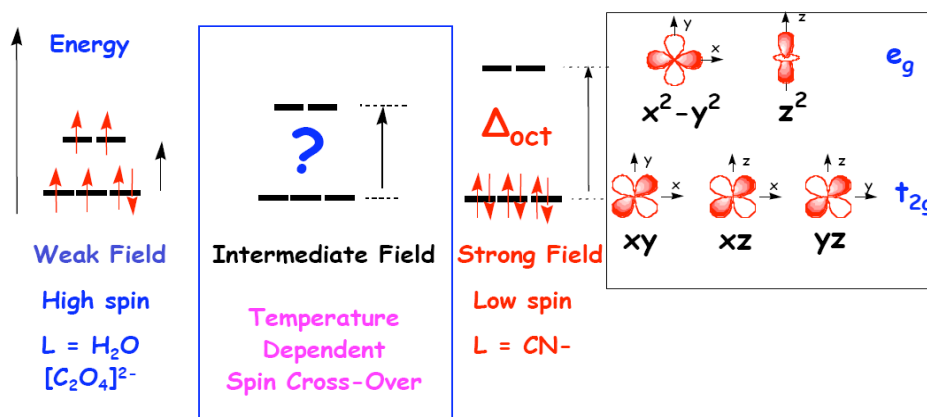
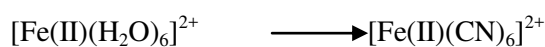
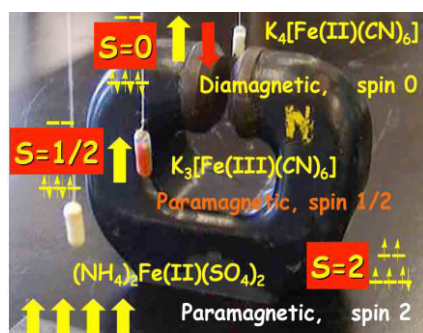


Figure 32. Splitting of the energy levels of Fe(II)-L<sub>6</sub> complex where L is being varied from weak field (water) to strong field (cyanide) and also spin-cross over is explained above.



We can consider ligand field splitting as  $\Delta_{\text{oct}}$ . In intermediate ligand field --- T or P causes switching between HS and LS – termed as spin cross over or spin transition.

Analysing magnetic properties:



Easiest way to detect the property of the sample is to explore the strength of attraction the sample felt which is primarily dictated by the number of lone electrons.

Figure 33. Description of Fe(II)-L<sub>6</sub> complex with its various magnetic properties.

## §9. Magnetic moment and ground state properties:

$$\mu_{so} = \sqrt{\frac{3k}{N\beta^2}} \sqrt{\chi T} = \sqrt{g^2 S(S+1)}$$

With no orbital contribution

Incorporating orbital contribution  $\mu_{LS}$  becomes,

$$\mu_{LS} = \sqrt{[g^2 S(S+1) + L(L+1)]} \quad \longrightarrow \text{Applicable only for free ions and for independent L \& S .}$$

S= total spin quantum number

L= total orbital angular momentum quantum number

g= a constant known as the (spin) g factor  $\approx 2.0023$

Effect of spin-orbit coupling:

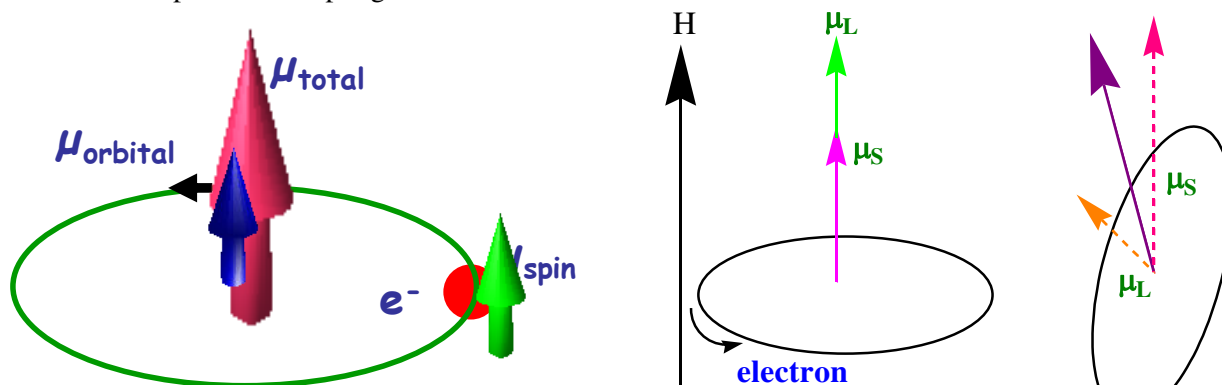


Figure 34. Contributory factors of total orbital angular momenta with applied magnetic field.

Actually, spin and orbital angular momenta couple, i.e. L and S no longer remain independent and not good quantum numbers given the strong nature of the coupling. We need a different quantum number, J.

J= total angular momentum quantum number.

J takes the absolute values from  $|L+S|$  to  $|L-S|$

$$\therefore \mu_{\text{eff}} = g_J \sqrt{J(J+1)} \quad g = 1 + \frac{S(S+1) - L(L+1) + J(J+1)}{2J(J+1)}$$

Eg. 1. Cr(III),  $d^3$ :

$$\begin{array}{cccccc} \uparrow & \uparrow & \uparrow & - & - & S=3/2; \\ +2 & +1 & 0 & -1 & -2 & L = \sum m_l = 3 \end{array}$$

$$J = 9/2, 7/2, 5/2, 3/2$$

These J states have different energies.

For shells less than half-filled, the minimum J is the ground state. For shells more than half-filled, the maximum J is the ground state. For half-filled shells  $L=0$  and  $J=S$ , i.e. only one state. For example, Cr(III) is associated with  ${}^4F_{3/2}$  or generally  $[{}^{2S+1}X_J]$  where  $\lambda$  and  $\xi$  are the measure of strength of interaction between L and S (SO).  $\xi$  is the strength for a one-electron system (a single unpaired electron).  $\lambda$  denotes SOC strength in presence of more than one unpaired electron.  $\xi$  is fundamentally a positive parameter,  $\lambda$  and  $\xi$  are related by,



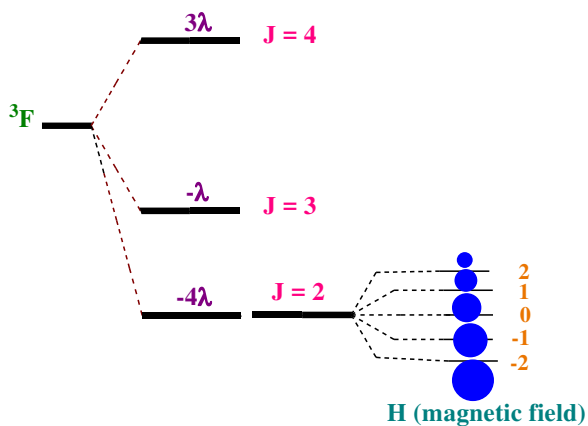


Figure 35. Energy level splitting in a system containing V(III), d<sup>2</sup>.

$$\lambda = \pm \frac{\xi}{2S} ; S = \text{total spin } \{ \lambda = \pm \xi \text{ for } S=1/2 \}$$

$\lambda > 0$  for less than half-filled shell ;  $\lambda < 0$  for more than half-filled shell

Eg. 2. V(III), d<sup>2</sup>: S = 1, L = 3, J=4, 3, 2 with <sup>3</sup>F<sub>2</sub> ground state

Remarkably, J states do not possess similar energy.

$$E_J = \frac{1}{2} \lambda [J(J+1) - L(L+1) - S(S+1)]$$

For <sup>3</sup>F ground state, J=2 so,

$$E_{J=2} = \frac{1}{2} \lambda [2(2+1) - 3(3+1) - 1(1+1)] = -4\lambda$$

The energy differences are measured in terms of  $\lambda$ .

$$\Delta E_{J, J+1} = \lambda (J+1); \text{ Hence, } \Delta E (J=4,3) = 4\lambda \text{ and } \Delta E (J=3,2) = 3\lambda$$

Each J is composed of M<sub>J</sub>, corresponding to allowed orientations in H. It is mentionworthy that, J split maintains a centre of gravity. <sup>3</sup>F=9\*3-7-5\*4= 0  $\lambda$ .

Magnetic moments of 1<sup>st</sup> row transition metal ions:

Practically, orbital contribution is often considerably less than the spin contribution...(S>>L):

$$\mu_{SO} = \sqrt{[g^2 S(S+1)]}$$

$$\mu_{SO} = \sqrt{[4S(S+1)]} = \sqrt{[n(n+2)]}$$

Ground terms for d<sup>n</sup> configuration:

Table 1. Ground term symbol for first row transition metal ions:

Configuration	Example	m <sub>l</sub>					L	S	Ground Term
		2	1	0	-1	-2			
d <sup>1</sup>	Ti <sup>3+</sup>	↑					2	1/2	<sup>2</sup> D
d <sup>2</sup>	V <sup>3+</sup>	↑	↑				3	1	<sup>3</sup> F
d <sup>3</sup>	Cr <sup>3+</sup>	↑	↑	↑			3	3/2	<sup>4</sup> F
d <sup>4</sup>	Mn <sup>3+</sup>	↑	↑	↑	↑		2	2	<sup>5</sup> D
d <sup>5</sup>	Mn <sup>2+</sup>	↑	↑	↑	↑	↑	0	5/2	<sup>6</sup> S
d <sup>6</sup>	Fe <sup>2+</sup>	↑↓	↑	↑	↑	↑	2	2	<sup>5</sup> D
d <sup>7</sup>	Co <sup>2+</sup>	↑↓	↑↓	↑	↑	↑	3	3/2	<sup>4</sup> F
d <sup>8</sup>	Ni <sup>2+</sup>	↑↓	↑↓	↑↓	↑	↑	3	1	<sup>3</sup> F
d <sup>9</sup>	Cu <sup>2+</sup>	↑↓	↑↓	↑↓	↑↓	↑	2	1/2	<sup>2</sup> D

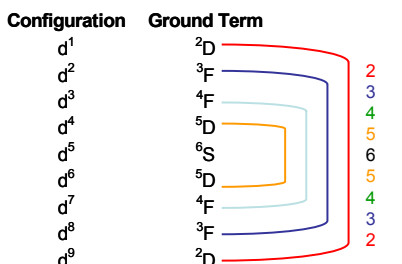


Figure 36. Schematic representation for ground state term symbol for d<sup>1</sup>-d<sup>9</sup> electronic configuration

Ground term: <sup>(2S+1)</sup>L

Where the maximum value of M<sub>L</sub> defines L

L=0,1,2 and 3 corresponds to S,P,D and F terms.

Where the maximum value of M<sub>S</sub> denotes S. Following enlisted the terms which arises from the d<sup>n</sup> electronic configuration which are

equivalent to the terms those generate from d<sup>10-n</sup> electronic

configurations.

**Orbital contribution to the magnetic moment:**

$$\mu_{LS} = \sqrt{[g^2 S(S+1) + L(L+1)]}$$

When orbital contribution arises?

In order that an electron can have orbital angular momentum, it must be possible to transform the orbital that it occupies into an exactly equivalent and degenerate orbital by rotation. The electron is then effectively rotating about the axis used for the orbital rotation.

(the circulation of an electron around the nucleus is like the circulation of a current through the turns of a solenoid)

Octahedral complexes: The degenerate  $t_{2g}$  orbitals ( $d_{xy}$ ,  $d_{xz}$ ,  $d_{yz}$ ) can be interconverted by  $90^\circ$  rotations. e.g. the  $d_{xz}$  orbital is transformed into the  $d_{yz}$  orbital by a rotation of  $90^\circ$  about the z-axis – during this rotation the electron is orbiting the nucleus. Thus, an electron in a  $t_{2g}$  orbital **can** contribute to orbital angular momentum.

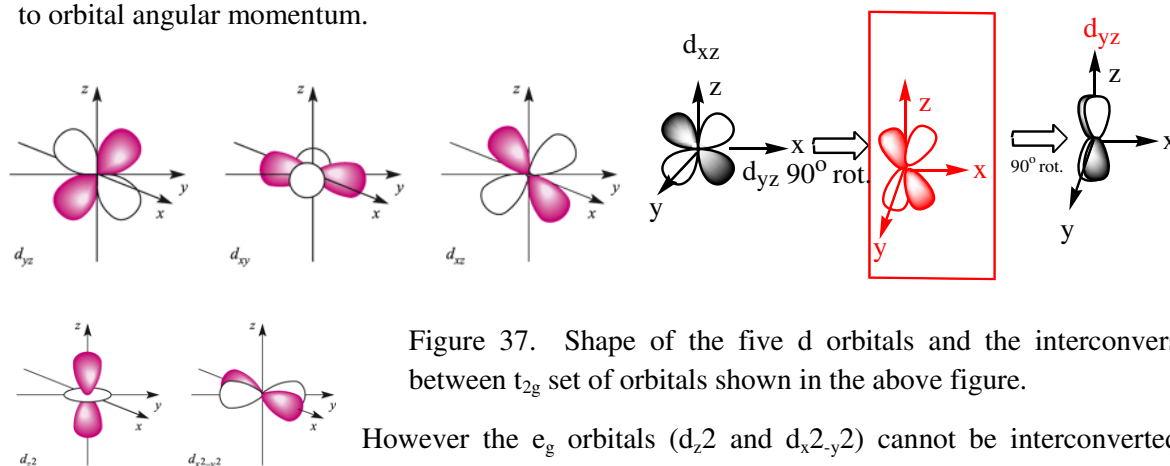
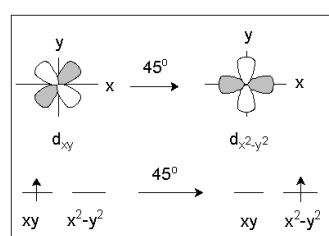


Figure 37. Shape of the five d orbitals and the interconversion between  $t_{2g}$  set of orbitals shown in the above figure.

However the  $e_g$  orbitals ( $d_{z^2}$  and  $d_{x^2-y^2}$ ) cannot be interconverted by rotation as they are different shapes. Thus an electron in an  $e_g$  orbital **can not** contribute to orbital angular momentum

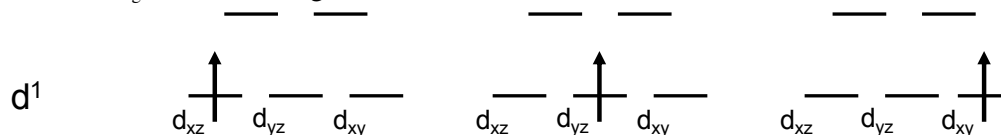


But an  $e_g \rightarrow t_{2g}$  transformation is possible.  
 $d_{xy} / d_{x^2-y^2}$  orbital motion about z axis  
 $d_{xz} / d_{yz}$  orbital motion about z axis  
 $d_{xz} / d_{xy}$  orbital motion about x axis  
 $d_{yz} / d_{xy}$  orbital motion about y axis

Figure 38. Figure depicting that interconversion between  $t_{2g}$  and  $e_g$  sets of orbitals is not possible.

Orbital contribution to the magnetic moment (high spin octahedral  $d^n$  ions)

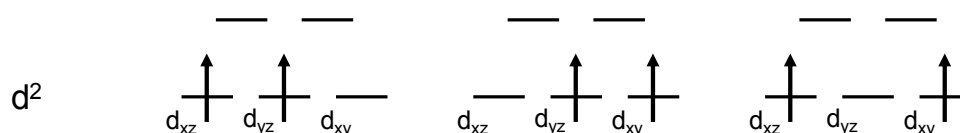
Plausible  $t_{2g}$  electron arrangements



Possible  $t_{2g}$  arrangements = 3

Orbital contribution = **no**

$d^1$  electronic configuration e.g. Ti(III)



Possible  $t_{2g}$  arrangements = 3

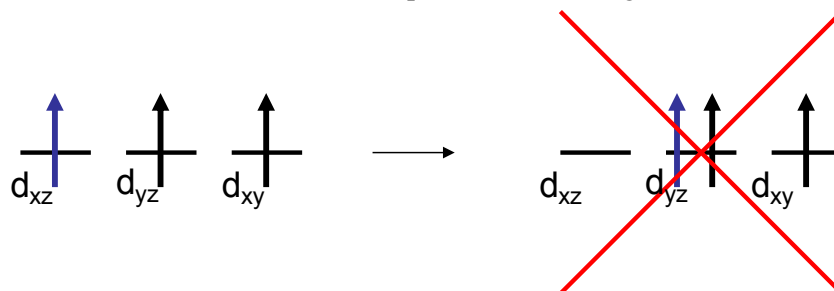
Orbital contribution = **yes**

$d^2$  e.g. V(III)

But, electrons in  $t_{2g}$  orbitals will not always contribute to orbital angular momentum

e.g. Consider octahedral Cr(III)  $d^3, t_{2g}^3$

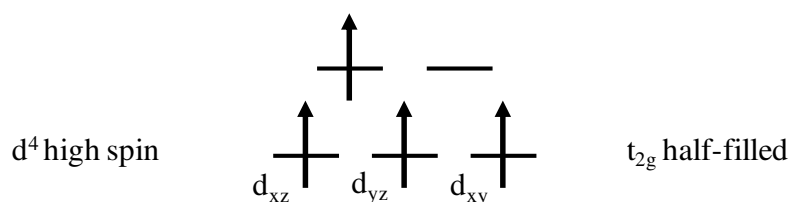
an electron in the  $d_{xz}$  orbital cannot by rotation be placed in e.g. the  $d_{yz}$  orbital because this orbital already contains an electron with the same spin as the incoming electron.



Therefore, there is only possible  $t_{2g}$  arrangement and **no orbital angular momentum**.

Orbital contribution to the magnetic moment (high spin octahedral  $d^n$  ions)

i)

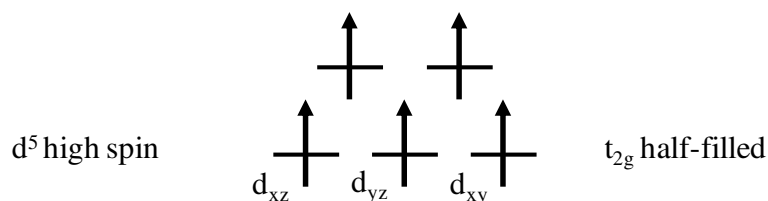


Possible  $t_{2g}$  arrangements = 1

Orbital contribution = **NO**

$d^4$  e.g. Cr(II)

ii)

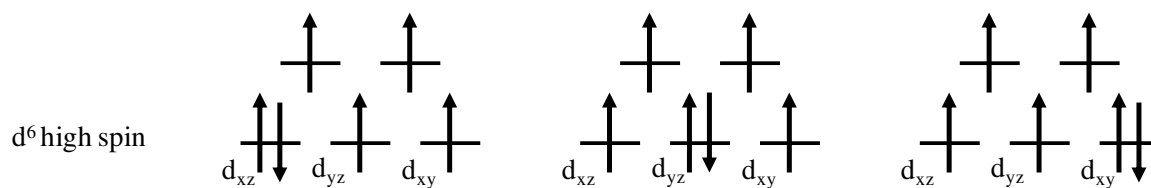


Possible  $t_{2g}$  arrangements = 1

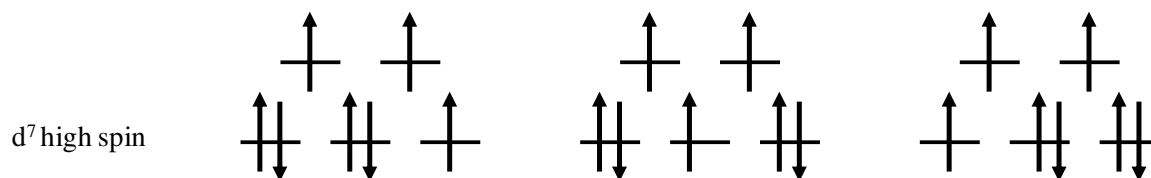
Orbital contribution =

$d^5$  e.g. Fe(III)

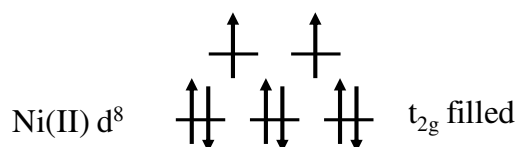
\_iii)

Possible t<sub>2g</sub> arrangements = 3Orbital contribution = **YES**d<sup>6</sup> e.g. Fe(II)

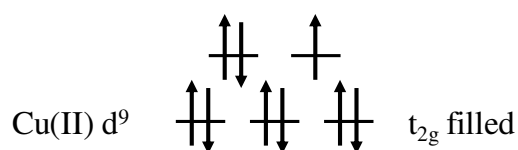
iv)

Possible t<sub>2g</sub> arrangements = 3Orbital contribution = **YES**d<sup>7</sup> e.g. Co(II)

v)

Possible t<sub>2g</sub> arrangements = 1Orbital contribution = **NO**d<sup>8</sup> e.g. Ni(II)

vi)

Possible t<sub>2g</sub> arrangements = 1

Orbital contribution =

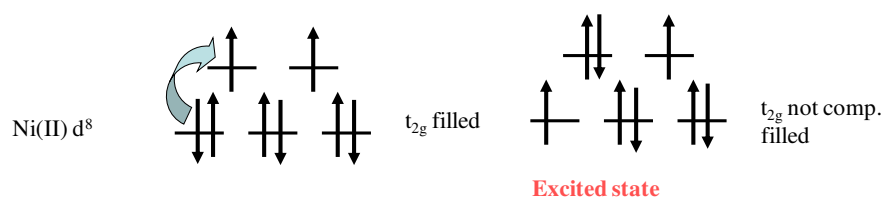
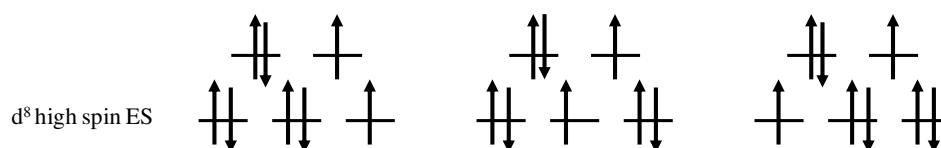
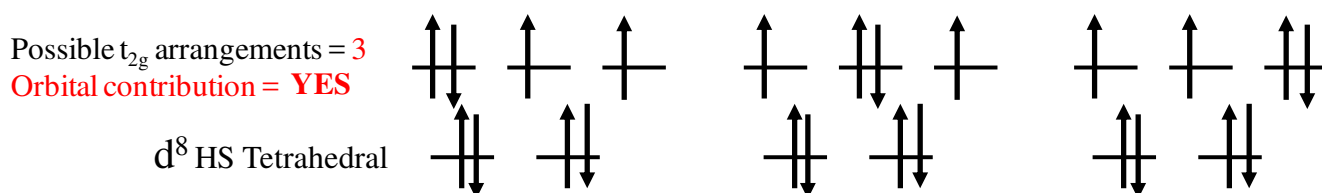
d<sup>9</sup> e.g. Cu(II)Contribution due to the excited state(s)**Orbital contribution to the magnetic moment****Contribution due to the excited state(s)**think of **possible** t<sub>2g</sub> electron arrangementsPossible t<sub>2g</sub> arrangements = 1Orbital contribution = **NO**Possible t<sub>2g</sub> arrangements = 3Orbital contribution = **YES** $\mu_{\text{exp}} > \mu_{\text{s}}$  for Oct. Ni<sup>2+</sup>

Table 2. Orbital contribution for  $d^1$ - $d^9$  ions in octahedral and tetrahedral stereochemistries:

d electrons	Octahedral complexes			Tetrahedral complexes		
	configuration	Ground term	Orbital contribution	configuration	Ground term	Orbital contribution
1	$t_{2g}^1$	${}^2T_{2g}$	Yes	$e^1$	${}^2E$	No
2	$t_{2g}^2$	${}^3T_{1g}$	Yes	$e^2$	${}^3A_2$	No
3	$t_{2g}^3$	${}^4A_{2g}$	No	$e^2 t_2^1$	${}^4T_1$	Yes
HS-4	$t_{2g}^3 e_g^1$	${}^5E_g$	No	$e^2 t_2^2$	${}^5T_2$	Yes
LS-4	$t_{2g}^4$	${}^3T_{1g}$	Yes	$e^2 t_2^3$	${}^6A_1$	No
HS-5	$t_{2g}^3 e_g^2$	${}^6A_{1g}$	No	$e^2 t_2^3$	${}^6A_1$	No
LS-5	$t_{2g}^5$	${}^2T_{2g}$	Yes	$e^3 t_2^3$	${}^5E$	No
HS-6	$t_{2g}^4 e_g^2$	${}^5T_{2g}$	Yes	$e^3 t_2^3$	${}^5E$	No
LS-6	$t_{2g}^6$	${}^1A_{1g}$	No	$e^4 t_2^3$	${}^4A_2$	No
HS-7	$t_{2g}^5 e_g^2$	${}^4T_{1g}$	Yes	$e^4 t_2^3$	${}^4A_2$	No
LS-7	$t_{2g}^6 e_g^1$	${}^2E_g$	No	$e^4 t_2^3$	${}^4A_2$	No
8	$t_{2g}^6 e_g^2$	${}^3A_{2g}$	No	$e^4 t_2^4$	${}^3T_1$	Yes
9	$t_{2g}^6 e_g^3$	${}^2E_g$	no	$e^4 t_2^5$	${}^3T_2$	yes

Henceforth, for  $O_h$  Ni(II), the magnetic moments are larger if the GS-ES gap is small:

But, for tetrahedral Ni(II) situation far differs:



$M_{\text{exp}} O_h \text{ Ni(II)} < M_{\text{exp}} T_d \text{ Ni(II)}$ . Exp example:  $\text{NiCl}_4^{2-}$ ,  $\text{Ni(HMPA)}_4^{2+}$  { HMPA: hexamethyl phosphoramidate } have magnetic moment larger than 4 BM. [larger the distortion smaller the magnetic moment] This distinction is extremely useful towards discrimination of  $O_h$  vs  $T_d$  structures.

### Terms arising in ligand fields:

So far we have considered the terms arising from free ions, but we should also consider the effect of ligand fields on the Russell-Saunders coupling scheme

Table 3. Terms arising from  $d^n$  configurations in octahedral and tetrahedral geometries:

Free ion term	Terms arising
S	$A_1$
P	$T_1$
D	$E + T_2$
F	$A_2 + T_1 + T_2$
G	$A_1 + E + T_1 + T_2$

Table 4. Magnetic moment comparison for  $d^1$ - $d^9$  electronic configurations:

d electrons	$\mu_{\text{LS}}$	$\mu_{\text{SO}}$	$\mu_{\text{eff}}$ (observed at 300 K)
0	0.00	0.00	0
1	3.00	1.73	1.7-1.8
2	4.47	2.83	2.8-2.9
3	5.20	3.87	3.7-3.9

	4	5.48	4.90	4.8-5.0
	5	5.92	5.92	5.8-6.0
	6	5.48	4.90	5.1-5.7
	7	5.20	3.87	4.3-5.2
	8	4.47	2.83	2.9-3.9
:	9	3.00	1.73	1.7-2.2
	10	0.00	0.00	0

### Orbital angular momentum in crystal field:

The splitting of the free ion terms in an octahedral crystal field can give components with states A, E, T:

We need to remember that: A states are singly degenerate, E states are doubly degenerate and T states are triply degenerate. We have seen that a crystal field reduces the orbital angular momentum: this is called quenching. In both A and E states, the orbital momentum is quenched. In T states, there is some residual orbital momentum.

Table 5. High spin octahedral transition metal ions with the term symbols:

		Free-ion Ground Terms	Ligand-field Ground Terms	Ligand-field Excited Terms
d <sup>1</sup>	Ti <sup>3+</sup>	2D	2T <sub>2g</sub>	2E <sub>g</sub>
d <sup>2</sup>	V <sup>3+</sup>	3F	3T <sub>1g</sub>	3T <sub>2g</sub> 3A <sub>2g</sub>
d <sup>3</sup>	Cr <sup>3+</sup> , V <sup>2+</sup>	4F	4A <sub>2g</sub>	4T <sub>2g</sub> 4T <sub>1g</sub>
d <sup>4</sup>	Mn <sup>3+</sup> , Cr <sup>2+</sup>	5D	5E <sub>g</sub>	5T <sub>2g</sub>
d <sup>5</sup>	Fe <sup>3+</sup> , Mn <sup>2+</sup>	6S	6A <sub>1g</sub>	<i>none from ground term</i>
d <sup>6</sup>	Fe <sup>2+</sup>	5D	5T <sub>2g</sub>	5E <sub>g</sub>
d <sup>7</sup>	Co <sup>2+</sup>	4F	4T <sub>1g</sub>	4T <sub>2g</sub> 4A <sub>2g</sub>
d <sup>8</sup>	Ni <sup>2+</sup>	3F	3A <sub>2g</sub>	3T <sub>2g</sub> 3T <sub>1g</sub>
d <sup>9</sup>	Cu <sup>2+</sup>	2D	2E <sub>g</sub>	2T <sub>2g</sub>

### Magnetic properties of complexes with A and E ground terms:

These complexes possess no orbital contribution in the ground state, so the magnetic moment is expected to follow the spin-only formula.

$$\mu_{LS} = \sqrt{[4S(S+1) + L(L+1)]} \text{ reduces to:}$$

$$\mu_{SO} = \sqrt{[4S(S+1)]} = \sqrt{[n(n+2)]}$$

The magnetic moment ( $\mu_{\text{eff}}$ ) is expected to be independent of temperature:

Eg. K<sub>2</sub>Mn(SO<sub>4</sub>)<sub>2</sub>·6H<sub>2</sub>O ; Mn<sup>2+</sup>, octahedral d<sup>5</sup> Measured:  $\mu_{\text{eff}}$ =5.9 $\mu_B$  at 300K, 5.9  $\mu_B$  at 80K

(calculated:  $\mu_{SO} = \sqrt{35} = 5.92 \mu_B$ )

Temperature independence is often the case, however the fit with the calculated spin only moment is not always good. Second-order spin-orbit coupling can mix in some orbital contribution from higher T terms of the same multiplicity as the ground term. In this context, we can cite an example of  $\text{Mn}^{2+}$  ion which could not produce good fit due to its associated  ${}^6\text{A}_{1g}$  ground state term which lacks higher sextet T terms, which subsequently prevents mixing of excited and ground terms.

$$\mu_{\text{eff}} = \mu_{\text{SO}} \left( \frac{1 - \alpha\lambda}{\Delta} \right) \quad \mu_{\text{SO}} = \sqrt{[4S(S+1)]} = \sqrt{[n(n+2)]}$$

$\alpha = 2$  for an E term and  $\alpha = 4$  for an  $\text{A}_2$  term ;  $\Delta$  is the crystal field splitting parameter.

The spin-orbit coupling constant,  $\lambda$  is positive for d-shells less than half filled (and visa versa). Thus, magnetic moments are slightly less than or more than the spin only moment depending on the sign of  $\lambda$ .

Table 6. Magnitude of spin-orbit coupling constant for first row transition metal ions:

metal ion	Ti(III)	V(III)	Cr(III)	Mn(III)	Fe(II)	Co(II)	Ni(II)	Cu(II)
$\lambda / \text{cm}^{-1}$	155	105	90	88	-102	-172	-315	-830

$\text{A}_2$  (from F) and E (from D) ground terms : The effect is normally a few tenths of a Bohr magneton

Eg.  $\text{KCr}(\text{SO}_4)_2 \cdot 12\text{H}_2\text{O}$  :  $\text{Cr}^{3+}$ , octahedral,  $d^3$

$\lambda$  is positive, hence  $\mu_{\text{eff}} < \mu_{\text{so}}$

$\mu_{\text{eff}} = 3.8 \mu\text{B}$  at 300K,  $3.8 \mu\text{B}$  at 80K (cal:  $\mu_{\text{so}} = \sqrt{15} = 3.87 \mu\text{B}$ )

eg.  $(\text{NH}_4)_2\text{Cu}(\text{SO}_4)_2 \cdot 6\text{H}_2\text{O}$  :  $\text{Cu}^{2+}$ , octahedral,  $d^9$

$\lambda$  is negative, hence  $\mu_{\text{eff}} > \mu_{\text{so}}$

$\mu_{\text{eff}} = 1.9 \mu\text{B}$  at 300K,  $3.8 \mu\text{B}$  at 80K (cal:  $\mu_{\text{so}} = \sqrt{3} = 1.73 \mu\text{B}$ )

Because the difference in energy between the ground term and excited T term is large ( $10,000 \text{ cm}^{-1}$  vs.  $kT$  of around  $200 \text{ cm}^{-1}$ ), the spin-orbit contribution to the magnetic moment is independent of temperature.

Table 7. effective magnetic moments for few complexes specified in the following table:

Number of d electrons	Compound	Geometry	$\mu_{\text{eff}}$ (B.M.)		
			80 K	300 K	Spin only
1	$\text{VCl}_4$	Tetrahedral	1.6	1.6	1.73
3	$\text{KCr}(\text{SO}_4)_2 \cdot 12 \text{H}_2\text{O}$	Octahedral	3.8	3.8	3.87
4	$\text{CrSO}_4 \cdot 6 \text{H}_2\text{O}$	Octahedral	4.8	4.8	4.90
5	$\text{K}_2\text{Mn}(\text{SO}_4)_2 \cdot 6 \text{H}_2\text{O}$	Octahedral	5.9	5.9	5.92
7	$\text{Cs}_2\text{CoCl}_4$	Tetrahedral	4.5	4.6	3.87
8	$(\text{NH}_4)_2\text{Ni}(\text{SO}_4)_2 \cdot 6\text{H}_2\text{O}$	Octahedral	3.3	3.3	2.83
9	$(\text{NH}_4)_2\text{Cu}(\text{SO}_4)_2 \cdot 6\text{H}_2\text{O}$	Octahedral	1.9	1.9	1.73

### Magnetic properties of complexes with T ground terms:

This is a more complex situation as the effects of spin-orbit coupling are first-order. The T terms are splitted by spin-orbit coupling to produce energy levels whose differences are often of the order of  $kT$  ( $\approx 200 \text{ cm}^{-1}$  at room temperature). Temperature thus has an effect on the population of the levels arising in a magnetic field *i.e.* the magnetic moment will now vary with temperature.

*e.g.*  $K_3[Mn(CN)_6]$  ; low-spin ;  $d^4$  system

For the ground state  $^3T_{1g}$ ,  $\lambda$  is found to be negative, and hence  $\mu_{\text{eff}} > \mu_{\text{SO}}$ .

$\mu_{\text{eff}} = 3.5 \mu_B$  at 300 K,  $3.31 \mu_B$  at 80 K

Magnetic moment T dependent... Reaches Zero at low T

(calc.  $\mu_{\text{SO}} = \sqrt{8} = 2.83 \mu_B$ )

Orb. momentum exist ...higher levels populate.. increases the observed magnetic moment

Table 8. effective magnetic moments for few more complexes specified in the following table:

Number of d electrons	Compound	Geometry	$\mu_{\text{eff}}$ (B.M.)		
			80 K	300 K	Spin only
1	$\text{Cs}_2\text{VCl}_6$	Octahedral	1.4	1.8	1.73
2	$(\text{NH}_4)\text{V}(\text{SO}_4)_2 \cdot 12 \text{H}_2\text{O}$	Octahedral	2.7	2.7	2.83
4	$\text{K}_3[\text{Mn}(\text{CN})_6]$	Octahedral	3.1	3.2	2.83
5	$\text{K}_3[\text{Fe}(\text{CN})_6]$	Octahedral	2.2	2.4	1.73
6	$(\text{NH}_4)_2\text{Fe}(\text{SO}_4)_2 \cdot 6\text{H}_2\text{O}$	Octahedral	5.4	5.5	4.90
7	$(\text{NH}_4)_2\text{Co}(\text{SO}_4)_2 \cdot 6\text{H}_2\text{O}$	Octahedral	4.6	5.1	3.87
8	$(\text{Et}_4\text{N})_2\text{NiCl}_4$	Tetrahedral	3.2	3.8	2.83

### Heavier elements (f-elem.) vs. Orbital contribution:

These ions have complete 5s and 5p shell and mag. moment arise from incomplete 4f shell. ( $4f^n 5s^2 5p^6$ ). Due to size and screening effect, 4f electrons do not interact strongly with diamagnetic ligands. The degeneracy of 4f shell thus maintains leading to LARGE orbital moment. For lanthanides – must include orbital contribution due to the downwards position in the periodic table and spin-orbit coupling: Ground State Term reveals the most stable term. We need to determine the number of 4f electrons in the ion.



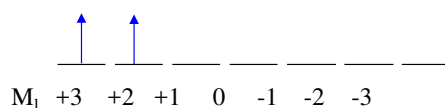
$$J = L+S, L+S-1, \dots, L-S$$

**Rule 1:** for a given electronic configuration, the state with highest S is lowest in energy

**Rule 2:** for a given electronic configuration and subject to Rule 1, the state with highest L is lowest in energy

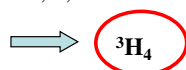
**Rule 3:** for a given electronic configuration and subject to Rules 1 and 2, the state with highest J is lowest in energy for ions with a greater-than-half-filled 4f sub-shell; converse true for ions with a less than half-filled shell.

e.g.  $\text{Pr}^{3+}, 4f^2$



$$2S+1 = 3; L = 5 \quad \longrightarrow \quad {}^3\text{H} \quad (2S+1)L_J$$

$$J = L+S, \dots, L-S = 6, 5, 4$$



$$g_J = 1 + \frac{S(S+1) + J(J+1) - L(L+1)}{2J(J+1)}$$

$$g = 1 + \left[ \frac{2+20-30}{40} \right] = 1 - 1/5 = 4/5$$

$$\mu = g_J \sqrt{J(J+1)}$$

$$\mu = 4/5 \sqrt{20} = 3.6$$

$$\mu_{\text{obs}} = 3.5$$

Table 9. Showing excellent agreement between our calculated with the experimental observation as elucidated in the below table:

$\text{Ln}^{3+}$	4f configuration	Ground state term symbol	$g$	$gJ\sqrt{J(J+1)}$	Exp $\mu_{\text{eff}}$ for $[\text{Ln}(\text{NO}_3)_3(\text{phen})_2]$
La	$4f^0$	${}^1\text{S}_0$	0	0	0
Ce	$4f^1$	${}^2\text{F}_{5/2}$	6/7	2.54	2.46
Pr	$4f^2$	${}^3\text{H}_4$	4/5	3.58	3.48
Nd	$4f^3$	${}^4\text{I}_{9/2}$	8/11	3.62	3.44
Pm	$4f^4$	${}^5\text{I}_4$	3/5	2.68	
Sm	$4f^5$	${}^6\text{H}_{5/2}$	2/7	0.84	1.64
Eu	$4f^6$	${}^7\text{F}_0$	1	0	3.36
Gd	$4f^7$	${}^8\text{S}_{7/2}$	2	7.94	7.97
Tb	$4f^8$	${}^7\text{F}_6$	3/2	9.72	9.81
Dy	$4f^9$	${}^6\text{H}_{15/2}$	4/3	10.63	10.6
Ho	$4f^{10}$	${}^5\text{I}_8$	5/4	10.6	10.7
Er	$4f^{11}$	${}^5\text{I}_{15/2}$	6/5	9.59	9.46
Tm	$4f^{12}$	${}^3\text{H}_6$	7/6	7.57	7.51
Yb	$4f^{13}$	${}^2\text{F}_{7/2}$	8/7	4.54	4.47

## §10. Assessment of theory based on experiment:

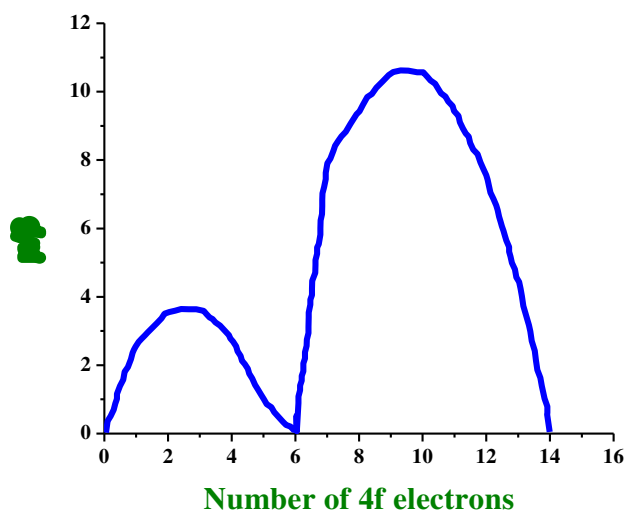


Figure 39. Correlation between 4f electrons and effective magnetic moment

Above approach works well for almost all lanthanide ions but substantial deviations occur for the  $4f^5$  ( $\text{Sm}^{3+}$ ) and  $4f^6$  ( $\text{Eu}^{3+}$ ) ions. Adjacent Figure 18 reveals the dependence of magnetic moment on core 4f electrons. Here excited (J) states may be thermally accessible at room temperature, leading to deviations from moments predicted just on the basis of the ground manifold of  $m_j$  state, need to use VV formula with more than one J manifold populated thermally. Most significant where J of GS smallest (the Lande

interval rule predicts that the operation between the states with J and J+1 is  $\lambda(J+1)$  ( $\lambda$  = spin orbit coupling constant). J is smallest near the middle of the series as here S is relatively large, L being small comparatively and they couple such that the contribution from S is opposed to that for L (less than half-filled shell). Eg:  $\text{Eu(III)} : ^7F$  gives rise to  $J=0,1,2,3,4,5,6$

$$(\chi T)_{HT} = \frac{N\beta^2}{3k} [g_L^2 L(L+1) + g_S^2 S(S+1)]$$

With  $g_L=1$  and  $g_S=2$ , at HT is 4.5. This limit is not reached, as only the first three states are significantly populated. At lower T since  $^7F_0$  is the ground state,  $\chi$  reaches zero.

## §11. Anomalous magnetic moments:

When the magnetic moment for a metal ion falls outside the range of predicted value based on the spin angular and orbital angular momenta of electrons, it is called anomalous value. These kind of systems are known as magnetically dilute systems.

Reasons underlying anomalous magnetic behaviour:

- (i) Equilibrium between two spin states.
- (ii) Magnetically non-equivalent sites in the unit cell.
- (iii) Solute-solvent interaction.
- (iv) Solute-solute interaction.
- (v) Configurational equilibrium.

(i) Equilibrium between two spin states:

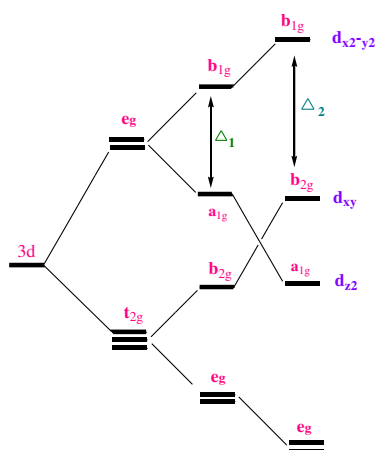


Figure 40. Tetragonal distortion of an octahedral complex

Equilibrium between high-spin and low-spin exists. Crystal field strength is in the region of the critical  $10Dq$ , a spin state equilibrium may arise for the  $d^4$ ,  $d^5$ ,  $d^6$  and  $d^7$  configurations but not for  $3d^8$  Ni(II) as the ground state is  $^3A_{2g}$ . But for  $Ni a_4 b_2$  type distortion the situation is different (a and b different donor ligands). If  $\Delta_1 \sim \Delta_2$  then  $\mu_{\text{eff}} = 3.0$  BM. But if b is weak LF than a, pairing is preferred leading  $S=0$ . Thus spin equilibrium occurs. For example: *Dichlorotetrakis (N,N'-diethylthiourea)nickel(II)*

Spin paired below 194 K and  $\mu = 0$  and becomes partially paramagnetic at higher T.

Singlet (low-spin)  $\rightleftharpoons$  Triplet (high-spin)

The equilibrium constant,

$$K = \frac{[\text{triplet}]}{[\text{singlet}]} = \frac{[\text{high-spin}]}{[\text{low-spin}]}$$

“k” can be calculated from the information of mole fractions,  $N_{\text{low-spin}}$  and  $N_{\text{high-spin}}$ .

The relation between  $\chi_M$  and mole fraction is given by the following expressions:

$$\chi_{M(\text{expected})} = N_{\text{low-spin}} \chi_{M(\text{low-spin})} + N_{\text{high-spin}} \chi_{M(\text{high-spin})} \quad \{ N_{\text{low-spin}} + N_{\text{high-spin}} = 1 \}$$

The above expression can be expressed in terms of magnetic moment as follows:

$$K = \frac{\mu_{\text{expected}}^2 - \mu_{\text{low-spin}}^2}{\mu_{\text{high-spin}}^2 - \mu_{\text{expected}}^2}$$

Difference between affixed mixture of two spin states and spin state equilibrium:

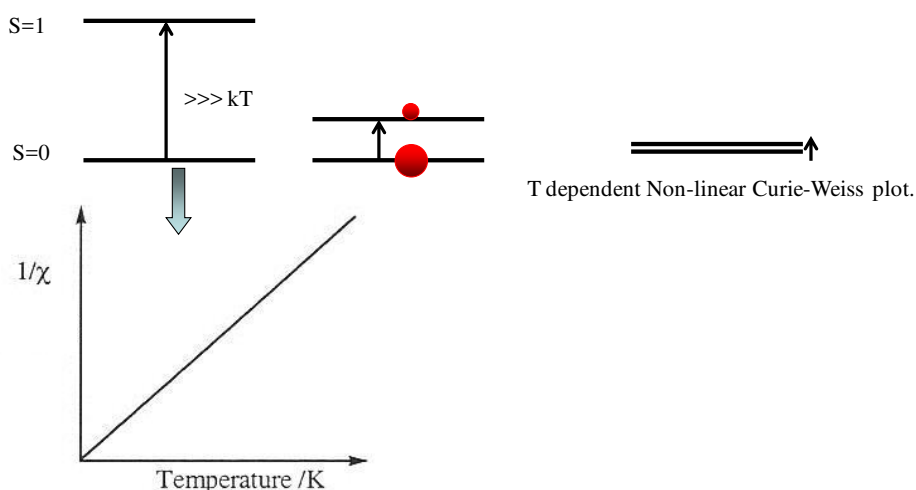


Figure 41. The above figure reveals transition between two different spin states and existence of spin-state equilibrium between two states.

In an octahedral crystal field, the spin-state equilibrium is possible for the following configurations:

For  $d^4$  :  $t_{2g}^3 e_g^1 - ^5E_g$  ;  $t_{2g}^4 - ^3T_{1g}$  eg :  $Cr^{2+}$  and  $Mn^{3+}$   
 For  $d^4$  :  $t_{2g}^3 e_g^2 - ^6A_{1g}$  ;  $t_{2g}^5 - ^2T_{2g}$  eg :  $Mn^{2+}$  and  $Fe^{3+}$   
 For  $d^6$  :  $t_{2g}^4 e_g^2 - ^5T_{2g}$  ;  $t_{2g}^6 - ^1A_{1g}$  eg :  $Fe^{2+}$  and  $Co^{3+}$   
 For  $d^7$  :  $t_{2g}^5 e_g^2 - ^4T_{1g}$  ;  $t_{2g}^6 e_g^1 - ^2E_g$  eg :  $Co^{2+}$

(ii) Magnetically non-equivalent sites in the unit cell:

In a unit cell, two situations may arise a) the metal ions may have the same coordination number b) the metal ions have the same set of ligands but different geometries c) the metal ions have different coordination numbers and subsequent different geometries. For example: \_\_\_Eg: dibromobis(benzylphosphine)nickel(II) is green colored and exhibits an anomalous magnetic moment of 2.7 B.M. The X-ray crystallographic revealed that the unit cell has three nickel(II) complexes constituted of **one square planar and two tetrahedral**.

Considering that square of the magnetic moment is additive and also the mole fractions of the different complexes, we get, square planar: tetrahedral equals to 1: 2; resulting total number of moles to be 3. Hence, mole fraction of square planar =  $1/3 = 0.33$  and that of tetrahedral =  $2/3 = 2 * 0.33$

$$\mu^2 = 0.33 * \mu^2 Ni^{2+} (\text{square planar}) + 2 * 0.33 * \mu^2 Ni^{2+} (\text{tetrahedral})$$

$$(2.7)^2 = 0.33 * 0 + 2 * 0.33 * \mu^2 Ni^{2+} (\text{tetrahedral}) \text{ resulted } \mu^2 Ni^{2+} (\text{tetrahedral}) = 3.3 \text{ BM}$$

(iii) Solute-solvent interaction.

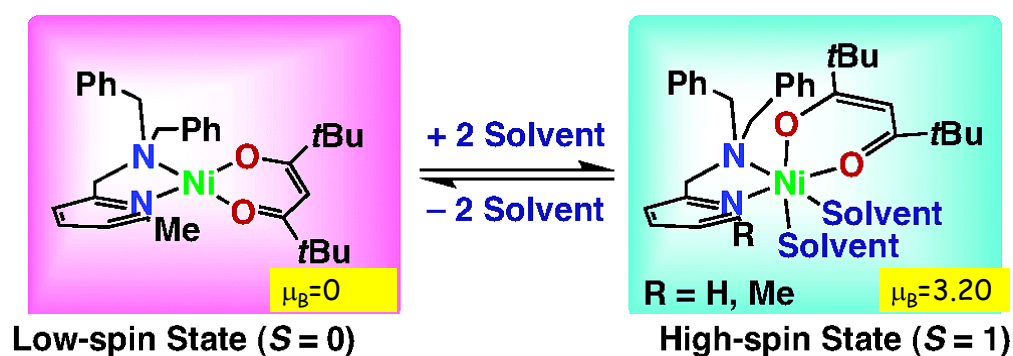
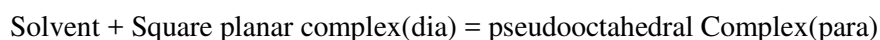


Figure 42. Schematic representation of solute-solvent interaction dictating low spin to high spin state conversion.

Anomalous magnetic moment may also arise when a particular complex interacts with a coordinating solvent. Thus many square planar diamagnetic nickel(II) complexes become partially paramagnetic due to an equilibrium of the following type:



(iv) Solute-solute interaction.

This is diamagnetic in the solid state. But, in solution, this shows anomalous magnetic moment in the

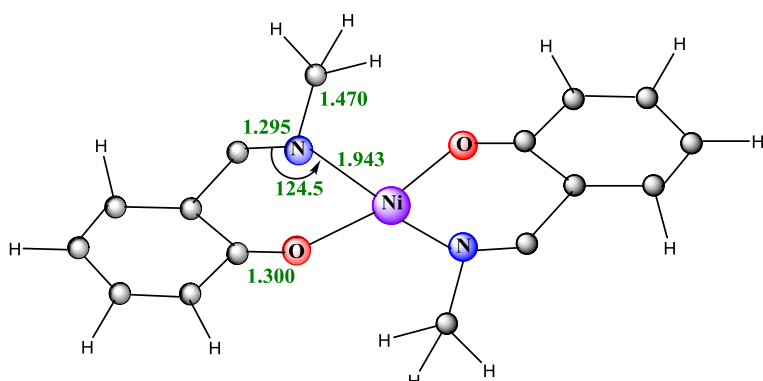


Figure 43. Structure of Bis(N-methylsalicylaldiminato)nickel(II)

range of 1.9 to 2.3 B.M. This arises not due to mutual transition between planar and tetrahedral geometry as the complex has zero dipole moment in benzene or dioxan. At higher concentration of the complex magnetic moment increase, indicating the presence of solute-solute interaction.

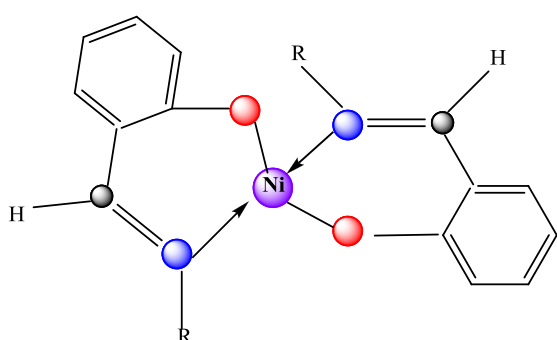


Figure 44. complex lacks paramagnetism

(v) Configurational equilibrium: Octahedral to square planar mutual equilibrium also leads to the observation of anomalous magnetic moment. Besides adjacent picture is the example of a complex possessing substituent in the ortho position which lacks paramagnetism (steric).

## §12. Calculation of magnetic susceptibilities:

### §12.1 The Van Vleck Equation.

In order to predict or calculate theoretical values of  $\chi$  we must determine the new energy levels in the applied magnetic field ( $H$ ) and the Boltzmann distribution among them.

Make two assumptions: (i) magnetically dilute system, (ii)  $\chi$  is independent of  $H$  (*i.e.*  $kT \gg \Delta E$ ).

The energy ( $E_n$ ) of the  $n^{\text{th}}$  energy level in field  $H$  can be described by a power series:

$$E_n = E_n^{(0)} + E_n^{(1)}H + E_n^{(2)}H^2 + \dots$$

where  $E_n^{(0)}$  = energy of level  $n$  in zero-field

$E_n^{(1)}$  = 1<sup>st</sup> order Zeeman coefficient (splits  $n$  into equally spaced components separated by  $g\beta H$ ).

$E_n^{(2)}$  = 2<sup>nd</sup> order Zeeman coefficient (mixes wavefunctions of ground state  $n$  with excited state  $m \rightarrow$  lowers energy of  $n$ , raises energy of  $m$ )

The macroscopic magnetisation,  $M$ , is given by the sum of the magnetic moments of each energy level (the microscopic magnetisation,  $-\delta E_n/\delta H$ ), weighted by Boltzmann distribution between them. We can derive:

$$M = \frac{NH \sum_n \left( \frac{E_n^{(1)2}}{kT} - 2E_n^{(2)} \right) \cdot \exp\left(-\frac{E_n^{(0)}}{kT}\right)}{\sum_n \exp\left(-\frac{E_n^{(0)}}{kT}\right)}$$

Then,  $\chi = M/H$  and

$$\chi = \frac{N \sum_n \left( \frac{E_n^{(1)2}}{kT} - 2E_n^{(2)} \right) \cdot \exp\left(-\frac{E_n^{(0)}}{kT}\right)}{\sum_n \exp\left(-\frac{E_n^{(0)}}{kT}\right)}$$

### Van Vleck Equation

Thus, if we know  $E_n^{(0)}$ ,  $E_n^{(1)}$  and  $E_n^{(2)}$  then we can calculate  $\chi$ .

### §12.2 Simplifications of the Van Vleck Equation.

- (i) Case with only one spin degenerate energy level in zero-field (hypothetical case).

Then,  $E_n^{(2)} = 0$ , because no excited state  $m$  to mix with.

$E_n^{(0)} = 0$ , set as reference level.

$$\chi = \frac{N \sum_n \left( \frac{E_n^{(1)2}}{kT} - 0 \right) \cdot \exp(0)}{\sum_n \exp(0)}$$

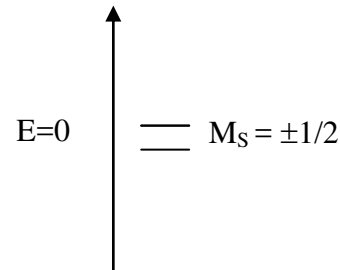


Figure 44. degenerate energy levels in absence of magnetic field.

but  $\exp(0) = 1$  and  $\sum_n E_n^{(1)2} = \text{constant}$  for any given system.  $\Rightarrow \chi = \frac{\text{constant}}{T}$  Curie Law

*i.e.* The empirical observation of Curie Law behaviour is consistent with a model in which there is a single degenerate electron spin energy level.

Ex. For  $S = 1/2$ , two energy levels  $M_S = \pm 1/2$  with  $E_n^{(1)} = \pm 1/2 g\beta$

$$\text{Thus, } \chi = \frac{N \left[ \left( \frac{g^2 \beta^2}{4kT} - 0 \right) \cdot \exp(0) + \left( \frac{g^2 \beta^2}{4kT} - 0 \right) \cdot \exp(0) \right]}{\left[ \exp(0) + \exp(0) \right]} = \frac{Ng^2 \beta^2}{4kT}$$

As expected from  $\chi = \frac{N\beta^2}{3kT} g^2 S(S+1)$

(ii) Singlet ground state (S=0) and a well separated ( $\gg kT$ ) degenerate excited state.

Then,  $E_n^{(1)} = 0$ , because ground state n is non-degenerate.

$E_n^{(0)} = 0$ , set as reference level.

$\Rightarrow \chi = N \sum_n E_n^{(2)}$ , but  $E_n^{(2)}$  only depends on ground state - excited state energy gap = constant for any given system.

$\Rightarrow \chi = N\alpha$  where  $\alpha$  is a constant. Temperature Independent Paramagnetism (TIP).

*i.e.* Can sometimes find weak paramagnetism in systems with a spin singlet ground state (no unpaired electrons)!

**Example:**  $[\text{Co}(\text{NH}_3)_6]^{3+}$ , Co(III) low-spin  $d^6$ ,  $S = 0$

$^1A_1$  ground state

$^1T_1$  excited state at *ca.* 20000  $\text{cm}^{-1}$

$\rightarrow \chi_{\text{TIP}} \approx 2 \times 10^{-4} \text{ cm}^3 \cdot \text{mol}^{-1}$

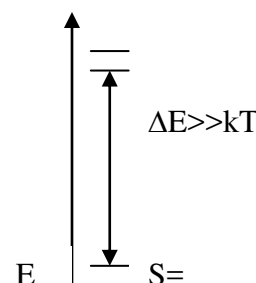


Figure 45. Singlet ground state and largely separated degenerate excited state

(iii) Degenerate ground state with all excited states well separated ( $\gg kT$ ).

$\chi$  has contributions from (i) + (ii).

$$\chi = \frac{C}{T} + N\alpha$$

**Example:** Any  $O_h$  or  $T_d$  ion with A or E ground term.

(iv) Degenerate ground state with thermally accessible degenerate excited states.

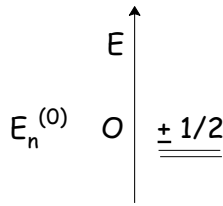
There is no simple reduction of Van Vleck formula because both  $E_n^{(1)}$  and  $E_n^{(2)}$  are non-zero [also  $E_m^{(1)}$  and  $E_m^{(2)}$ ]. However, in practice often find  $\chi$  obeys Curie-Weiss type behaviour.

**Example:**  $O_h$   $d^1$  complexes (T ground term) often obey Curie-Weiss behaviour with  $\theta \approx -200$  K.

Note: Curie-Weiss behaviour does not necessarily imply intermolecular interactions!

### §12.3 Applications of Van Vleck equations to certain situations

**a) In H = 0, there is only one spin state (S), and all its m<sub>s</sub> levels are degenerate**



For example, S = 1/2 (m<sub>s</sub> = ± 1/2) is the ground state, and no excited states are considered. Conventionally, energy of the ground state is considered to be zero. i.e. E<sub>n</sub><sup>(0)</sup>=0 and E<sub>n</sub><sup>(2)</sup>=0 (no excited state present).

$$\chi = \frac{N \sum_n \left( \frac{E_n^{(1)2}}{kT} - 0 \right) \cdot \exp(0)}{\sum_n \exp(0)}$$

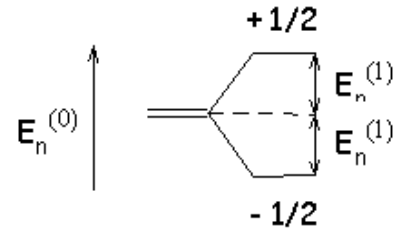


Figure 46. Splitting of degenerate energy levels

But,  $\exp(0) = 1$  and  $\sum_n E_n^{(1)2}$  constant for any given system,  
 $= \chi = \frac{\text{constant}}{T}$  which is known as Curie Law.

for S = 1/2, m<sub>s</sub> = ± 1/2,  $E_n = E_n^{(0)} + E_n^{(1)}H$

$$E_n = 0 + m_s g \beta H$$

i.e.  $E_n^{(1)} = m_s g \beta$

$$\chi = \frac{N \left[ \left( \frac{g^2 \beta^2}{4kT} - 0 \right) \cdot \exp(0) + \left( \frac{g^2 \beta^2}{4kT} - 0 \right) \cdot \exp(0) \right]}{[\exp(0) + \exp(0)]} = \frac{Ng^2 \beta^2}{4kT}$$

Similarly for other S values:

$$\chi = \frac{N\beta^2}{4kT} g^2 S(S + 1) \text{ which is what we had before in H}$$



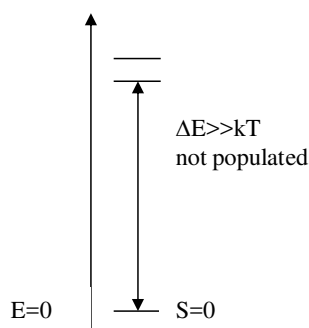
To be noted: Although the Curie Law is approximately obeyed by many systems, there are, of course, no systems that have just one energy level. Thus what we've just done is never exactly valid.

**b) In H = 0, there is only one spin state (S), and all its m<sub>s</sub> levels are degenerate**

If spin singlet remains the only thermally populated state without first-order angular momentum then the paramagnetic susceptibility is to be purportedly zero, and the measured susceptibility will be negative. For other situations, Van Vleck formula can be easily applied. Assuming energy of the ground state E<sub>0</sub><sup>(0)</sup> as origin, this state lacks angular momentum and termed as diamagnetic; E<sub>0</sub><sup>(1)</sup> can be taken as zero which converts Van Vleck formula to  $\chi = 2NE_0^{(2)}$



The diamagnetic ground state may couple with the excited states through Zeeman perturbation provided the presence of smaller energy gaps. This has resulted magnetic susceptibility to be temperature independent. This contribution is known as temperature-independent paramagnetism (TIP). TIP contribution is rather small, often of the same order of magnitude as the diamagnetism, but of opposite sign. As an example, it is estimated to be about  $60 \cdot 10^{-6} \text{ cm}^3 \text{ mol}^{-1}$  for Cu(II) mononuclear species,  $100 \cdot 10^{-6} \text{ cm}^3 \text{ mol}^{-1}$  for Ni(II) mononuclear species and  $200 \cdot 10^{-6} \text{ cm}^3 \text{ mol}^{-1}$  for the octahedral complex  $[\text{Co}(\text{NH}_3)_6]^{3+}$  possessing a  $^1\text{A}_{1g}$  ground state. TIP is not restricted to compounds with a diamagnetic ground state. The coupling between a magnetic ground state and nonthermally populated excited states may also give a weak temperature-independent contribution, which subsequently superimposes to the dominant temperature-dependent contribution arising from the ground state. Generally, we assume that the measured susceptibilities have been corrected not only for diamagnetism, but also for TIP.



$E_n^{(1)} = 0$ , because ground state  $n$  is non-degenerate.  $E_n^{(0)} = 0$ , set as reference level.

but  $E_n^{(2)}$  only depends on ground state - excited state energy gap = constant for any given system. Hence,  $\chi$  equals to  $N\alpha$  where  $\alpha$  is a constant. Temperature Independent Paramagnetism (TIP). Can

**sometimes find weak paramagnetism in systems with a spin singlet ground state (no unpaired electrons)!**

Figure 47. Population of energy level depends on the ground and first excited level gap

**Example:**  $[\text{Co}(\text{NH}_3)_6]^{3+}$ , Co(III) low-spin  $d^6$ ,  $S = 0$

$^1\text{A}_1$  ground state

$^1\text{T}_1$  excited state at *ca.*  $20000 \text{ cm}^{-1}$

→  $\chi_{\text{TIP}} \approx 2 \cdot 10^{-4} \text{ cm}^3 \text{ mol}^{-1}$

Other examples include:  $\text{MnO}_4^-$ ,  $\text{CrO}_4^{2-}$  ....

Often same order of magnitude as diamagnetic but **opposite sign** (+ive) . TIP not limited to diamagnetic sample .... for paramagnetic sample possessing  $^1\text{A}_{1g}$  ES has TIP contribution, TIP not limited to diamagnetic ground state .... A magnetic ground state too! Coupling between magnetic ground state and nonthermally populated ES can give a WEAK TIP. The ground state mixes with ES which could make an orbital contribution in H.

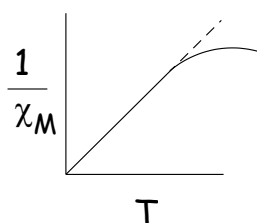
$TIP = \frac{4.089}{D}$  where  $D =$  energy of the  $^1\text{A}_{1g} \rightarrow ^1\text{T}_{1g}$  transition and is obtained experimentally.

The ratio of the experimental T.I.P. and the theoretical T.I.P. gives  $k^2$ , where  $k$  is the orbital reduction factor. A  $k$  value in the range 0.5- 0.9 indicates the covalent nature, and a  $k$  value of 1, the ionic nature of a complex. HS  $d^5$  system ( $Fe^{3+}$  and  $Mn^{2+}$ ) has the  ${}^6A_{1g}$  ground state term in an octahedral field --- No orbital angular momentum. No excited term with the spin multiplicity six. Therefore, NO TIP.

**c) Ground state is  $S \neq 0$  and degenerate; excited states all  $\gg kT$  above this**

This is simply the sum of cases (A) and (B) i.e. we now have an  $S > 0$  ground state, with unpopulated excited states that can only influence the magnetic properties through the 2nd order Zeeman term.....Therefore, we find the Curie Law, plus a TIP term:

$$\chi_M = \frac{N\beta^2 g^2}{4kT} S(S+1) + N\alpha \quad \chi_M = \frac{C}{T} + N\alpha$$



$N\alpha$  small, the Curie (or Curie-Weiss) Law term will dominate unless  $T$  gets very high. At most temperatures,  $T \approx \frac{C}{\chi_M}$  i.e. a straight line. When  $T$  tends

big,  $\chi_m$  tends to be small and  $N\alpha$  is noticeable as a curvature in the plot.

Figure 48. Reverse of susceptibility vs  $T$  plot

**d) Ground state is  $S \neq 0$  and degenerate; excited states are thermally-accessible (i.e. populated) and degenerate**

Energy  $\uparrow$

$E_n^{(0)} = 0$

k  $\equiv E_{ni}^{(0)} = 0 \therefore \exp\left(\frac{-E_{ni}^{(0)}}{kT}\right) = 1$

j  $\equiv$  but no other simplification is possible.

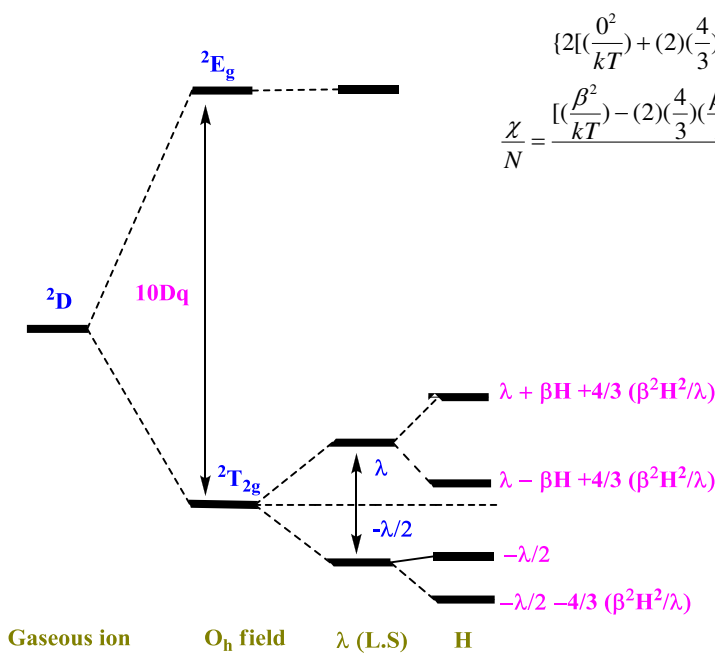
i  $\equiv \therefore$  We may expect a complicated temperature dependence of the susceptibility, so consider case-by-case (see later).

Above possibility is commonly found for (i) mononuclear transition metal complexes with a  $T$  ground state, and lanthanide complexes, because they have orbital contributions giving several levels ( $i, j, k$ , etc) due to spin-orbit coupling; and (ii) molecules with two or more metal ions interacting with each other and giving different spin ( $S$ ) possibilities.

**e) Some real examples**

(i)  $Ti^{3+}$  with  $d^1$  electronic configuration:

◆  $Ti^{3+}$  in  $O_h$  splits in to  ${}^2T_{2g}$  and  ${}^2E_g$  with  ${}^2T_{2g}$ - ${}^2E_g$  gap very large.



$$\chi = \frac{2 \left[ \left( \frac{0^2}{kT} \right) + (2) \left( \frac{4}{3} \right) \left( \frac{\beta^2}{\lambda} \right) e^{\frac{\lambda}{kT}} \right] + 2 \left[ \left( \frac{0^2}{kT} \right) - (2)(0) e^{\frac{\lambda}{kT}} \right] + \left[ \left( \frac{\beta^2}{kT} \right) - (2) \left( \frac{4}{3} \right) \left( \frac{\beta^2}{\lambda} \right) e^{\frac{\lambda}{kT}} \right] + \left[ \left( \frac{\beta^2}{kT} \right) - (2) \left( \frac{4}{3} \right) \left( \frac{\beta^2}{\lambda} \right) e^{\frac{\lambda}{kT}} \right]}{2 \left[ e^{\frac{\lambda}{kT}} + e^{\frac{\lambda}{kT}} + e^{\frac{\lambda}{kT}} \right]}$$

As,  $\chi = \frac{N\beta^2}{3kT} \mu_{eff}^2$

Hence,  $\mu_{eff}^2 = \frac{8 + \left[ \frac{3\lambda}{kT} - 8 \right] + e^{\frac{-3\lambda}{2kT}}}{\frac{\lambda}{kT} \left[ 2 + e^{\frac{-3\lambda}{kT}} \right]} \beta^2$

Curie-law will not obey. As  $T \rightarrow \infty \mu_{eff}^2 \rightarrow$  zero. As  $\lambda \rightarrow$  zero  $\mu_{eff}^2 \rightarrow 3$ . As  $T \rightarrow$  Zero, susceptibility reaches ZERO. Systems with

Figure 49. d orbitals splitting for a system containing  $Ti^{3+}(d^1)$

one unpaired electron have zero magnetic susceptibility due to cancellation of spin and orbital contribution.

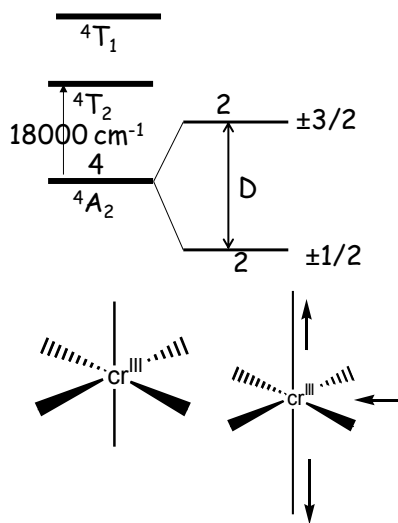


Figure 50. energy levels splitting in  $Cr^{3+}$  system.

(ii)  $Cr^{3+}$  with  $d^3$  electronic configuration:

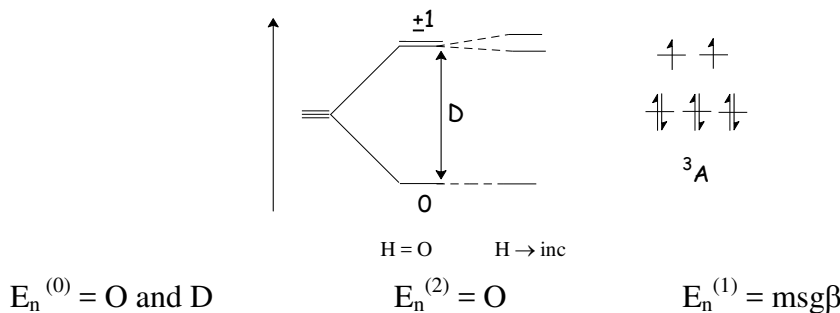
If D assumed axial then  $D\hat{S}_z^2$  has to be considered. Then,  $\chi$  in parallel direction will be procured with  $E_n^1$  of  $(1/2)g\beta$  and  $(3/2)g\beta$ . With  $E_n^{(0)}=0$  for lower and D for higher, then

$$\chi = \frac{g_z^2 \beta^2}{4kT} \frac{[1 + 9e^{\frac{-D}{kT}}]}{[1 + e^{\frac{-D}{kT}}]}$$

When  $D/KT \ll 1$  (small distortions or high T)  $\chi_z$  becomes  $(5/4)Ng^2\beta^2/kT$ . As  $T \rightarrow$  Zero or large D, spin only  $S=1/2$  results.

(iii) Calculation of effect ZFS on  $\chi$  using van vleck:

Ni(II)... $d^8$ :



$$\chi_M'' = N \frac{\sum_n (E_n^{(1)2} / kT - 2E_n^{(2)}) \exp\left(\frac{-E_n^{(0)}}{kT}\right)}{\sum_n \exp\left(\frac{-E_n^{(0)}}{kT}\right)}$$

$$\chi_M'' = N \left[ \frac{0 \exp(0) + \frac{g^2 \beta^2}{kT} \exp\left(\frac{-D}{kT}\right) + \frac{g^2 \beta^2}{kT} \exp\left(\frac{-D}{kT}\right)}{\exp(0) + 2 \exp\left(\frac{-D}{kT}\right)} \right]$$

$$\chi_M'' = \frac{2Ng^2\beta^2}{kT} \left[ \frac{\exp\left(\frac{-D}{kT}\right)}{1 + 2 \exp\left(\frac{-D}{kT}\right)} \right]$$

(NH<sub>4</sub>)<sub>2</sub>Ni(SO<sub>4</sub>)<sub>2</sub>·6H<sub>2</sub>O  
 $g_z = 2.25; D = 2.24 \text{ cm}^{-1}$   
 $\chi_{Ml}(\text{expt}) = 4230 \times 10^{-6} \text{ cm}^3 \text{ mol}^{-1}$   
 $\chi_{Ml}(\text{calc}) = 4260 \times 10^{-6} \text{ cm}^3 \text{ mol}^{-1}$   
 $\chi_{Mls.o}(D=0) = 3359 \times 10^{-6} \text{ cm}^3 \text{ mol}^{-1}$

Important points to be noted:

- a)  $g = g_x = g_z$  b) As  $D \rightarrow 0$ ,  $\chi \rightarrow$  Curie Law for  $S = 1$ . At low  $T$  and large  $D$ ,  $\chi \rightarrow 0$ , i.e. has 2 unpaired electrons but behaves as if none. c) more accurate way of determining the magnitude and sign of  $D$  (and  $g$ ) is EPR spectroscopy.

## §13. Magnetic Anisotropy:

### §13.1 The $\chi$ Tensor.

So far we have implicitly assumed that  $\chi$  is isotropic, i.e. independent of molecular orientation with respect to the applied magnetic field. In general, this is not true because molecules (and assemblies of molecules) are not generally isotropic with the exception of strictly  $O_h$  and  $T_d$  (cubic) symmetry.

$\chi$  is a tensor quantity, i.e. can be described by a 3x3 matrix.

$$\begin{pmatrix} \chi_{xx} & \chi_{xy} & \chi_{xz} \\ \chi_{yx} & \chi_{yy} & \chi_{yz} \\ \chi_{zx} & \chi_{zy} & \chi_{zz} \end{pmatrix}$$

However, we can always define 3 orthogonal principal axes such that  $\chi$  is diagonal (only  $\chi_{xx}$ ,  $\chi_{yy}$  and  $\chi_{zz}$  are non-zero).  $\chi_{xx}$ ,  $\chi_{yy}$  and  $\chi_{zz}$  can be measured independently on single-crystals if the x, y, z axes

can be located. In practice,  $\chi$  is normally measured from powdered or polycrystalline samples, in which case the average susceptibility,  $\bar{\chi}$ , is measured.

$$\bar{\chi} = \frac{\chi_{xx} + \chi_{yy} + \chi_{zz}}{3}$$

If  $\chi_{xx} = \chi_{yy} = \chi_{zz}$ , then  $\chi$  is said to be isotropic.

If  $\chi_{xx} = \chi_{yy} \neq \chi_{zz}$ , then  $\chi$  is said to be axial.

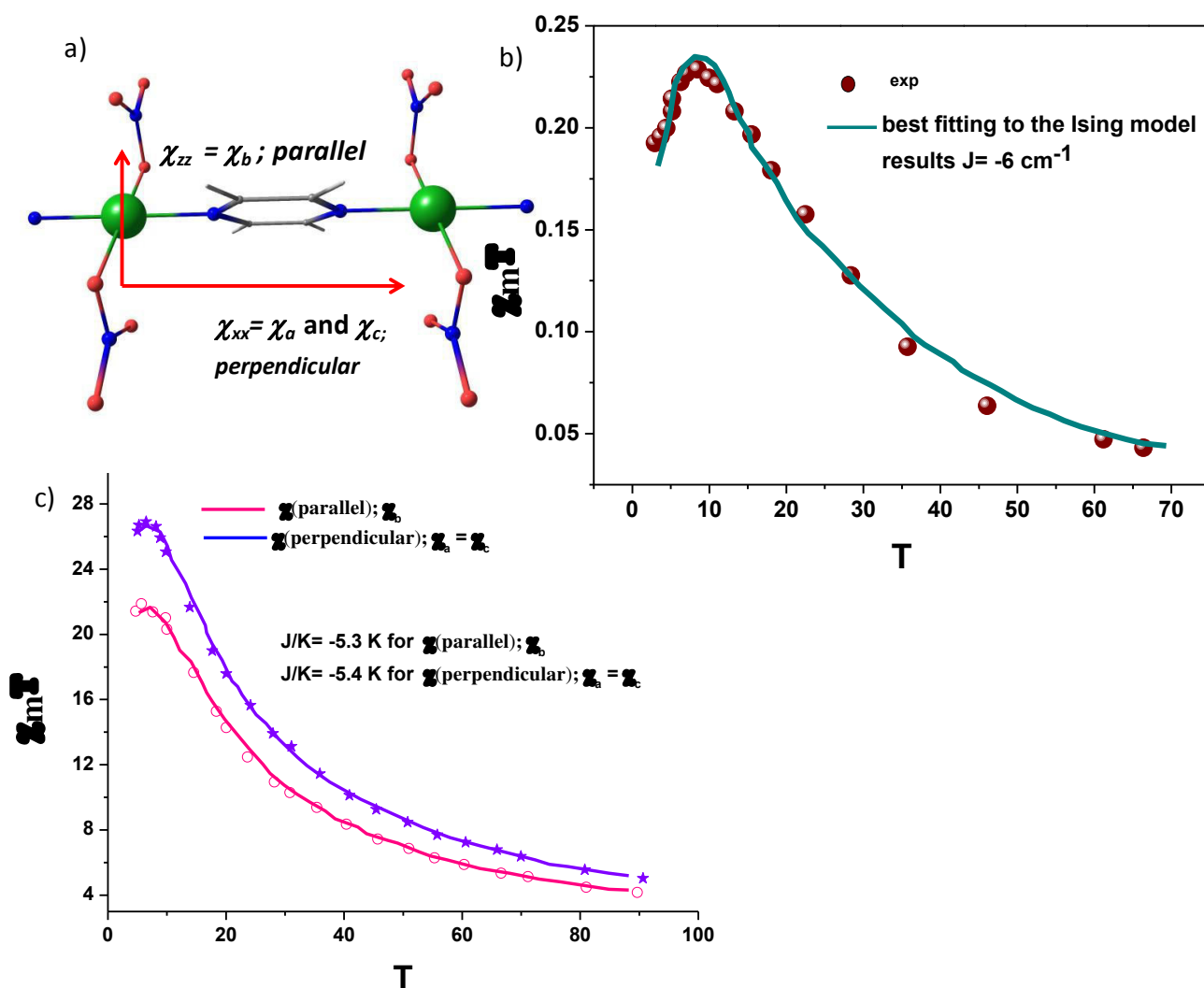


Figure 51. (a) crystal structure of  $\{Cu(pyrazine)(NO_3)_2\}_5$  (b) product of experimental magnetic susceptibility and  $T$  vs  $T$  plot with respect to that obtained by the best fitting of the Ising model leading to the observation of  $J$  value of  $-6 \text{ cm}^{-1}$ .<sup>6</sup> (c) If the same complex would have been isotropic  $J$  value would have been instead  $-5.5 \text{ K}$ . However, owing to its axiality  $J$  value of  $-5.3 \text{ K}$  is witnessed with susceptibility parallel to the applied magnetic field ( $\chi$  parallel) while  $-5.4 \text{ K}$  is indicated for susceptibility perpendicular to the applied magnetic field.<sup>7</sup>

### §13.2 Sources of Magnetic Anisotropy.

#### (i) g-anisotropy

The energy of a level in a magnetic field depends on the g-value. We have assumed up to now that  $g \approx 2$  and is isotropic. In fact, g often deviates from 2 due to mixing in of excited states via spin-orbit coupling, and in general is anisotropic.

**Example:** tetragonal Cu(II),  $d^9$   $S = 1/2$ : commonly has  $g_{zz} \approx 2.3$ ,  $g_{xx}, g_{yy} \approx 2.1$ .

g-values and g-anisotropy are poorly defined by magnetic susceptibility measurements and are best measured by EPR spectroscopy [EPR spectrum of square-planar Cu(II),  $d^9$ ,  $S = 1/2$ ].

Magnetic data of powdered materials should be interpreted with the average g-value

$$\bar{g} = \frac{g_{xx} + g_{yy} + g_{zz}}{3}$$

Spin-Orbit coupling results if the ground state orbital commutes with an excited state orbital along any axis x, y or z.

Consider  $D_{4h}$  sym. with  $d^1$  ion.

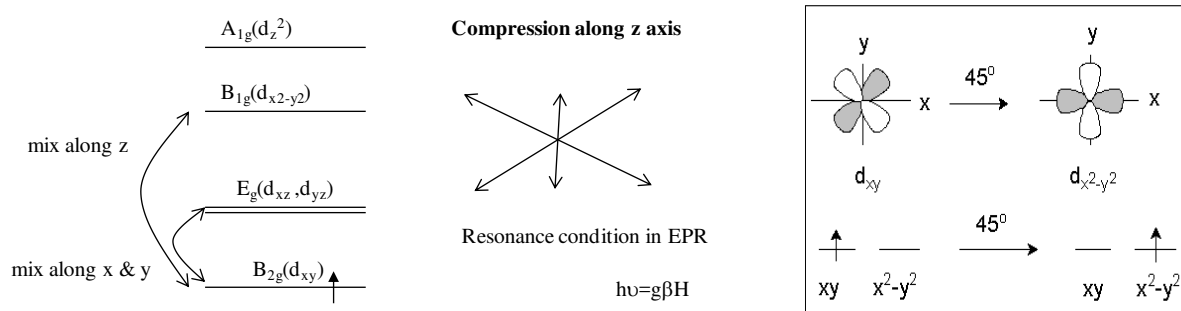


Figure 52. energy level splitting in  $D_{4h}$  symmetry with  $d^1$  electronic configuration.

Anisotropy in g-values are best described by **EPR spectroscopy** rather than by bulk magnetic susceptibility studies. H is applied along z direction (parallel) due to the mixing of  $d_{xy}$  and  $d_{x^2-y^2}$  orbital a small electric current will generate opposing the  $\Delta H$ . Therefore the new resonance in a EPR spectrum will appear at,

$$h\nu = g_{||}\beta (H + \Delta H)$$

Here  $g_{||}$  must be less than the free electron g-value of 2.0023 ( $\nu$  is a constant) For the applied field  $H_{\perp}$  or along x or y then  $d_{xy}$  will commute with  $d_{yz}$  and  $d_{xz}$ . The orbital contribution will then be  $g_{\perp} < 2.0023$ . If the ground state orbital commutes with a filled level, the induced magnetic field is now in the same direction as the original field.  $h\nu = g'_{\perp}\beta (H - \Delta H)$  and here  $g'_{\perp} > 2.0023$

### For, Lower symmetry cases

This arises often with mixed ligands. The shift in the g-values can be predicted with the following equation

$$g = g_0 \pm \frac{n\lambda}{\Delta}$$

$g_0$  is 2.0023,  $\lambda$ - SO coupling constant,  $\Delta$  is the energy separation between orbitals containing unpaired electrons and the orbitals that they commute . n is the co-efficient,  $\pm$  with filled or empty orbitals.

The n value may be deduced from the magic pentagon...

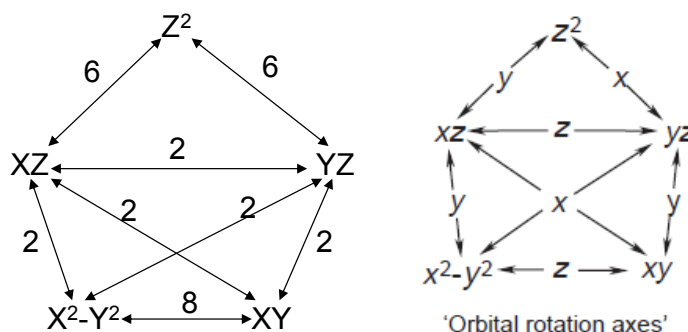


Figure 53. Illustrating inter-correlation between the stipulated d orbitals.

For ex.,  $d^9$  ( $\text{Cu}^{\text{II}}$ ) case with tetragonal distortion

(i) Case A. Elongation along z: Unpaired electron in  $d_{xy}$  orbital

$$g_{\parallel} = g_0 \pm \frac{8\lambda}{\Delta E(d_{xy} - d_{x^2-y^2})} \quad g_{\perp} = g_0 \pm \frac{2\lambda}{\Delta E(d_{xy} - d_{xz}, d_{yz})}$$

(ii) Case B. Compression along z: Unpaired electron in  $d_z^2$  orbital

$$g_{\parallel} = g_0 \quad g_{\perp} = g_0 \pm \frac{6\lambda}{\Delta E(d_z^2 - d_{xz}, d_{yz})}$$

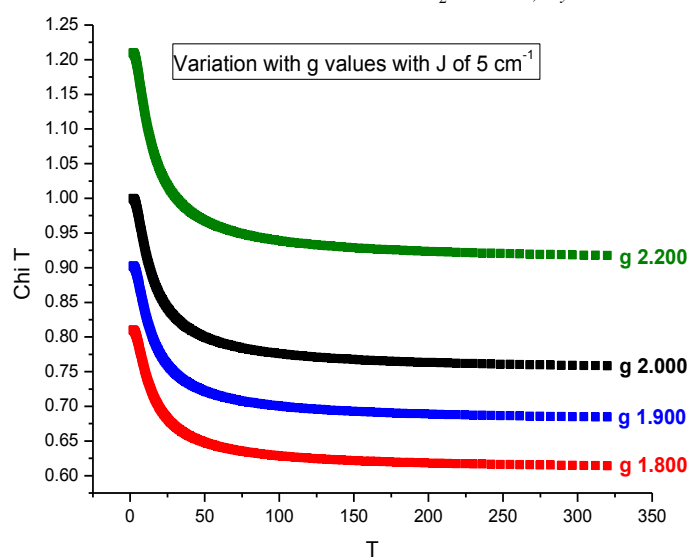


Figure 54. Graph showing variations of g tensor parameter on changes in the magnetic susceptibility.

Example:

tetragonal Cu(II),  $d^9 S = 1/2$ : commonly has  $g_{zz} \approx 2.3$ ,  $g_{xx}, g_{yy} \approx 2.1$ . g-anisotropy are poorly defined by magnetic susceptibility measurements while it is best measured by EPR spectroscopy. Magnetic data of powdered materials should be interpreted with the average g-value

$$\bar{g} = \frac{g_{xx} + g_{yy} + g_{zz}}{3}$$

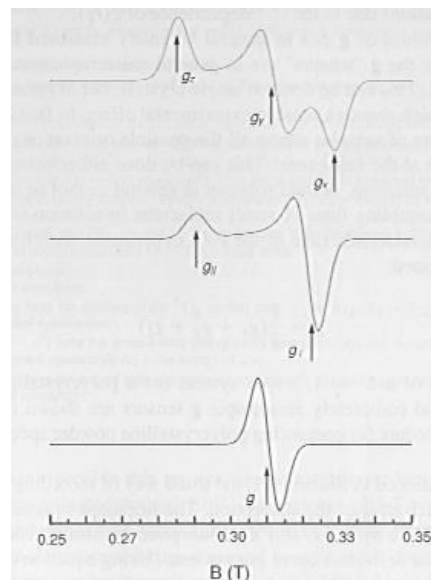
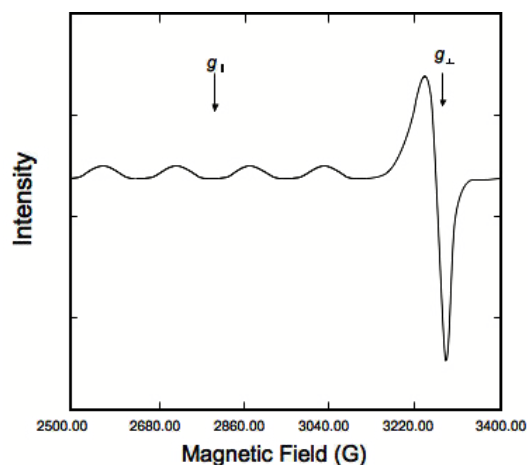
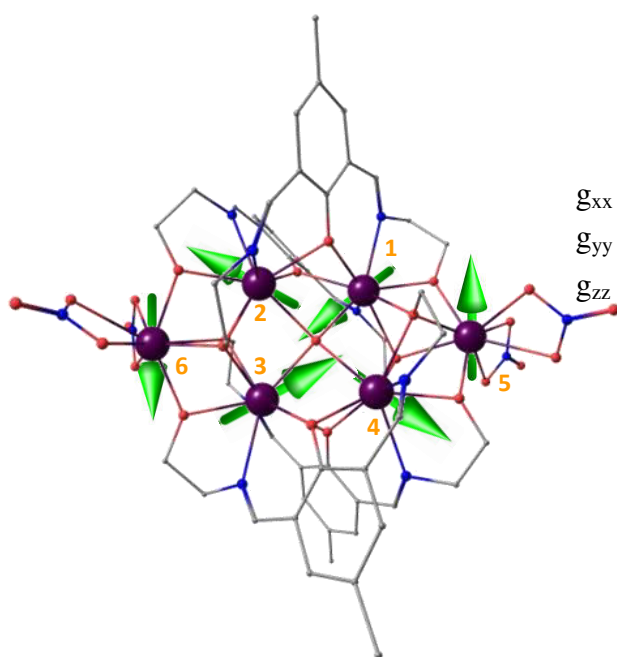


Figure 55. EPR spectrum showing distinct g parallel and g perpendicular signals while right hand side figure reveals rhombic, axial and isotropic nature of EPR spectrum respectively.

#### Examples:

Dy(III) ( $4f^9$ ) triangle AF coupled – Very large anisotropy in g tensor



	Dy1	Dy2	Dy3	Dy4	Dy5	Dy6
$g_{xx}$	0.01	0.01	0.01	0.01	0.00	0.01
$g_{yy}$	0.02	0.01	0.01	0.02	0.01	0.00
$g_{zz}$	19.73	19.66	19.74	19.69	19.78	19.82

highly anisotropic due to large magnetic moment;  $S=5/2$

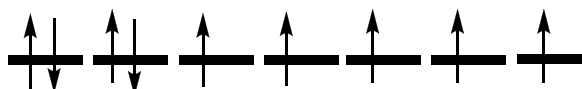


Figure 56.  $Dy_6$ -complex<sup>8</sup> composed of two  $Dy_3$  triangles show strong anisotropy arising from the intrinsic high magnetic moment (large  $J=15/2$ ) associated with Dy(III) ion.



## (ii) Zero-Field Splitting

When  $S > \frac{1}{2}$  (i.e. more than one unpaired electron), the coupling of the ground state with excited states *via* spin-orbit coupling can also result in partially removing the degeneracy of the  $M_S$  states in zero-field. The separation of the  $M_S$  states in zero-field is the zero-field splitting ( $D$ ). In magnetic studies this is often referred to as the single-ion anisotropy. The energies of the  $M_S$  states in zero-field is given by  $M_S^2 D$ .

In strictly cubic symmetry  $D = 0$ .

Example: Tetragonally distorted octahedral Ni(II),  $d^8$ ,  $S = 1$ .

Zero-field splitting removes the 3-fold degeneracy ( $M_S = 0, \pm 1$ ) of the spin triplet state with  $M_S = \pm 1$  separated by  $D$  (in energy units) from  $M_S = 0$ .

Note: 1. If  $D > 0$ , then  $M_S = 0$  lies lowest in energy. If  $D < 0$  then  $M_S = \pm 1$  lie lowest. Important because population of levels, and hence magnetic behaviour, is determined by Boltzmann distribution among the levels.

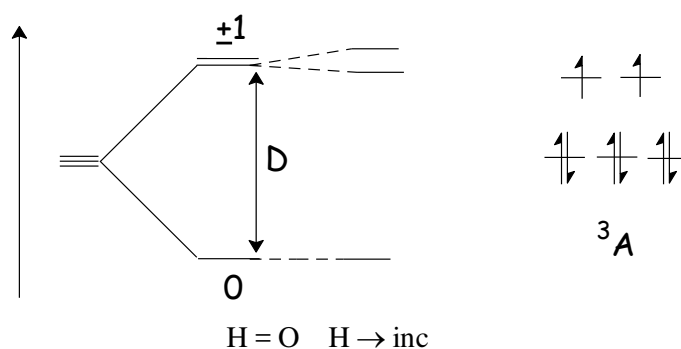


Figure 57. Example of energy level splitting of  $S=1$  state in absence of magnetic field, incurred onto the zero-field splitting( $D$ ), i.e.  $D < 0$ .

Example: Tetragonally distorted octahedral Ni(II),  $d^8$ ,  $S = 1$ . Zero-field splitting removes the 3-fold degeneracy ( $m_s = 0, \pm 1$ ) of the spin triplet state with  $m_s = \pm 1$  separated by  $D$  (in energy units) from  $m_s = 0$ .

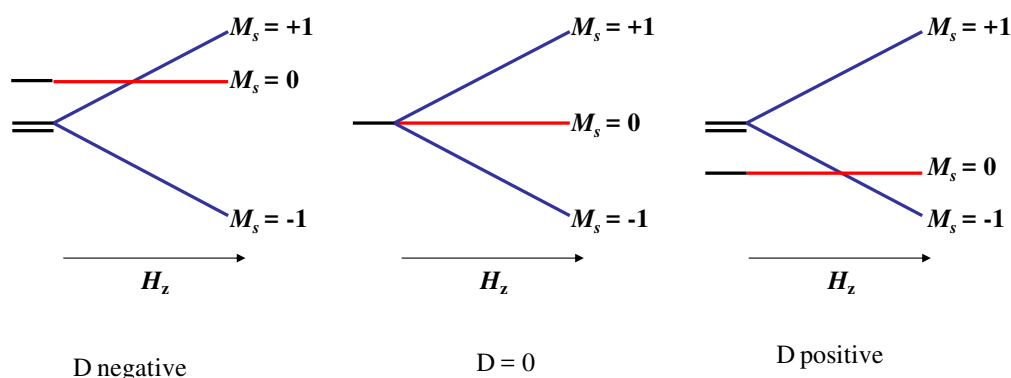


Figure 58. Variational cases of zero-field splitting which gives rise to different ground state.

### Quantitative approach to zero-field splitting:

The ZFS within a multiplet state without first-order angular momentum is given by phenomenological Hamiltonian (Spin Hamiltonian)

Here  $D$  is symmetric traceless tensor. In general, 
$$H_{ZFS} = S \bullet D \bullet S$$

$$H = \mu_B B \cdot g_1 \cdot S_2 + S_1 \cdot D_1 \cdot S_1 + \sum_j S_1 \cdot A_{1j} \cdot I_j + \dots$$

$\uparrow$                        $\uparrow$                        $\uparrow$   
 Electronic Zeeman    Zfs (electron-        Hyperfine (electron-  
 interaction)            nuclear interaction)

Zero-field splitting for different symmetry:

Cubic ( $O_h, T_d$ ):                       $D = 0, E = 0$   
 Axial ( $D_{4h}, C_{4v}, D_{3h}, \text{etc}$ ):         $D \neq 0, E = 0$   
 Rhombic ( $C_{2h}, D_{2h}, C_{2v} \text{ etc}$ ):       $D \neq 0, E \neq 0$

For,  $C_{2v}$  and higher symmetry:  $g$  and  $D$  have co-parallel principal axes. General method to obtain ZFS energies:

$E(m_s) = \text{energy of an } m_s \text{ state}$      $E(m_s) = m_s^2 D$

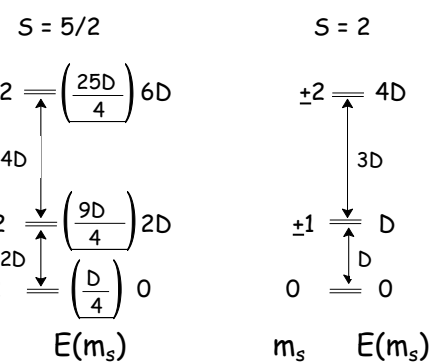


Figure 59. Pattern of energy level splitting as induced by  $D$  for half-integer and integer  $S$  value respectively.

Quantitative ligand field (LF) approach

The spin Hamiltonian (SH) parameters can be obtained by best fit of the calculated energies

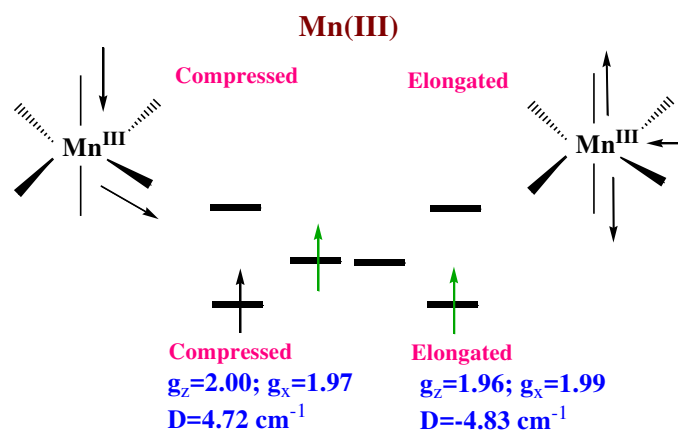


Figure 60. Impact of Jahn-Teller distortion on the magnitude of  $D$  as shown for Mn(III) octahedral complex above.

(ii) Direct measurement of D: susceptibility measurements

Direct measurement of D has been performed from single crystal of FeSiF<sub>6</sub>.6H<sub>2</sub>O (adjacent figure 24).

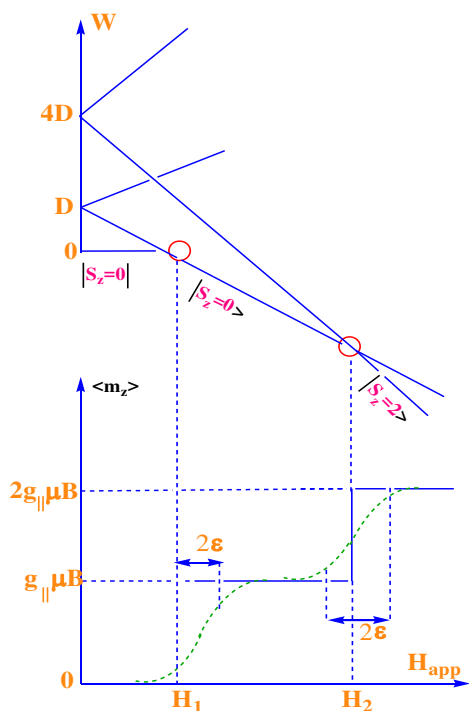


Figure 61. Schematic diagram representing direct measurement of D from single crystal.

The <sup>5</sup>D gives two doubly degenerate levels at D and 4D. At H<sub>1</sub> and H<sub>2</sub> doubly degenerate GS. At H<sub>1</sub>=g<sub>||</sub>μ<sub>B</sub>D and H<sub>2</sub>=3g<sub>||</sub>μ<sub>B</sub>D. Assuming g<sub>||</sub>=2, H<sub>1</sub>=132 G, D =12.2± 0.2 cm<sup>-1</sup> (Magnetic measurements. 10.5-10.9 cm<sup>-1</sup>) And H<sub>2</sub> occurs at 410 G.

Examples:

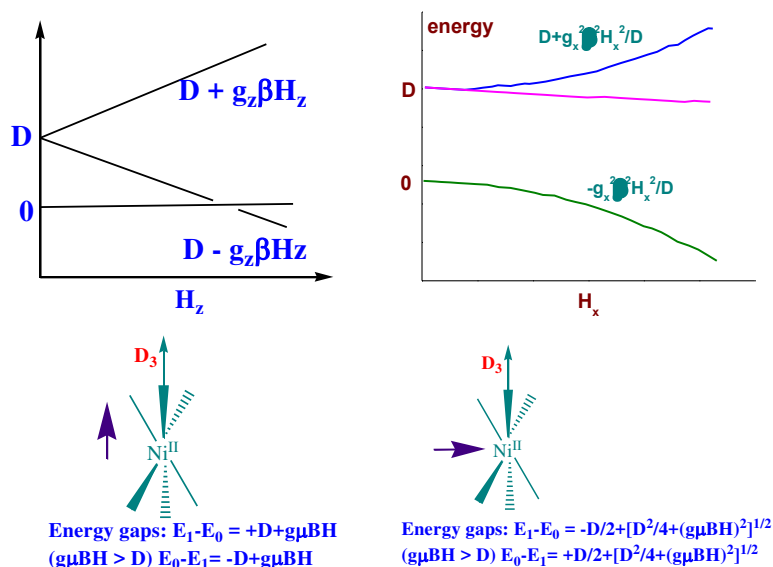


Figure 62. Energy gap between the splitted energy levels is dictated by zero-field splitting .

(iv) Behaviour of susceptibility( $\chi$ ) of zfs parameter(D):

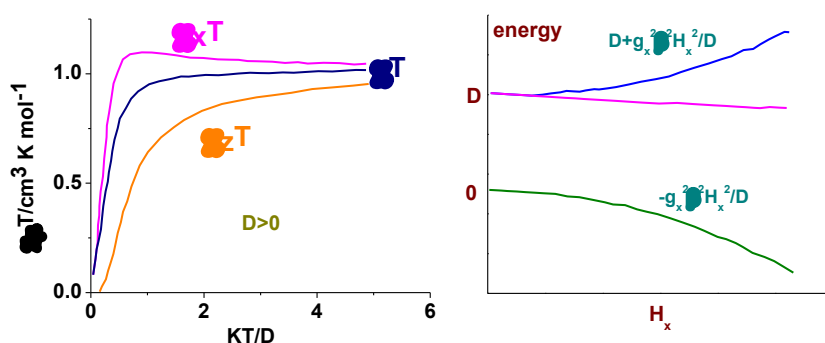


Figure 63. Diagram exhibiting dependence of magnetic susceptibility on zero field splitting.

For +ve D,  $\chi_x$  and  $\chi_z$  tend to zero as T tends to zero ( $\chi_x$  passes through a maximum). For -ve D,  $\chi_z$  increases and has finite value of  $Ng_z^2\beta^2/k$  when T tends to zero. The average magnetic susceptibility plotted is approximated by  $\chi = (\chi_z + 2\chi_x)/3$ . Examples: Cr(III); d<sup>3</sup> electronic configuration:

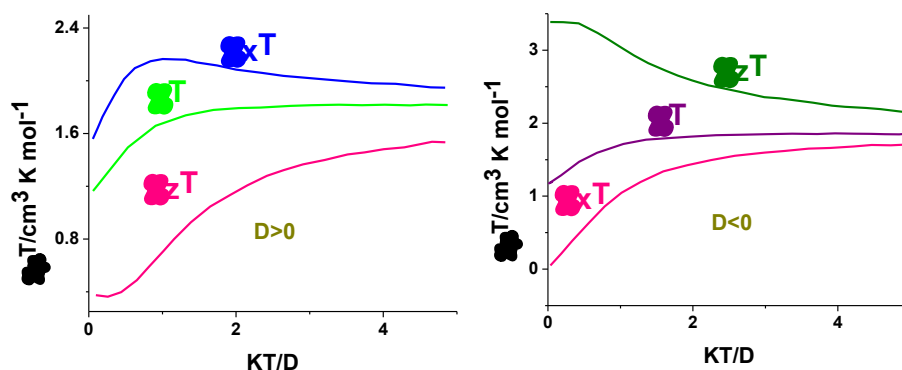
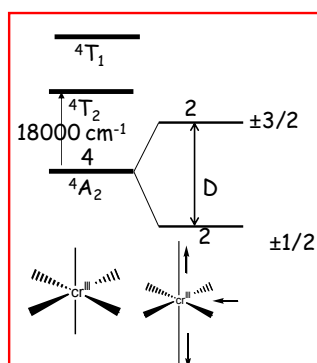


Figure 64. Impact of D on magnetic susceptibility for d<sup>3</sup> electronic configuration.



$$E_{\pm 1/2} = \pm g_z \beta H_z / 2 \text{ and } E_{\pm 3/2} = 2D \pm 3g_z \beta H_z / 2$$

$$\frac{\chi_z}{N} = \frac{g_z^2 \beta^2}{4kT} \left[ \frac{1 + 9e^{-\frac{D}{kT}}}{1 + e^{-\frac{D}{kT}}} \right]$$

Figure 65. energy levels splitting in Cr<sup>3+</sup> system.

For +iv D  $\chi_z$  decreases on cooling and tend to  $N g_z^2 \beta^2 / 4k$  when  $kT/|D| \rightarrow 0$  while  $\chi_x$  pass through a maximum and then tend to  $N g_z^2 \beta^2 / k$  when  $kT/|D| \rightarrow 0$ . For -ive D  $\chi_z$  increases and has finite value of  $9N g_z^2 \beta^2 / 4k$  when  $kT/|D| \rightarrow 0$ . while  $\chi_x$  decreases continuously tend to zero as  $kT/|D| \rightarrow 0$ . Finally,  $\chi T$  is insensitive to sign of D. It is worthwhile to mention that ,  $\chi_z$  is the magnetic susceptibility along Z direction/along the symmetry axis of the molecule/parallel to direction along which magnetic field has been applied. On the other hand,  $\chi_x$  is such contribution to the magnetic susceptibility which has been applied perpendicular to the applied magnetic field.

Examples: Fe(III);Mn(II); d<sup>5</sup> electronic configuration:

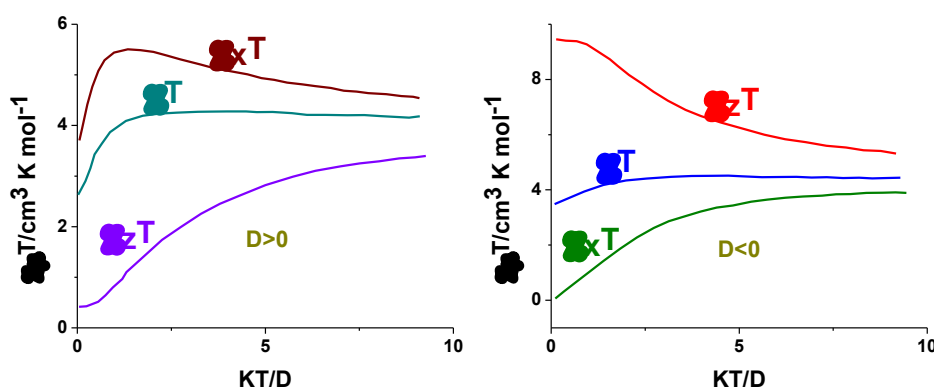


Figure 66. Impact of D on magnetic susceptibility for d<sup>5</sup> electronic configuration.

The above example shows similar feature for that observed in d<sup>3</sup> electronic configuration except the detection of larger susceptibility values.

Important points to be noted: The axial field (tetragonal distortion) establishes a symmetry axis in the molecule (z). It is important to specify the orientation of the axis with respect to *H*.

We can calculate the effect of the zero-field splitting on  $\chi$  via Van Vleck using the  $E_n$  levels above.

[ Example: monomeric Ni(II),  $D \approx +2 \text{ cm}^{-1}$ ,  $g_z = g_{xy} = 2$ ,  $S = 1$  ]

$$\chi = \frac{N \sum_n \left( \frac{E_n^{(1)2}}{kT} - 2E_n^{(2)} \right) \cdot \exp\left(-\frac{E_n^{(0)}}{kT}\right)}{\sum_n \exp\left(-\frac{E_n^{(0)}}{kT}\right)} \quad [\text{assume } E_n^{(2)} = 0]$$

$$\chi = \frac{N \left[ 0 + \frac{g^2 \beta^2}{kT} \cdot \exp\left(-\frac{D}{kT}\right) + \frac{g^2 \beta^2}{kT} \cdot \exp\left(-\frac{D}{kT}\right) \right]}{\left[ 0 + \exp\left(-\frac{D}{kT}\right) + \exp\left(-\frac{D}{kT}\right) \right]} = \frac{Ng^2 \beta^2}{kT} \left[ \frac{2 \exp\left(-\frac{D}{kT}\right)}{1 + 2 \exp\left(-\frac{D}{kT}\right)} \right]$$

Note: 1. As  $D \rightarrow 0$ ,  $\chi \rightarrow$  Curie Law for  $S = 1$ . At low T and large D,  $\chi \rightarrow 0$ , i.e. has 2 up e but behaves as if none.

2.  $\chi$  calculated above is  $\chi_z$  (i.e. H along molecular z axis). Can do slightly more involved sum for  $\chi_{xy}$ .  $\chi_z$  and  $\chi_{xy}$  behave differently. Magnetic anisotropy arising from zero-field splitting.

3.  $\chi$  follows Curie-Weiss behaviour. Another example of Curie-Weiss behaviour not arising from intermolecular interactions.

4. To determine D can least squares fit experimentally determined, variable temperature  $\chi$  data to appropriate equation where D and g are variables. However, a far more accurate way of determining the magnitude and sign of D (and g) is EPR spectroscopy.

#### §14. Low spin- High spin transition:

Config.	$\Delta \gg P$	$\Delta \ll P$
$d^4$	${}^3T_{1g}$	${}^5E_g$
$d^5$	${}^2T_{2g}$	${}^6A_{1g}$
$d^6$	${}^1A_{1g}$	${}^5T_{2g}$
$d^7$	${}^2E_g$	${}^4T_{1g}$

Configurations  $d^{4-7}$  in Oh has either LS or HS ground state. (determined by  $\Delta$  and mean spin pairing energy P).

$\Delta \gg P \rightarrow$  LS and if  $\Delta \ll P \rightarrow$  HS. However when  $\Delta \ll$  or  $\gg P$  not true, a LS  $\leftrightarrow$  HS transition can occur. But often  $|\Delta - P| \sim kT$ . A temperature induced LS  $\leftrightarrow$

HS transition is characterised by  $x = f(T)$  with x being mole fraction of HS and (1-x) being LS molecules. Determination from magnetic measurements,

$$x = \frac{\chi T - (\chi T)_{LS}}{(\chi T)_{HS} - (\chi T)_{LS}}$$

Magnetic measurements are not unique here. Other measurements Mossbauer, Temp dependent-IR, EPR can be used also. Types of transition observed for  $x=f(T)$ . Transition may be abrupt or smooth. It may be incomplete or complete at low or high T. The curve can be strictly identical in cooling and heating or exhibit hysteresis effect.

*(i) Mechanism of spin transition at the molecular scale:*

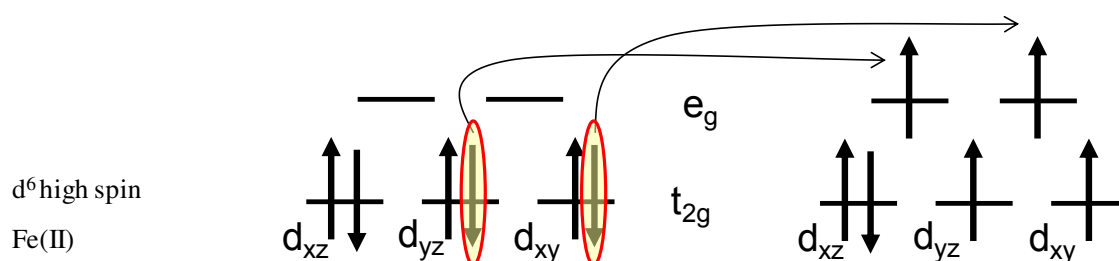


Figure 67. Electronic spin transition in a complex containing Fe(II) in presence of weak field.

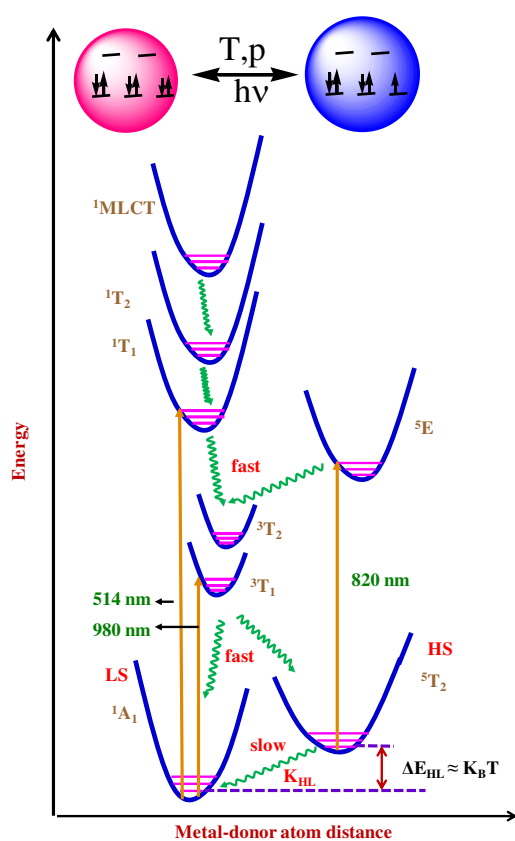


Figure 69. Schematic representation of the excited higher LF states of a  $d^6$  complex  $[\text{Fe}(\text{ptz})_6](\text{BF}_4)_2$  for LF strengths in the spin crossover range. This scheme provides explicit idea about the mechanism of LIESST.

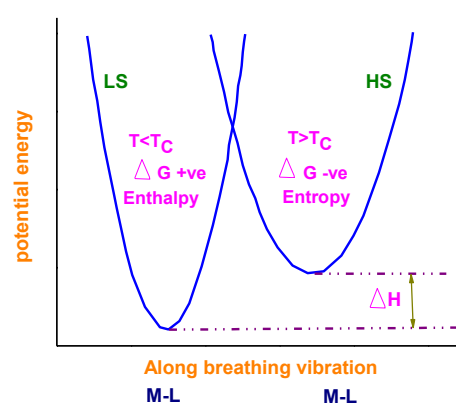


Figure 68. Spin cross over vs metal-ligand bond distance

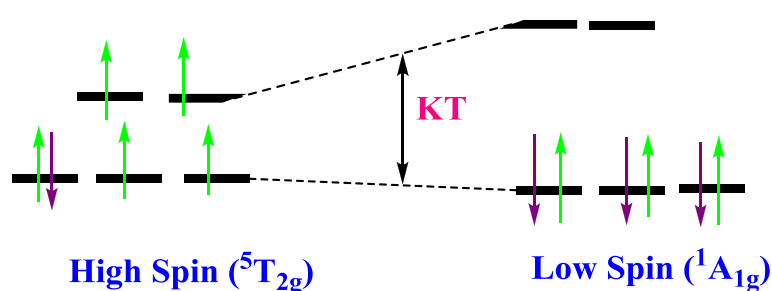


Figure 70. High-spin and Low-spin states in iron(II) compounds.

Spin transition corresponds to an intraionic electron transfer. For Fe(II)  $\Delta S$  corresponds to 2. The occupancy of  $e_g$  orbitals in the HS state causes elongation of M-L bonds. For Fe(II) 0.14-0.24 Å for Fe(III) 0.11-0.15 Å ( $\Delta S=2$ ). For Co(II) 0.09-0.11 Å  $\Delta S=1$ .  $\Delta G = \Delta H - T\Delta S$  With  $\Delta G = G_{\text{HS}} - G_{\text{LS}}$ .  $\Delta H = H_{\text{HS}} - H_{\text{LS}}$  while

$\Delta S = S_{HS} - S_{LS}$ . At equilibrium temperature  $T_c$ ,  $\Delta G = 0$ , hence  $T_c = \Delta H / \Delta S$ . To have +ve  $T_c$ ,  $\Delta H$  must have same sign.  $\Delta S = \Delta S_{el} + \Delta S_{vib}$  and  $\Delta S_{el} = Nk \ln(D_{HS}/D_{LS})$ . For Oh Fe(II)  $D_{HS}/D_{LS}$  is 15 then  $\Delta S_{el} = 1.882 \text{ cm}^{-1} \text{ K}^{-1}$ . At low sym.  $D_{HS}/D_{LS}$  will be 5 then  $\Delta S_{el} = 1.119 \text{ cm}^{-1} \text{ K}^{-1}$ . Thus  $\Delta S_{el}$  is +ive so is  $\Delta S_{vib}$ . HS bond lengths are longer than LS, more vibrational disorder thus both  $\Delta H$  and  $\Delta S$  are +ive. In order for ST to occur, the minimum of LS PES must be slightly lower than HS PES. The existence of two minima in the PES leads to LIESST (Light induced excited state trapping). Electronic spectrum recorded at 10K and at RT differs for  $[\text{Fe}(\text{ptz})_6](\text{BF}_4)_2$ . This complex exhibits transition from the diamagnetic LS state to the strongly paramagnetic state (Spin transition; ST) at 135 K with a hysteresis effect of around 7K. In the adjacent figure 69 clearly three different transitions<sup>9</sup> ( $^1A_1$  to  $^3T_1$ ,  $^1A_1$  to  $^3T_2$ ,  $^1A_1$  to  $^1T_1$ ) are visible which corresponds to the middle diagram of the below figure 71. The figure implies the presence of two very weak and broad bands which can be correlated to  $^1A_1$  to  $^1T_1$  transition.

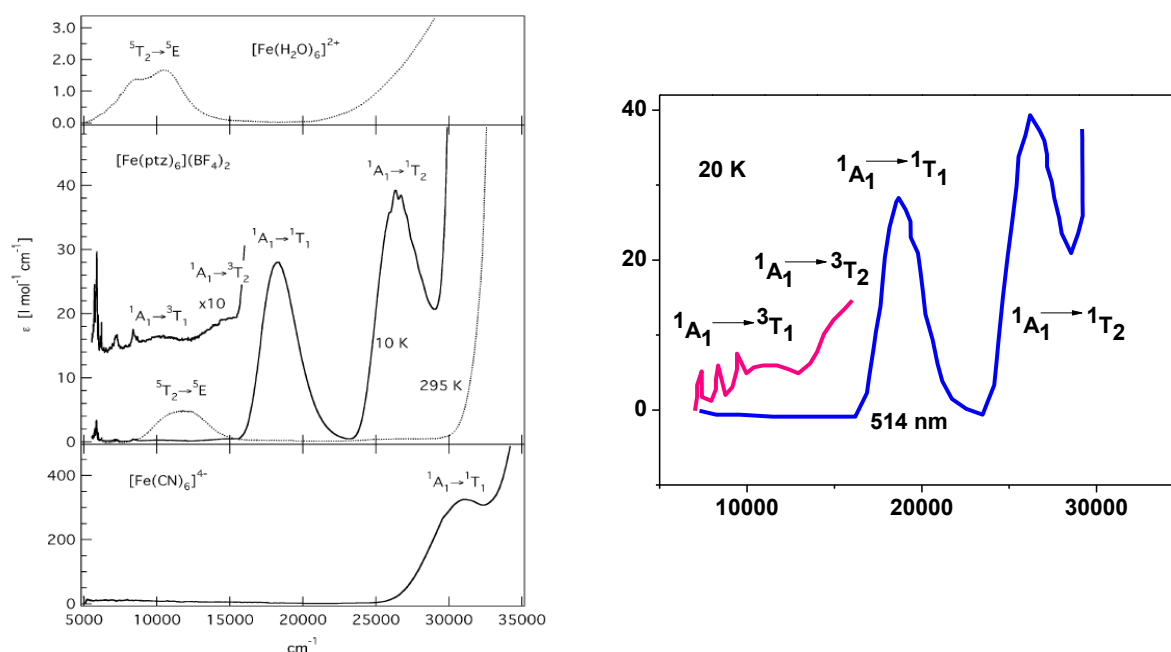
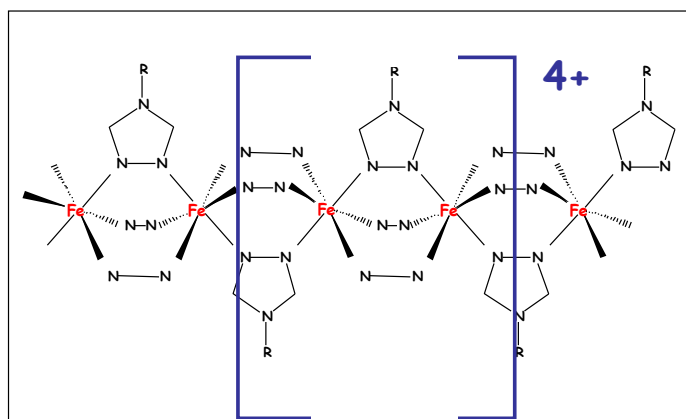
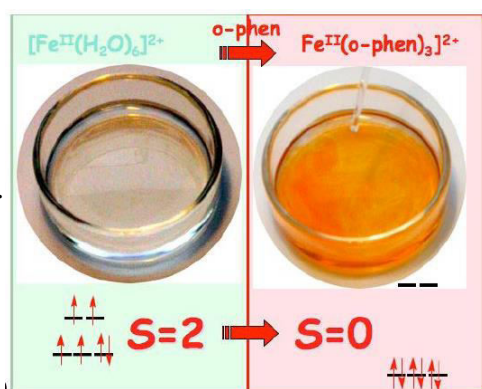


Figure 71. Single crystal absorption spectra for  $[\text{Fe}(\text{ptz})_6](\text{BF}_4)_2$ ,  $[\text{Fe}(\text{H}_2\text{O})_6]^{2+}$  and  $[\text{Fe}(\text{CN})_6]^{4-}$  where in all the complexes Fe possesses +2 oxidation state. Represents excitation from LS to excited LS effected by irradiation. This subsequently decays back to LS but due to SO coupling alternative path would be to decay to lowest spin triplet state  $^3T_{2g}$ . This is irreversible unless using a light that could affect  $^5T_{2g} \rightarrow ^5E_g$  transition thus pumping back to LS state.



(a)

(b)

Figure 72. a) Manifestation of LS-HS transition and b) Fe(II) « Chain » with spin cross-over

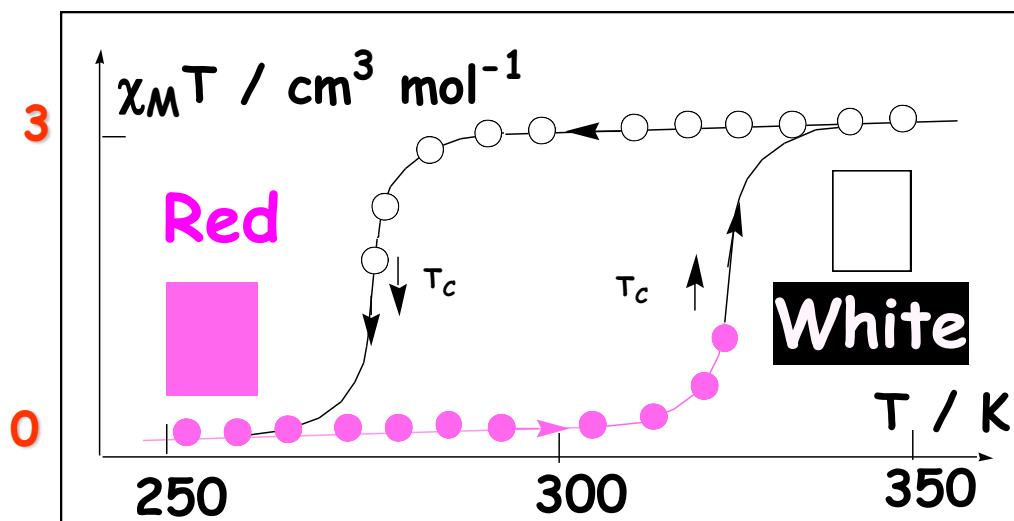


Figure 73. Diagram implies Spin cross over at room temperature. Most importantly, the system remembers its thermal past and in its bistability domain.

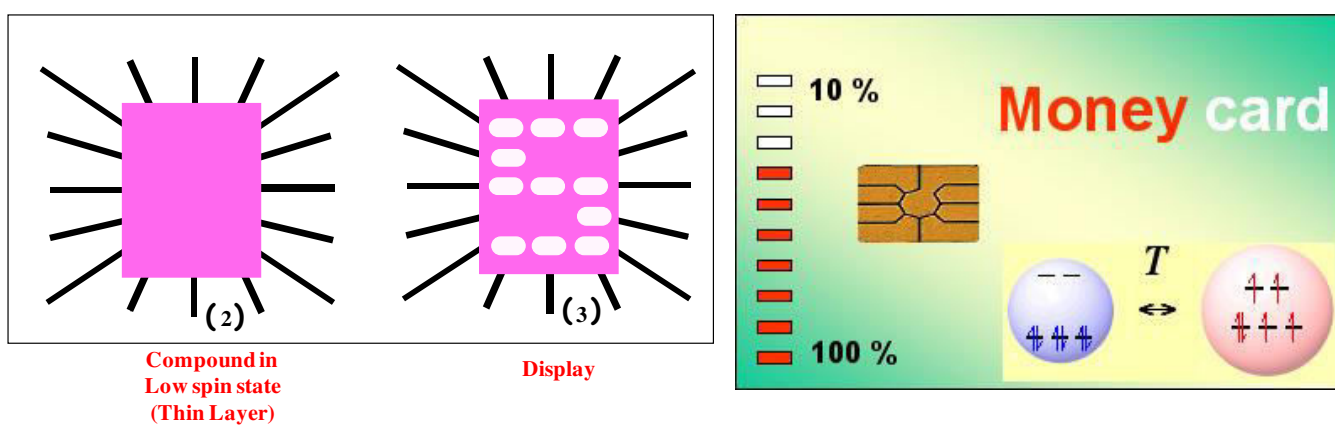
Applications of LS-HS transition:

Figure 74. Picture depicting display devises as a potential application of LS-HS transition.

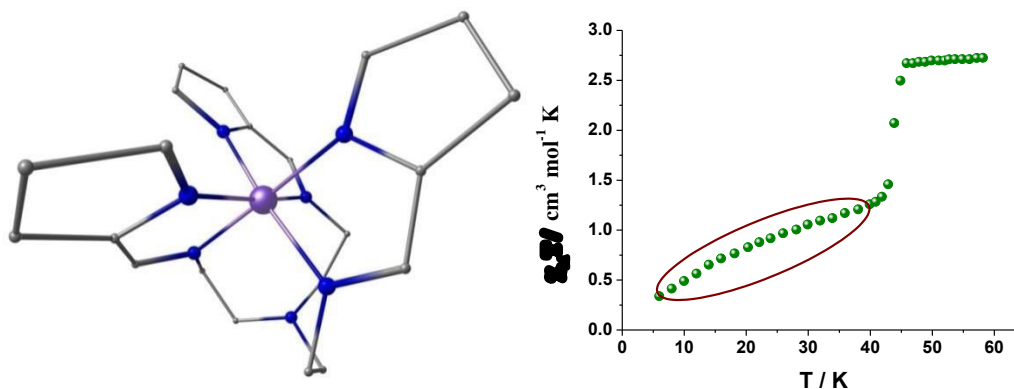
Other applications of LS-HS transition in transition metal ions:i) Ex: 1: The first report of  $d^4$  systems exhibiting LS-HS transition is  $[\text{Mn}(\text{pyrol})_3\text{tren}]$ 



Figure 75. Exhibits an abrupt change at 41K from  $S=2$  to  $S=1$  is clearly visible which is also one of the lowest  $T_c$  ever observed.

ii) Example II:  $[\text{CrI}_2(\text{depe})_2]^{10}$  with  $\text{depe}=1,2\text{-bis}(\text{diethylphosphino})\text{ethane}$

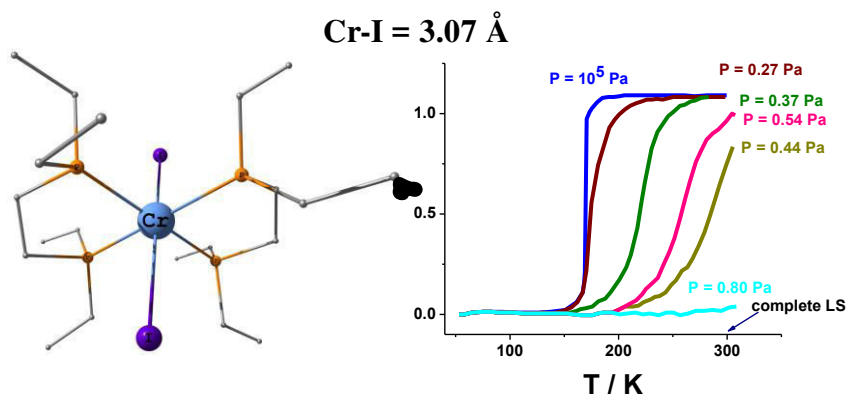


Figure 76. Example of  $[\text{CrI}_2(\text{depe})_2]$  complex which exhibits a sharp and complete ST around  $T \sim 170$  K between HS (**brown**) ( $S=2$ ) and LS ( $S=1$ ) (**violet**) states without any detectable hysteresis at ambient pressure. With increasing pressure,<sup>11</sup> the ST curves are shifted towards higher temperatures.

iii) triple-decker chromium dinuclear complexes of formula  $[(\eta^5\text{-C}_5\text{Me}_5)(\text{Cr}(\mu^2\text{-}\eta^5\text{-P}^5)\text{Cr}(\eta^5\text{-C}_5\text{Me}_5))]^{12}$  (A) (A anion= $\text{PF}_6^-$ ,  $\text{SbF}_6^-$ )

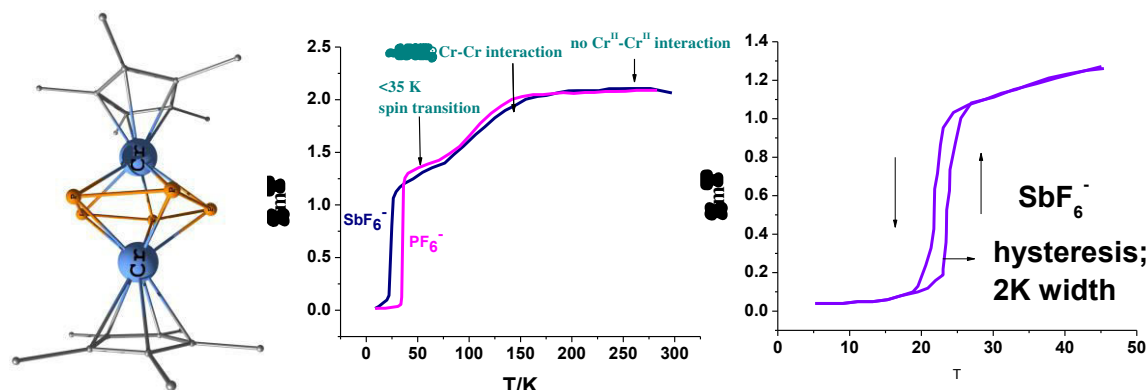


Figure 77. Above compound exhibits unconventional magnetic properties below room temperature.

iv) Magnetic interaction vs spin transition:

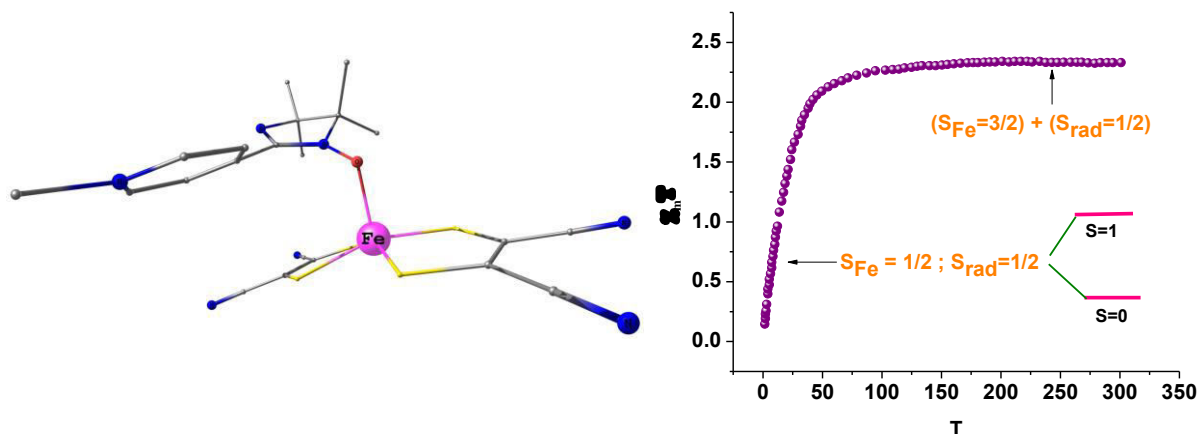


Figure 78. Crystal structure of bis(cis-1,2-dicyano-1,2-ethylenedithiolato)[2-(para-N-methylpyridinium)-4,4,5,5,-tetramethylimidaxolin-1-oxyl]iron(III) and participating spin-cross over for Fe metal ion within the complex.

The complex <sup>13</sup> (figure 78) bis(cis-1,2-dicyano-1,2-ethylenedithiolato)[2-(para-N-methylpyridinium)-4,4,5,5,-tetramethylimidaxolin-1-oxyl]iron(III) is composed of two bidentate cis-1,2-dicyano-1,2-ethylenedithiolates combined with a monodentate coordinated organic radical. Between 100 and 300 K non-exchange-coupled radical spin ( $S_{\text{radical}}=1/2$ ) and the quartet spin state of Fe(III) ( $S_{\text{Fe}}=3/2$ ) led to  $\chi T$  2.33 cm<sup>3</sup> K mol<sup>-1</sup>. Below 100 k  $\chi T$  abruptly decreases and reaches zero due to LS-Fe(III) ( $S=1/2$ ) and  $S_{\text{radical}}=1/2$  AF interaction. This leads a high energised  $S=1$  state, which is gradually depopulated in compliance with the reduction in temperature while simultaneous population of the  $S=0$  state has been witnessed. Here ST involves  $S=1/2$  to  $S=3/2$ . For six co-ordinate systems the spin crossover generally involves an  $S=1/2 \rightarrow S=5/2$  change, whereas for five-coordinate materials an intermediate (quartet) spin state is involved in  $S=1/2 \rightarrow S=3/2$  transitions. ST are rapid and hysteresis is rare.

The complex [Fe(phen)<sub>2</sub>(NCS)<sub>2</sub>] is found to show abrupt transition(as revealed by the effective magnetic moment vs temperature plot in the above figure 79). This was the first invented Fe(II) complex exhibiting a temperature dependent <sup>5</sup>T<sub>2g</sub> to A<sub>1g</sub>(O<sub>h</sub>) spin transition. <sup>14</sup> This prompted the scientists to ascertain the determining factors behind spin transition<sup>15</sup> which was concluded to be appreciable enhancement in entropy for transition from the LS to HS state. For this complex, similar space group was procured above and below the curie temperature ( $T_C$  of 176K) despite observed hysteresis effects by spin transition. This complex possesses purely HS behaviour at room temperature while cooling down to 185K only results discontinuous spin transition to a LS state. Such spin transition is associated with hysteresis without any concomitant variations in the crystal structure. This complex is a prolific example of a crystalline spin crossover<sup>17</sup> compounds which are

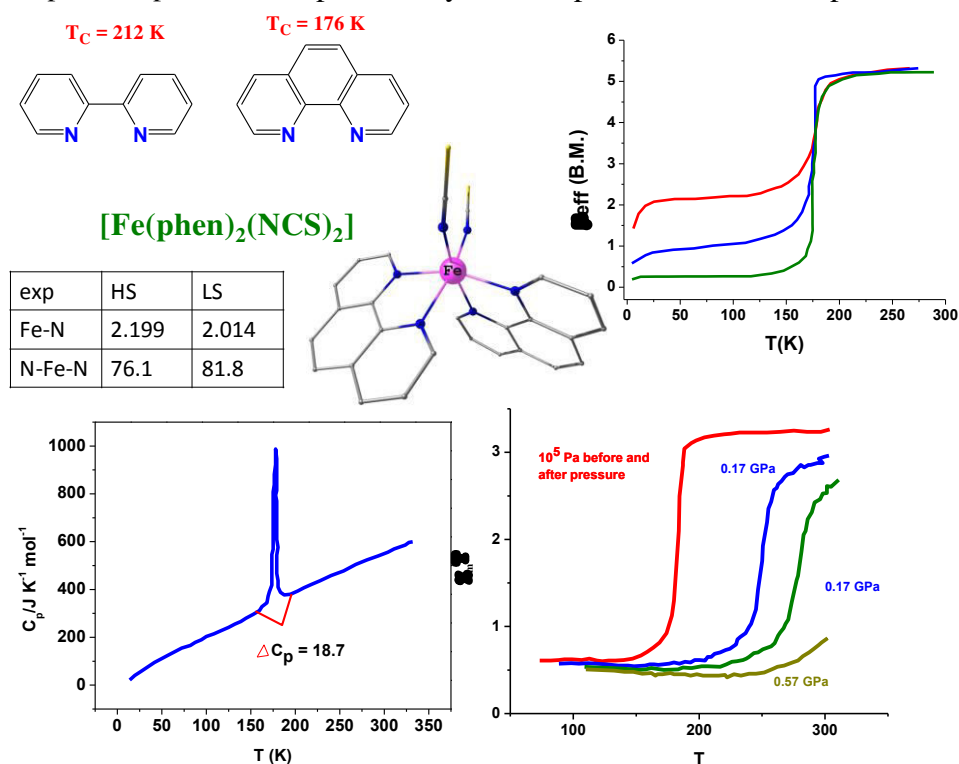


Figure 79. Diagram showing crystal structure of complex  $[\text{Fe}(\text{phen})_2(\text{NCS})_2]$  (H atoms omitted for clarity)<sup>16</sup>, effect of pressure on its spin transition and molar heat capacity indicating the spin crossover temperature.

uncharged, possess anions essential for electrical neutrality coordinated directly to the metal site. The critical temperature above which these molecules in its HS state by LIESST<sup>18</sup> (light induced excited spin state trapping) supposedly relax back to the normal LS state is found to be around 55K. Thermal spin transition at 175 K is also further corroborated by the magnetic susceptibility vs temperature plot. With increasing pressure the transition curves shift to higher temperatures owing to the stabilisation of the LS state and become slightly more gradual. At the largest pressure of 0.57 GPa, the paramagnetic HS state is found to be almost suppressed at the room temperature region. Upon releasing pressure, the ST behaviour practically remains same as before under ambient pressure. It is notable that, in this compound, NCS<sup>-</sup> anion acts as direct codeterminant of the ligand field strength at the metal site. The molar heat capacity ( $C_p$ )<sup>19</sup> at constant pressure is recorded between 10 to 350K which clearly show beginning of the heat capacity anomaly at 162K, culmination at 175K and termination at 187K. The starting temperature represents quadrupole split doublet due to the HS component and terminating temperature denotes the disappearance of the LS component.

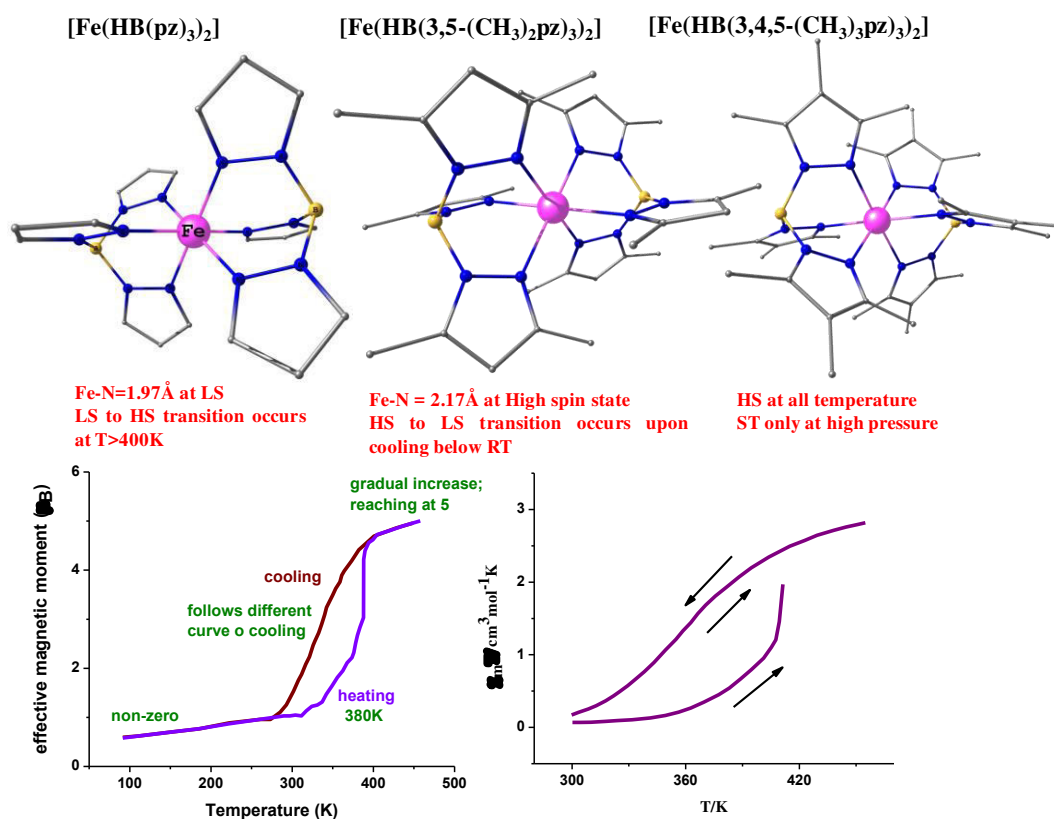


Figure 80. Figure shows crystal structure of complexes  $[\text{Fe}(\text{HB}(\text{pz})_3)_2]$ ,  $[\text{Fe}(\text{HB}(3,5\text{-(CH}_3)_2\text{pz})_3)_2]$  and  $[\text{Fe}(\text{HB}(3,4,5\text{-(CH}_3)_3\text{pz})_3)_2]$ . Figure shows also effect of temperature on magnetic moment of  $[\text{Fe}(\text{HB}(\text{pz})_3)_2]$  complex and its magnetic susceptibility data as effected by temperature.

For complex  $[\text{Fe}(\text{HB}(\text{pz})_3)_2]$ <sup>20</sup> slight increase of magnetic moment from  $0.6 \mu_B$  at 78K is typical of

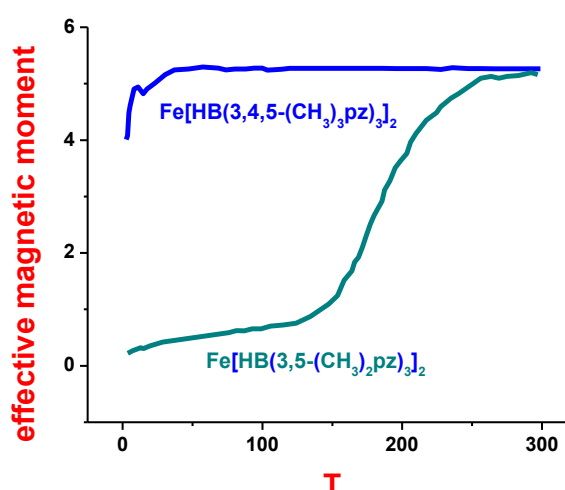


Figure 81. Variation in magnetic moment with temperature for complexes  $\text{Fe}(\text{HB}(3,5-(\text{CH}_3)_2\text{pz})_3)_2$  and  $[\text{Fe}(\text{HB}(3,4,5-(\text{CH}_3)_3\text{pz})_3)_2]$

low spin Fe(II) complexes and resulted due to the second order Zeeman mixing of magnetic excited state wave functions with the nonmagnetic ground state wave function (known as temperature independent Paramagnetism; TIP). The product of magnetic susceptibility and temperature for complex  $[\text{Fe}(\text{HB}(\text{pz})_3)_2]$  showed apparent hysteresis for the first thermal cycle and note-worthily, its spin crossover is revealed by change in the colour of the complex. It is notable that, in the solid state  $[\text{Fe}(\text{HB}(\text{pz})_3)_2]$  remains at low spin state at ambient temperature making transition to the high spin state at higher temperatures,<sup>21</sup> while complex  $[\text{Fe}(\text{HB}(3,5-(\text{CH}_3)_2\text{pz})_3)_2]$ <sup>22</sup> remains at high spin state (mentioned in above figure 80) at ambient temperatures changing to the low spin state at lower temperatures (figure 82). Contrary to this, in solution state  $[\text{Fe}(\text{HB}(3,5-(\text{CH}_3)_2\text{pz})_3)_2]$ <sup>23</sup> remains at high spin state between 200 & 295 K which is true for  $[\text{Fe}(\text{HB}(3,4,5-(\text{CH}_3)_3\text{pz})_3)_2]$ . For complex  $[\text{Fe}(\text{HB}(3,4,5-(\text{CH}_3)_3\text{pz})_3)_2]$ . The magnetic moment retains at  $5.22 \mu_B$  at ambient temperature and remains constant down till 210K. Minuscule decrease in the moment to  $5 \mu_B$  at the low temperatures owes to the varying populations of the sublevels in the E state of the axially distorted  $^5T_2$  state. The  $[\text{Fe}(\text{HB})(\text{pz})_3)_2]$  compound exhibits fascinating spin state transitions in solution and at ambient temperature possesses magnetic moment of  $2.71 \mu_B$  exemplifying simultaneous presence of high spin and low spin states. At 295K (shown in figure 81) less amount of low-spin Fe(II) presence was detected (corresponds to the large magnetic moment) for complex  $[\text{Fe}(\text{HB}(3,5-(\text{CH}_3)_2\text{pz})_3)_2]$ . Hence, at ambient pressure the sample can contain only few percent of low spin Fe(II) which is significantly less. So, by assuming a Boltzmann distribution between the high-spin and low-spin state separated in energy by  $D$ , it is possible to calculate the changes in the energy between the two states with increasing pressure. The absence of the low-spin state at ambient pressure indicated that this state is at least  $600 \text{ cm}^{-1}$  above the high-spin ground state. At 2 kbar this separation has decreased to ca.  $175 \text{ cm}^{-1}$  and at 4 kbar the two states are approximately equivalent in energy. At 6, 8, 15, 40, and 70 kbar the low-spin state is the ground state and the high-spin state is, respectively, at 85, 140, 270, 340, and  $360 \text{ cm}^{-1}$  above the ground state. Hence, as might be expected for a compound with a long iron–nitrogen bond, there is a gradual shift in the relative energy of the two spin states with increasing pressure. This behaviour is quite different from the sudden change in spin state with pressure that is observed in  $[\text{Fe}(\text{phenanthroline})_2(\text{NCS})_2]$ .

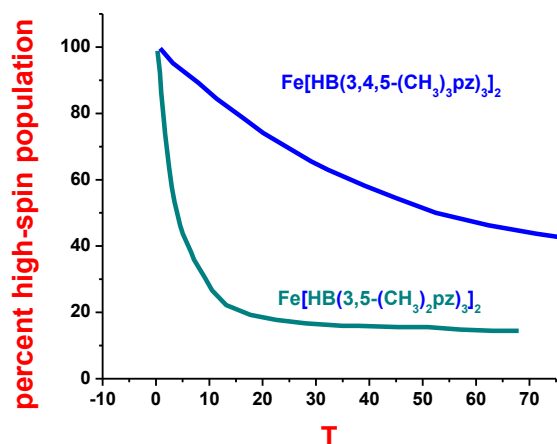


Figure 82. HS state contribution in complexes  $\text{Fe}[\text{HB}(3,5\text{-(CH}_3)_2\text{pz})_3]_2$  and  $[\text{Fe}(\text{HB}(3,4,5\text{-(CH}_3)_3\text{pz})_3)_2]$

Differences among the aforementioned compounds arise due to difference in Fe-N bond lengths. It has been observed that longer bond lengths favour HS. Steric hindrance due to bulkiness of ligands enforces longer Fe-N bonds. Application of pressure leads to shorter Fe-N distances i.e. the HS-LS gap reduces. At very high P even switching of ground state occurs due to shorter bond length. For  $[\text{Fe}(\text{HB}(3,4,5\text{-(CH}_3)_3\text{pz})_3)_2]$  larger pressure is required to produce LS state. At constant T, the magnetic moment

decreases in the order :  $[\text{Fe}(\text{HB}(3,5\text{-(CH}_3)_2\text{pz})_3)_2] > [\text{Fe}(\text{HB}(\text{pz})(3,5\text{-(CH}_3)_2\text{pz})_2)_2] > [\text{Fe}(\text{HB}(\text{pz})_2(3,5\text{-(CH}_3)_2\text{pz}))_2] > [\text{Fe}(\text{HB}(\text{pz})_3)_2]$

implying direct correlation between larger number of substituents on the pyrazoyl rings with the stability of high spin state.

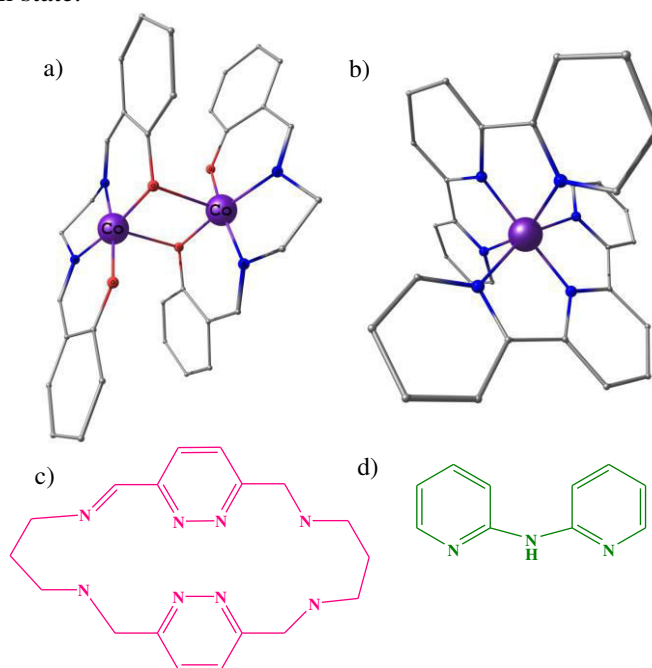


Figure 83. Crystal structure of a) dincular  $\text{Co}(\text{II})$  complex  $[\text{Co}^{\text{II}}(\text{salen})]_2$ <sup>24</sup> b)  $[\text{Co}^{\text{II}}(\text{terpy})_2]\text{Br}_2$ <sup>25, 26</sup> and structure of the c) condensed macrocyclic ligand composed of 3,6-diformylpyrazine and 1,3-diaminopropane and d) dpa(di(2-pyridyl)amide anion) ligand which can be coordinated to the  $\text{Co}(\text{II})$  ion to induce SCO characteristics.

Octahedral  $\text{Co}(\text{II})(d^7)$ <sup>27</sup> compounds are viable towards spin-crossover(SCO) mechanism between the HS( $S=3/2$ ;  $t_{2g}^5e_g^2, 4.7\mu_B$ ) and LS ( $S=1/2$ ;  $t_{2g}^6e_g^1, 1.8\text{--}2.2\mu_B$ ) state. They can spontaneously undergo oxidation to  $\text{Co}(\text{III})$ . SCO of  $\text{Co}(\text{II})$  is found to have minute effect on the structural variation in  $\text{Co}(\text{II})$  complexes. This leads to the observation of gradual, incomplete thermal SCO in octahedral

mononuclear Co(II) compounds containing terpyridine, salen, dpa, 3-formylsalicylic acid derived, pyrazine derived amide ligands.  $[\text{Co}^{\text{II}}(\text{salen})]_2$  compound shows SCO and antiferromagnetic exchange interaction ( $-21 \text{ cm}^{-1}$ ) between the two Co(II) ions. Magnetic susceptibility measurements undertaken on  $[\text{Co}_3(\text{dpa})_4\text{Cl}_2]$  complex indicates the presence of  $S=1/2$  ground state at low temperature which shows gradual spin-crossover at higher temperature.<sup>28</sup> Trinuclear  $[\text{Co}^{\text{II}}_3(\text{dpa})_4\text{Cl}_2]$  compound possesses consistent LS state which further shows incomplete SCO to an  $S=5/2$  delocalised [LS-HS-LS] state. It is mentionworthy that, SCO has also been observed in  $\text{NiF}_6^{3-}$  (containing  $d^7$  configuration) complex.<sup>29</sup>

v) Spin transition and co-operativity:

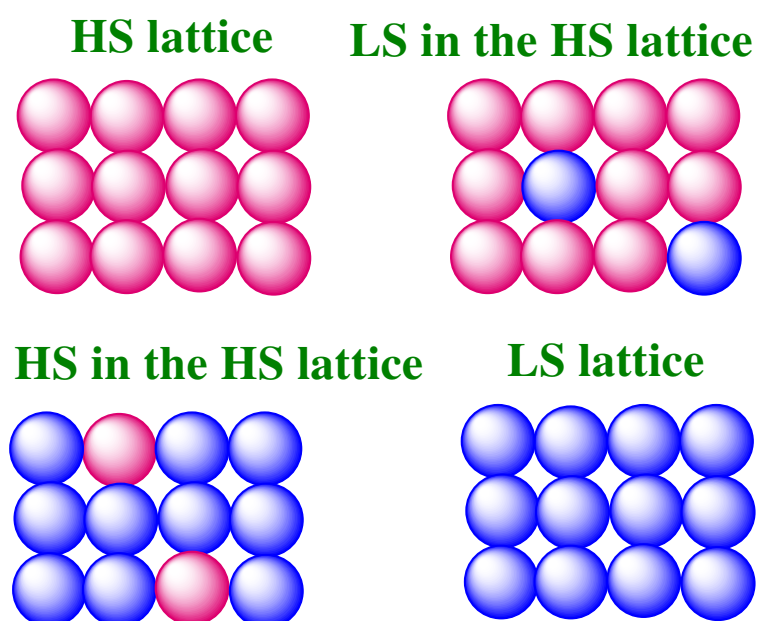


Figure 84. correlation between lattice architecture and cooperativity

Compounds showing SCO effects can be termed as attention seeker owing to their potential applications as sensing devices (temperature, pressure or gas).data storage, displays, molecular switches etc. To catalyse the use of SCO material as binary data storage, switching between the low-spin(LS) and the high-spin (HS) state must be associated with the hysteresis loop providing a applicable memory effect. SCO is purported to be elucidated using ligand field theory. Manipulation

of spin transition type (hysteresis, abruptness),being dictated by SCO cooperativity acts as a building block for technologically useful SCO material. $[\text{Fe}(\text{NCS})_2(\text{PM-PEA})_2]$  is known to be the first ever complex exhibiting most cooperative spin-crossover(SCO) which profoundly relies on thje form of the sample(either in powder form or in single crystal form). Co-operativity of a spin-crossover system is represented by the similar number of molecules and same short- and long-range magnetic interaction parameters, which increases on transition from a 1D chain to a 1D ladder type lattice and 2D square lattice. Lattice architecture (number of composite molecules), size, pressure, edge effects have strong impact on the width of the observed hysteresis.<sup>30</sup> The dependence of SCO on lattice structure arises from their simultaneous huge variations in size and shape which propagates through the material in the solid state. Size effect is preponderantly correlated with the residual HS fraction, which increases with proportionate decrease in the switching temperatures. This consequently spurs reduction of the size of the SCO system. Such decrease has led to the comparison between the number of molecules from the

edge of the lattice and those arise from the inner of the lattice influencing both the gap energy and the cooperativity of the system.

Here we assume an assembly of  $N$  molecules showing a LS to HS transition and we can define the

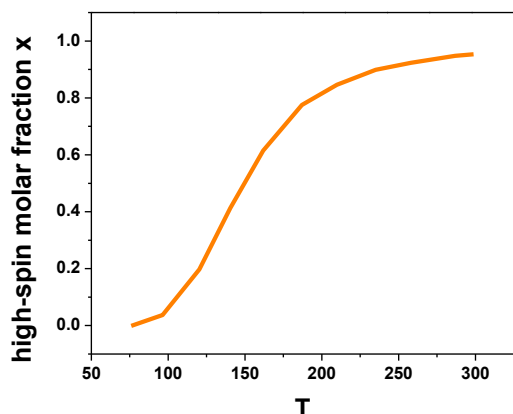


Figure 85. fractional contribution from HS state vs temperature plot correlating the spin-cooperativity with spin crossover.

taken to be zero. All the molecules are LS. On the other hand, at high temperature, the transformation is incomplete. It is noteworthy that, transition is very smooth, covering a large temperature range. Such smooth transitions are normally observed in solution, but are exceptional in solid state. Hence, it is not legitimate to ignore intermolecular interaction. Molecular nature of the spin transition phenomena arises due to the subtle balance between enthalpy and entropy factors being affected by the cooperativity within the assembly of molecules.

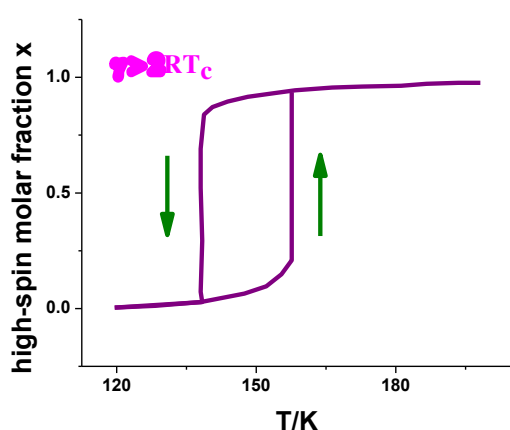


Figure 86. Importance of interaction parameter in the correlation between high-spin molar fraction and temperature

model was first applied to pressure induced transitions, we consider its activity at constant pressure. For case-I, when  $\gamma < 2RT_c$ , the transition is relatively smooth and occurs without a hysteresis effect. For case-II, when  $\gamma = 2RT_c$ , transition becomes abrupt around  $T=T_c$  but proceeds without hysteresis. For case-III, when  $\gamma > 2RT_c$ , pronounced spin transition takes place with a hysteresis effect. The adjacent figure 37 here denotes high-spin molar fraction  $x$  versus  $T$  plot for  $\Delta H=600 \text{ cm}^{-1}$ ,  $\Delta S=4 \text{ cm}^{-1} \text{ K}^{-1}$  and  $\gamma=300 \text{ cm}^{-1}$  in the

molar fraction of HS molecules as  $x$  and that of LS molecules as  $1-x$ . In absence of intermolecular interaction, each molecule ignores its neighboring molecules, we must introduce an additional entropy term, the mixing entropy; to the Gibbs free energy  $G$ . This accounts for the fact that there are many ways of distributing  $xN$  HS molecules and  $(1-x)N$  LS molecules within the assembly of  $N$  molecules. The

figure shown here is an example of  $x$  vs  $T$  plot where  $\Delta H$  has been taken equal to  $600 \text{ cm}^{-1}$  and  $T_c$  to be  $150 \text{ K}$ . At  $T=0 \text{ K}$ ,  $x$  can be

Regular solution model: This model is based on the hypothesis of regular solutions and on the formation of domains within the molecular assembly. This model will be investigated for their ranges of validity and their limits. Slichter and Drickamer have proposed this model based on the addition of the interaction term to the Gibbs free energy. This model incorporates only the  $\chi$  dependence and  $\gamma$  (interaction parameter) has been  $T$  independent in a first approximation. Although this

model was first applied to pressure induced transitions, we consider its activity at constant pressure. For case-I, when  $\gamma < 2RT_c$ , the

regular solution model.  $\gamma$  is larger than  $2RT_c$ ; the transition is abrupt with hysteresis around 150K having the maximum width of 19.2K. The important advantage from regular solution model arises from the fact that it can be useful for continuous as well as discontinuous transitions. Additionally, it is responsible for hysteresis in few complexes including Fe(II) chemistry. As mentioned earlier, given  $\gamma > 2RT_c$ , pronounced hysteresis effect has been observed subject to the minimum secondary free energy for the system. It is to be noted that, tunnelling through the barrier between the two minima due to a demixing process can decrease/suppress hysteresis.

Domain model: This model was established by Sorai and Seki; based on the like spin domain distribution rather than random fashion within the assembly for LS/HS molecules. The domains are assumed to have uniform size around critical temperature ( $T_c$ ). This model enables calculation of molar heat capacity at constant pressure ( $C_p$ ) which is impossible to derive by regular solution model. Domain wall has advantage to boast easily understood primary basics. However, recent model incorporates some extent complexity and fails to account for hysteresis. Hysteresis could appear if the sizes of the domains were different in the cooling and warming modes.

Spin transition and molecular electronics : Most fascinating future of molecular chemistry lies in the utilization of the isolated molecules in electronic circuits and devices. This is a long term issue and the problem is not to replace classical (silicon) electronics; rather to use molecular systems to perform functions those fail for silicon. Success has been achieved in the field of switching, amplification, information storage and signal processing. The spin transition is the most spectacular example of transition between two electronic states in molecular chemistry, devices for display and data recording incorporating spin transition molecular materials have been described. For viable molecular electronics property, a molecular system must be potent enough to evolve from a stable (metastable) electronic state to another one in reversible (perturbation in the initial way is opposing to that of in the final state)/detectable (potent to measure response for any value of the applied perturbation) fashion on application of an appropriate (concept of transition includes the system as well as the perturbation) and controllable (possible to fix the value of perturbation) perturbation. The foremost requirement is the existence of double minimum energy curves. In case of spin transition compounds, hysteresis arises due to the intermolecular interactions within the assembly of molecules.

## **§15. Magnetic interactions:**

Up to now we have considered monomeric transition metal ions. In polynuclear (cluster) compounds the magnetic behaviour is determined by the interactions between the unpaired electron spins on adjacent centres.



If the two paramagnetic centres A and B interact then the local spins  $S_A$  and  $S_B$  are not good quantum numbers for the system. The ions are said to be magnetically coupled, or are undergoing magnetic exchange. This exchange is described by a spin-Hamiltonian, which involves only spin operators ( $\hat{S}_A$  and  $\hat{S}_B$ ) and allows the wavefunctions (energy levels) of the system to be expressed in terms of spin functions only.

$$\hat{H} = -J\hat{S}_A \cdot \hat{S}_B$$

where  $J$  the isotropic exchange parameter.

Solving the Hamiltonian gives a new set of quantum numbers ( $S'$ ) describing the total spin:

$$S' = |S_A - S_B|, |S_A - S_B| + 1, \dots, |S_A + S_B|$$

The energies of the resultant  $S'$  states are, in general, not equal and are given by:

$$E(S') = -\frac{J}{2} S'(S' + 1)$$

### **§15.1 Copper(II) monomer: Copper(II) acetate monohydrate.**

For Cu(II) acetate monohydrate; which contains only one Cu(II) ion with  $d^9$  electronic configuration has free ion ground term as  $^2D$  which converts to  $^2E_g$  in octahedral ligand field.

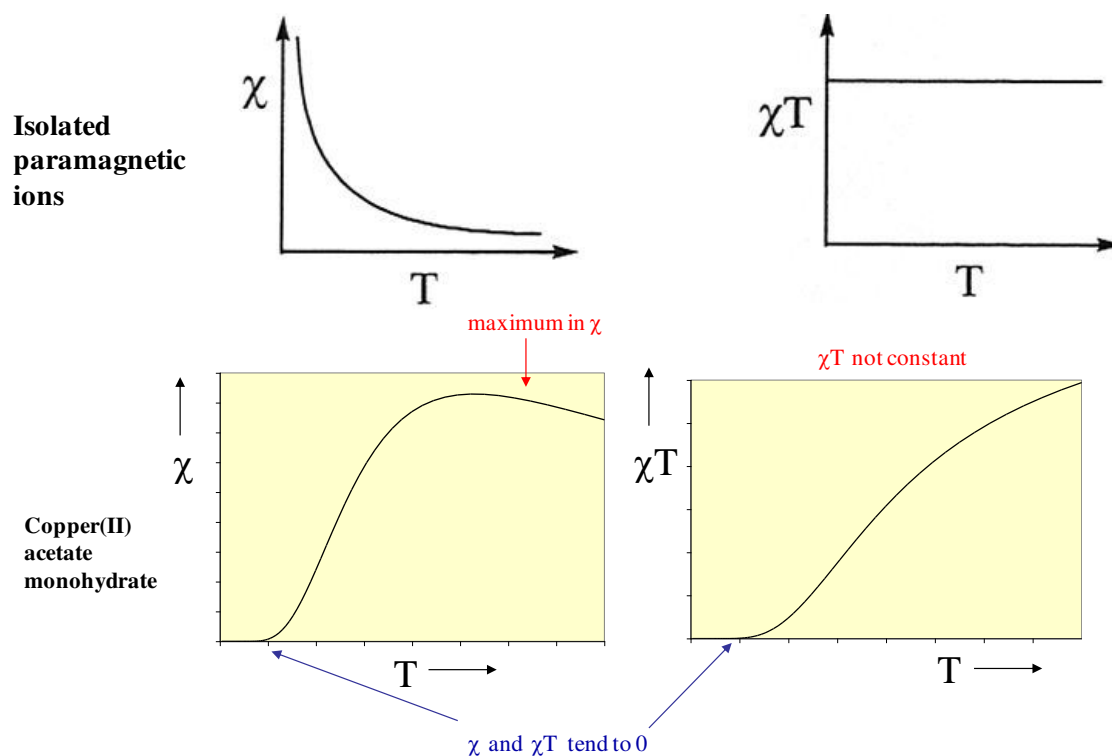


Figure 87. Magnetic susceptibility vs temperature plot for Copper(II) acetate monohydrate.

Due to aforementioned points, the magnetic moment ( $\mu_{\text{eff}}$ ) or  $\chi T$  becomes independent of temperature as depicted in top right figure 38.

### §15.2 Copper(II) dimers: dimeric structure of Copper(II) acetate monohydrate.

Side figure 88 describes the structure of dimeric Cu(II) acetate monohydrate  $\{\text{Cu}_2(\text{OAc})_2(\text{H}_2\text{O})_2\}$

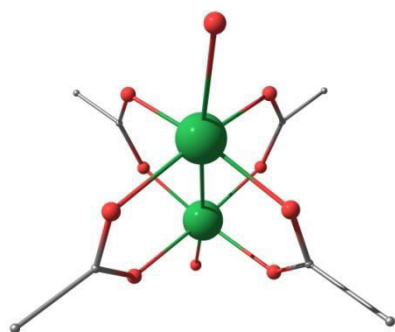


Figure 88. Crystal structure of complex  $\{\text{Cu}_2(\text{OAc})_2(\text{H}_2\text{O})_2\}$ . H atoms are omitted for clarity.

where also Cu(II) possesses one unpaired electron in  $d_{x^2-y^2}$  orbital. This denotes the first ever example of discovery to have antiferromagnetic coupling in a dimer in 1952. It is noteworthy that, the unpaired electrons on each Cu(II) centres can interact with each other. Variations exist in the type of exchange coupling; to induce such interactions spin vectors do add up or could be subtracted. Moreover, a new quantum number is

required to depict the behaviour of interacting system: (i) magnetic dipolar interaction : in this type, one electron feels the field of the other. This is very weak but can gain importance in magnetic properties below 1K. (ii) exchange interaction: this correlates to the properties of a two-electron wavefunction. It is variable in strength and has importance in magnetic properties over a wide temperature range.

For  $\{\text{Cu}_2(\text{OAc})_2(\text{H}_2\text{O})_2\}$ , strong magnetic interaction exists within the cluster and for magnetically dilute system negligible magnetic interaction lies between the clusters due to intrinsic molecular packing. Coupling of electron spins between adjacent magnetic sites indicates the exchange coupling. This exchange deals with the overlap between ligand atomic orbitals and the metal d-orbitals possessing unpaired electrons. Numerical approaches towards procuring the exact solution of the exchange coupling can be complex for large systems. Modelling of the magnetic properties were performed using effective exchange parameter ( $J$ ). Sign of  $J$ , magnitude of  $J$  vs  $KT$  (thermal energy) will govern the magnetic properties in a system.

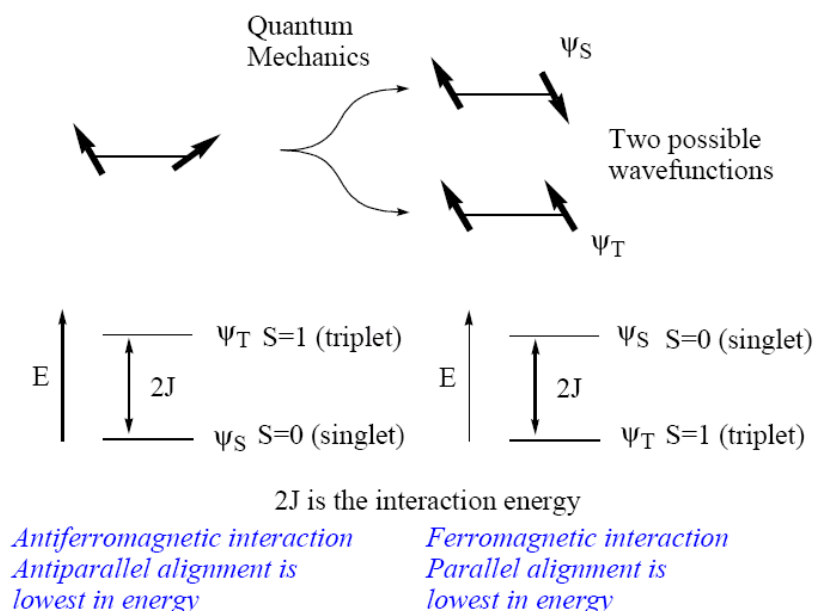


Figure 89. The figure explains the dependence of the type of magnetic exchange on the energy of the levels.

To represent exchange interaction spin Hamiltonian  $\hat{H}$  has been proposed which involves the spin operators  $\hat{S}$ . Three different formalism for exchange spin Hamiltonian as invented by Heisenberg and termed as Heisenberg-Dirac-Van Vleck Hamiltonian has been proposed:

$$(i) \quad \hat{H} = -\sum_{i,j} J_{ij} \hat{S}_i \cdot \hat{S}_j \quad J>0; \text{ Ferromagnetic and } J<0; \text{ Antiferromagnetic interaction}$$

$$(ii) \quad \hat{H} = \sum_{i,j} J_{ij} \hat{S}_i \cdot \hat{S}_j \quad J<0; \text{ Ferromagnetic and } J>0; \text{ Antiferromagnetic interaction}$$

$$(iii) \quad \hat{H} = -2\sum_{i,j} J_{ij} \hat{S}_i \cdot \hat{S}_j \quad J>0; \text{ Ferromagnetic and } J<0; \text{ Antiferromagnetic interaction}$$

and here  $J$  of equation (i) has been substituted by  $2J$  for the use by some authors.

As per the Schrodinger equation,  $\hat{H}\Psi = E\Psi$ ; the spin Hamiltonian operates on the spin part of the wavefunction which is correlated to the relative energies of the spin states. This coupling is of scalar type; which is a phenomenological description.

Exchange coupling possesses three different kind of strengths:

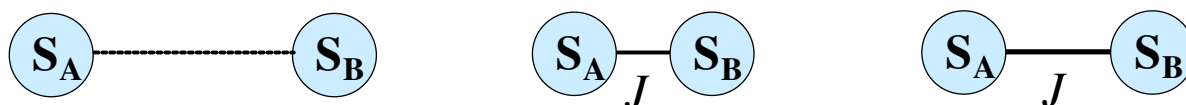


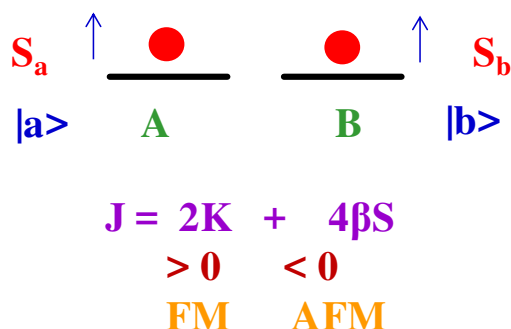
Figure 90. Schematic diagram explaining magnetic exchange interaction between two metal ions possessing different spins ( $S$ =spin quantum number of respective A/B metal site).

Case-I: magnetic properties of the dimer remain unaltered from that of the monomer for non-interacting spins.

Case-II: relatively strong metal-metal bond has been formed for strongly interacting spins arising from the diamagnetic behaviour of even numbers of unpaired electrons.

Case-III: weak exchange coupling owes to the weakly interacting spins and subsequently has resulted low-lying excited states of different spin which can be populated at thermal energies. The exchange

interaction can be considered as the extreme case of very weak bond.



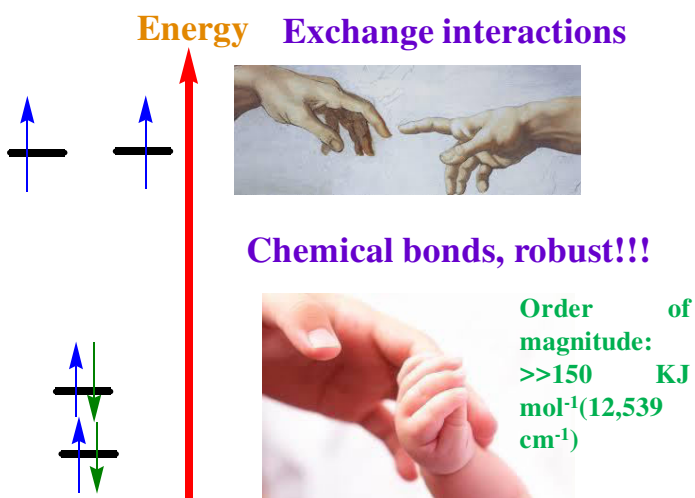
Challenges in calculating the exchange interaction in the interaction models between localised electrons owes to the spin-spin interaction (magnetic dipolar) and does not possess the right order of magnitude which can be remedied by the

Figure 91. Orbital model interactions as proposed by Prof. Kahn and Briat

use of non-magnetic (dipolar) and electrostatic (exchange) nature of interaction. Two orbital models of interaction exist between localised electrons: a) weak interaction (localised electrons) suggested by Prof. Heitler and London b) strong interaction (delocalised electrons) predicted by Prof. Hund and Mulliken. Kahn and Briat model ( adjacent figure 91) ,Hay , Thibault and Hoffmann model and Anderson model were proposed to elucidate the orbital models of interaction between localised models.

For  $\{\text{Cu}_2(\text{OAc})_2(\text{H}_2\text{O})_2\}$  complex, singlet becomes the ground state.  $S=1$  and  $S=0$  are Separated in

### Exchange interactions can be very weak...



Michelangelo, Sixtin Chapel, Rome (Italy)

Figure 92. Effect of the sign of magnetic interaction on the fundamental energy state (singlet or triplet).

do this using Boltzmann distribution.

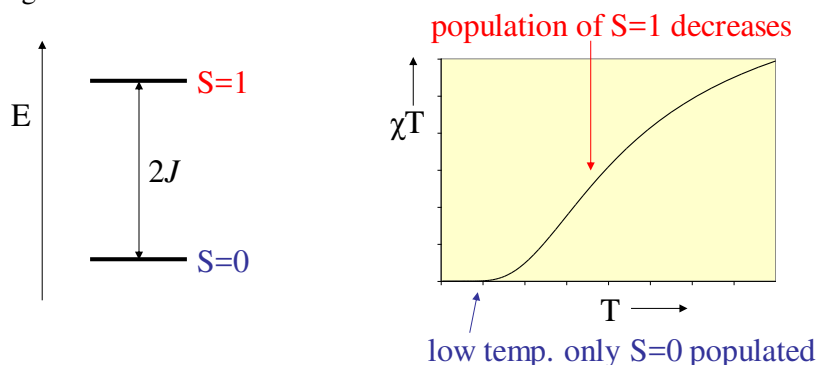


Figure 93. Diagram illustrating the exchange interaction between two spin energy levels and variation in the population with respect to change in the product of magnetic susceptibility and temperature ( $\chi T$ ) vs T curve.

For two interacting Cu(II) ions:  $S_A = S_B = \frac{1}{2} \rightarrow S' = 0, 1$ . The relative energies are  $E(0) = 0$  and  $E(1) = -J$  i.e. we have a spin-singlet state and a spin-triplet state separated by an energy gap  $J$ :

energy by  $2J$ , where  $J$  is the isotropic exchange (units  $\text{cm}^{-1}$  or K). For copper acetate monohydrate exchange coupling turns out to be very strong:  $2J = -240 \text{ K}$  (strong coupling).

It is fascinating to explore the thermal behaviour of the bulk sample: The two states represent two different magnetic moments i.e.  $\mu = \sqrt{g^2 S(S+1)}$ . Dimers in the  $S=1$  state have  $\mu = 2.83$  B.M. while  $S=0$  states possess  $\mu$  of 0 B.M. Towards the calculation of the average moment,  $\langle \mu \rangle$  and the magnetic susceptibility, we must know the numbers of clusters in the  $S=1$  and  $S=0$  states, and we can

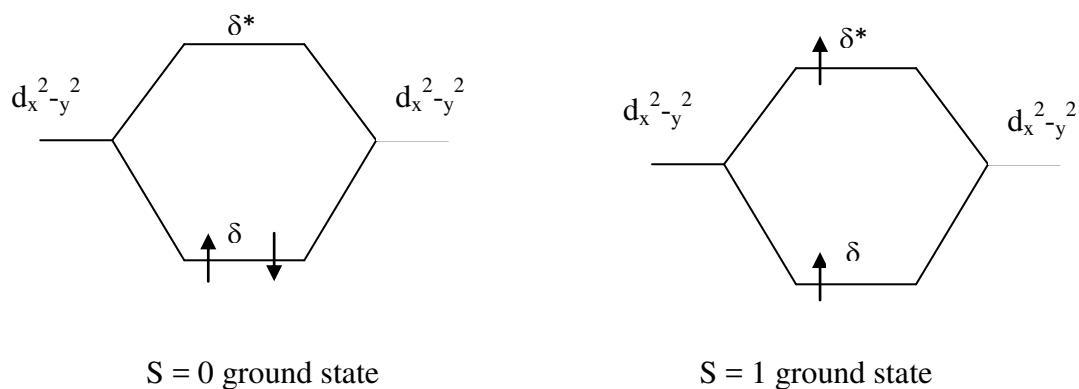


Figure 94. Showing  $\delta\delta^*$  overlap for square planar Cu(II), unpaired electron is in the  $d_{x^2-y^2}$  orbital

Which we can represent as:

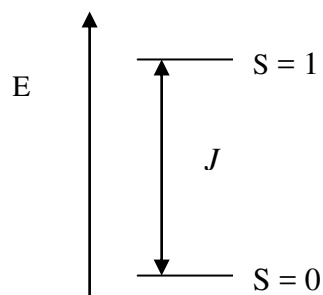


Figure 95. Ground and excited state energy level splitting with the mention of its corresponding  $S$  value.

When  $J < 0$ ,  $S' = 0$  is the ground state, *i.e.* the two unpaired electrons align oppositely in the ground state ( $A\uparrow, B\downarrow$ ) and the interaction is said to be antiferromagnetic.

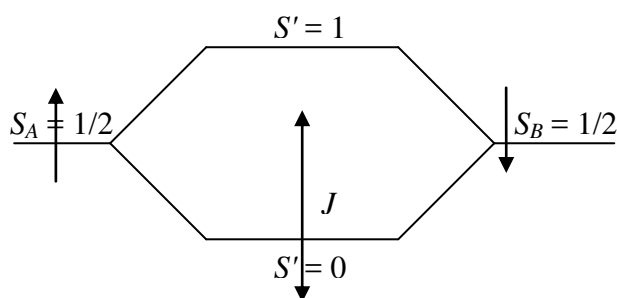


Figure 96. Schematic representation of antiferromagnetic interaction between two oppositely lying spin values.

When  $J > 0$ ,  $S' = 1$  is the ground state, *i.e.* the two unpaired electrons align parallel in the ground state ( $A\uparrow, B\uparrow$ ) and the interaction is ferromagnetic (much less common).

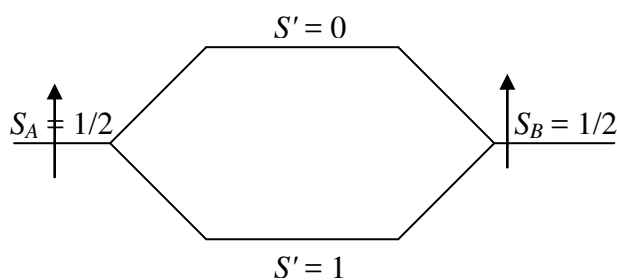


Figure 97. Schematic representation of ferromagnetic interaction between two parallelly lying spin values.

Thus, if  $kT \ll J$  (i.e. only the lowest spin state is populated) then the system will behave as an  $S = 0$  ( $\chi T = 0$ ) or 1 ( $\chi T \approx 1.1 \text{ cm}^3 \cdot \text{K} \cdot \text{mol}^{-1}$ ) object rather than the sum of two  $S = 1/2$  objects ( $\chi T \approx 2 \times 0.41 = 0.82 \text{ cm}^3 \cdot \text{K} \cdot \text{mol}^{-1}$ ).

l).

[Remember  $\chi T \approx \frac{g^2}{8} S(S+1)$  and  $\bar{g}_{Cu} \approx 2.1$ ]

### §15.3 Bleaney-Bowers Equation.

Consider antiferromagnetic case: Two  $S=1/2$  interacting

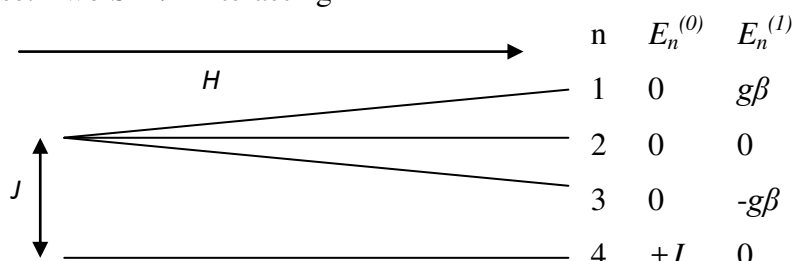


Figure 98. Splitting of the energy levels on application of magnetic field (H).

Remember:  $E_n = E_n^{(0)} + E_n^{(1)}H + E_n^{(2)}H^2$

Define energy of  $S' = 1$  state as  $E = 0$  (hence  $S' = 0$  has  $E = +J$ ), assume  $E_n^{(2)} = 0$ , and use Van Vleck equation:

$$\chi = \frac{N \sum_n \left( \frac{E_n^{(1)2}}{kT} - 2E_n^{(2)} \right) \cdot \exp\left(-\frac{E_n^{(0)}}{kT}\right)}{\sum_n \exp\left(-\frac{E_n^{(0)}}{kT}\right)} = \frac{N \sum_n \left( \frac{E_n^{(1)2}}{kT} \right) \cdot \exp\left(-\frac{E_n^{(0)}}{kT}\right)}{\sum_n \exp\left(-\frac{E_n^{(0)}}{kT}\right)}$$

$$\Rightarrow \chi = \frac{N \left[ \frac{g^2 \beta^2}{kT} \cdot 1 + 0 + \frac{g^2 \beta^2}{kT} \cdot 1 + 0 \right]}{\left[ 1 + 1 + 1 + \exp\left(-\frac{J}{kT}\right) \right]}$$

$$\Rightarrow \chi = \frac{2Ng^2\beta^2}{kT \left[ 3 + \exp\left(-\frac{J}{kT}\right) \right]} : \text{ This is known as Bleaney-Bower equation.}$$

Table 10. Shows variation in  $|J| / KT_{\max}$  with the changes in S value.

$S_A$	$ J  / KT_{\max}$
1/2	1.599
1	0.976
3/2	0.648
2	0.462
5/2	0.347

Using the Bleaney-Bowers equation we can predict the behaviour of  $\chi$  (and  $\chi T$ ) for ferromagnetic (positive  $J$ ) and antiferromagnetic (negative  $J$ ) interaction between the Cu(II) ions.

For any general spin-coupled system:

Plugging in the constants provides:

$$\chi = \frac{0.125g^2 \text{ emuK / mol}}{T} \frac{\sum_S S(S+1)(2S+1) \exp\left(\frac{-E_S}{k_B T}\right)}{\sum_S (2S+1) \exp\left(\frac{-E_S}{k_B T}\right)}$$

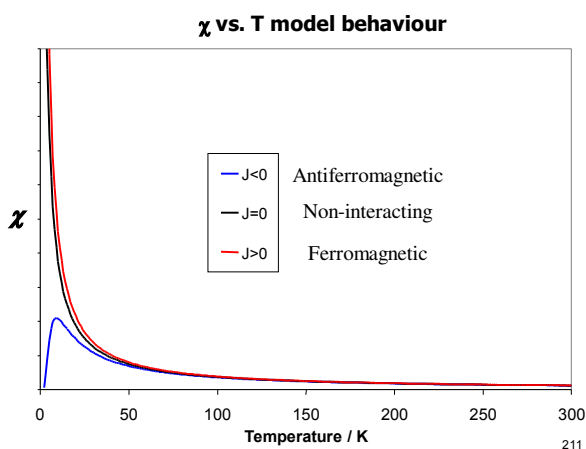


Figure 99. Prediction of magnetic properties based on Bleaney-Bowers equation.

temperature only the diamagnetic ground state is populated. The value of  $T_{max}$  can be used to estimate  $J$ , from the empirical relationship (only valid for  $S_A = S_B = 1/2$ ).

$$\frac{|J|}{kT_{max}} = 1.599 \quad \{ K = 0.695 \text{ cm}^{-1} \text{ K}^{-1} \}$$

Ratio  $|J| / kT_{max}$  relating the interaction parameter  $J$  and the temperature  $T_{max}$  for which a maximum

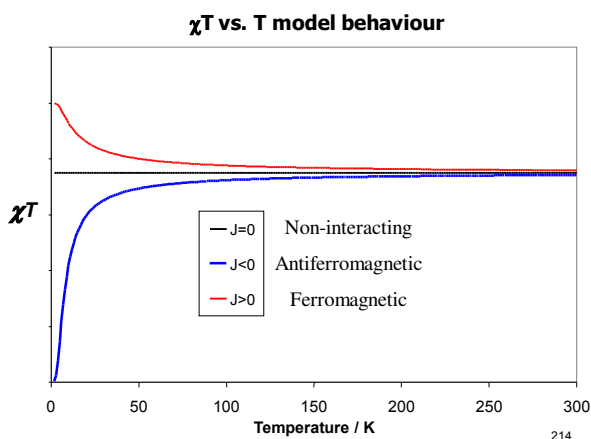


Figure 99. Elucidates  $\chi T$  vs.  $T$ :  $J=0 \rightarrow$  constant (Curie Law behaviour, with  $\chi T$  characteristic of the spin state of the monomer.

Using the Bleaney-Bowers equation we can predict the behaviour of  $\chi$  (and  $\chi T$ ) for ferromagnetic (positive  $J$ ) and antiferromagnetic (negative  $J$ ) interaction between the Cu(II) ions. The adjacent figure 99 describes  $\chi$  vs.  $T$ :  $J=0 \rightarrow$  Curie Law behaviour,  $J>0 \rightarrow \chi$  rises faster than expected from Curie Law. Not very different from  $J=0$  curve,  $J<0 \rightarrow \chi$  goes through a maximum at  $T_{max}$  and tends to

zero as  $T \rightarrow 0$ . This is a signature for antiferromagnetic coupling. At low

of  $\chi$  is observed for pairs of local spins  $S_A$  coupled antiferromagnetically.

$$\chi T \approx 2 \times \frac{g^2}{8} S_A(S_A + 1) \approx 0.75 \text{ cm}^3 \text{ K mol}^{-1}$$

$$\chi T \approx \frac{g^2}{8} S'(S' + 1) \approx 1 \text{ cm}^3 \text{ K mol}^{-1}$$

$J < 0 \rightarrow \chi T$  decreases continuously with  $T$   $J > 0 \rightarrow \chi T$  increases on cooling, reaching a plateau at low temperatures (diamagnetic excited state is fully depopulated), *i.e.* Curie Law at low  $T$  with  $\chi T$  characteristic of the ground spin state.

Practically, approach should be to measure experimental  $\chi$  vs  $T$  curve, followed by the determination of  $J$  by fitting of the experimental data to the Bleaney-Bowers equation with  $J$  as a variable.

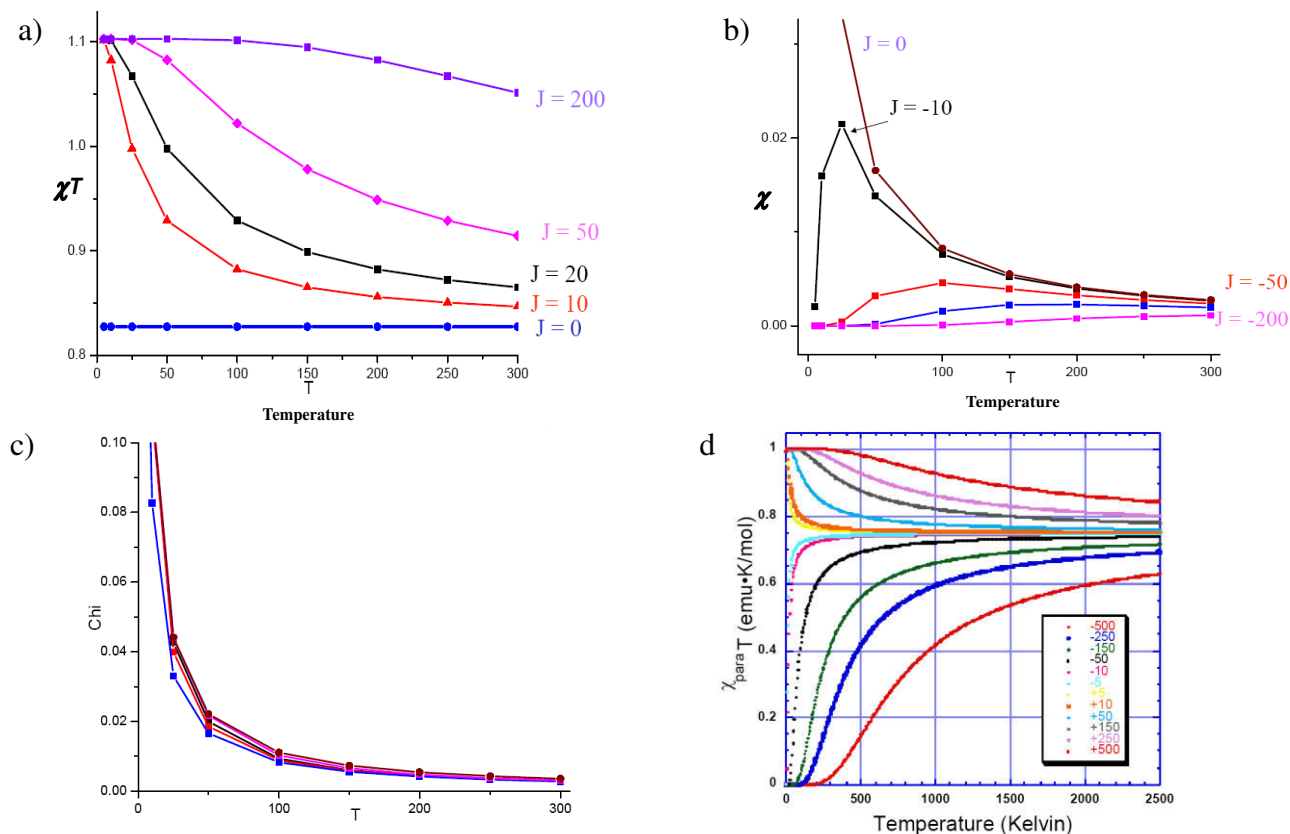


Figure 100 . (a) explanation of antiferromagnetic exchange in Copper dimer (b) explanation of ferromagnetic exchange in Copper dimer (c) ferromagnetic exchange in Copper dimer (d)  $\chi T$  vs  $T$  for  $-500 \text{ cm}^{-1} \leq J \leq +500 \text{ cm}^{-1}$ .

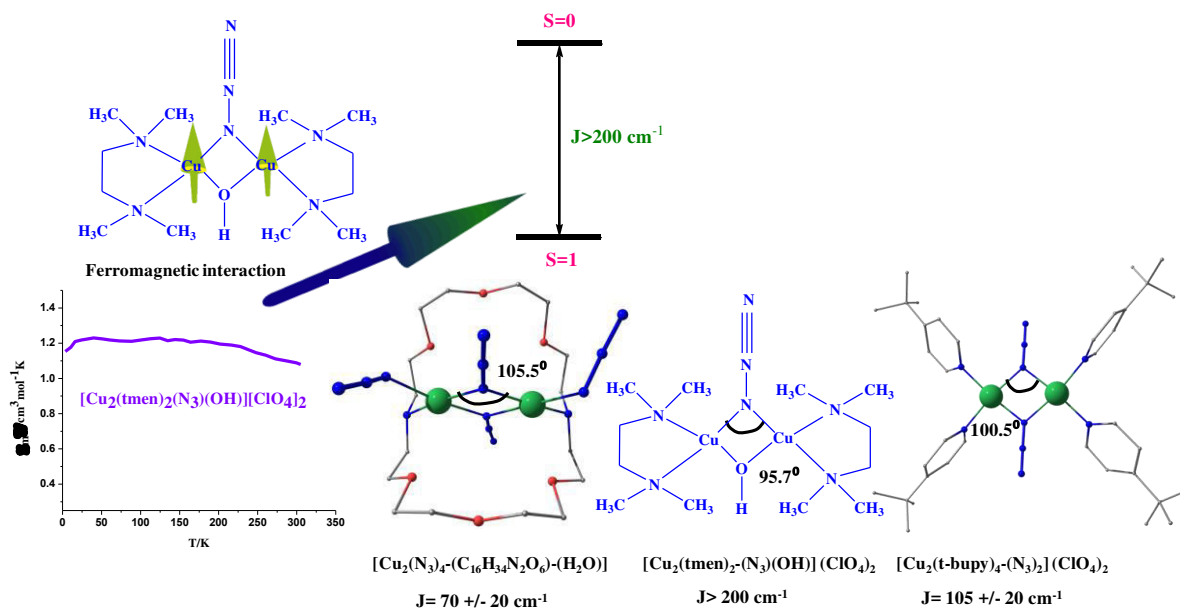




Figure 101. The above picture represents extremely strong ferromagnetic ( $>200 \text{ cm}^{-1}$ ) interaction for  $[\text{Cu}_2(\text{tmen})_2(\text{N}_3)(\text{OH})][\text{ClO}_4]_2$ .<sup>31</sup> Additionally, the other two crystal structures with formula  $[\text{Cu}_2(\text{t-bupy})_4(\text{N}_3)_2]^{30, 32}$   $(\text{ClO}_4)_2$  and  $[\text{Cu}_2(\text{N}_3)_4(\text{C}_{16}\text{H}_{34}\text{N}_2\text{O}_6)(\text{H}_2\text{O})]^{33}$  were also shown in order to gain deeper insights into the magnetic interaction. Furthermore, analysis on other similar type of bridged  $\text{Cu}_2$  dimers enables us to conclude the dependence of magnetic exchange ( $J$ ) on Cu-N-Cu bridging angle (i.e. decrease of Cu-N-Cu bridging angle results increase in  $J$  magnitude).

### §15.4 Other symmetrical dinuclear complexes.

Our previously mentioned Heisenberg-Dirac-Van Vleck (HDVV) Hamiltonian is valid for any pair of the interacting magnetic centres (possess local spins of  $S_A$  and  $S_B$ ) provided the local states lack first order angular momentum. The variations of  $\chi$  and  $\chi T$  as a function of  $T$  are qualitatively similar to those obtained with copper(II) dinuclear species. When  $J$  is negative, the ground state is diamagnetic and  $\chi$  represents a maximum at a finite temperature  $T_{\text{max}}$ . The ratio of  $|J| / K T_{\text{max}}$  as a function of local spin  $S_A (= S_B)$  is mentioned above in the tabular format.

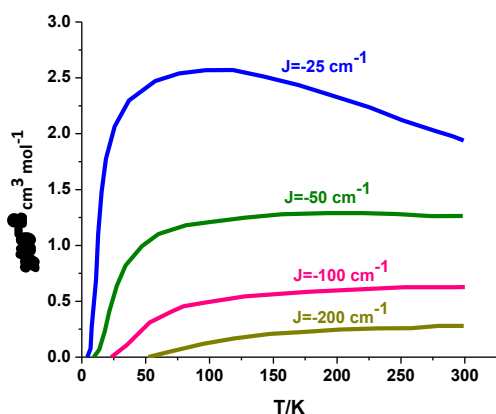
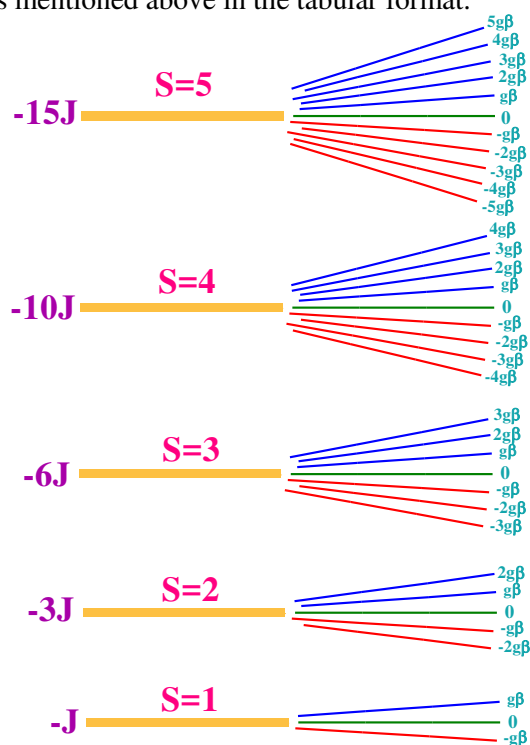


Figure 102. The figure below in the next page illustrates the example of the spectrum of the low-lying states and the first order Zeeman coefficients incorporated with the Zeeman perturbation in order to explicitly gain insight into the exchange parameter in a pair of local spins  $S_A =$

Figure 103.  $\chi$  vs  $T$  curves for a high spin Fe(III) dinuclear compound (containing symmetrical dinuclear units with more than two unpaired electrons) with various values of  $J < 0$ .

$S_B = 5/2$  {high spin Fe(II) or Mn(II)}.

The Zeeman factor is considered to be equal to 2. Such Fe(III)<sup>34</sup> high spin complexes can be cited by [Fe(salen)]<sub>2</sub>O which possess  $\mu$ -oxo derivatives with the Fe-O-Fe bridging linkage significantly

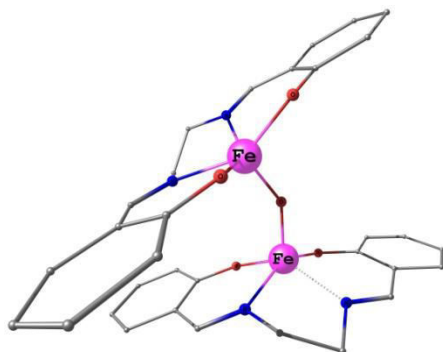


Figure 103. Crystal structure of [Fe(salen)]<sub>2</sub>O complex.

smaller than 180°(145°). The magnetic susceptibility of [Fe(salen)]<sub>2</sub>O<sup>35</sup> (structure shown beside below), corrected for the uncoupled impurity, continuously decreases on cooling from room temperature, characterizing a strong antiferromagnetic interaction. The energy levels are separated by multiples of  $J$  with higher level lies at  $S'J$  gap with respect to the ground level. The deduced  $J$  from magnetic as well as

theoretical data is found to be as  $-178 \text{ cm}^{-1}$  which is in well agreement with the observation for those classes of compounds possessing  $J$  in the range of  $170\text{-}230 \text{ cm}^{-1}$ . Most importantly, in these series of complexes  $J$  does not seem to be dependent on the small variation of bridging angle values. The reaction of [Fe(salen)]<sub>2</sub>O with (Me<sub>3</sub>Si)<sub>2</sub>S in DMF affords the  $\mu$ -sulfido compound [Fe(salen)]<sub>2</sub>S. The Fe-S-Fe angle, equal to  $121.8^\circ$ , is substantially smaller than the Fe-O-Fe angle. At equal bridging angles the antiferromagnetic interaction would be expected to be more pronounced in the  $\mu$ -sulfido than in the  $\mu$ -oxo derivatives, due to a stronger delocalization of the spin density toward the bridging atom in the sulfur-containing compound. If the bridge X remained the same, then a decrease of the Fe-X-Fe bridging angle should lead to a weaker antiferromagnetic interaction. Apparently, in the present case, the two factors almost exactly compensate each other. Indeed  $J$  in [Fe(salen)]<sub>2</sub>S was reported as  $-172 \text{ cm}^{-1}$ .

The mentioned magnetic data have been interpreted by neglecting the zero-field splittings within the excited magnetic states. Such an approximation is quite valid so long as the isotropic interaction is antiferromagnetic and the magnitude of the zero-field splitting is much smaller than that of the isotropic interaction. The EPR spectrum of  $\mu$ -oxalato-tetrakis(acetylacetonato)diiron(III) dissolved in a 1/1 toluene-chloroform mixture reveals a zero-field splitting of  $0.10(6) \text{ cm}^{-1}$  between the  $M_S = \pm 1$  and the  $M_S = 0$  components of the triplet state located at  $7.22 \text{ cm}^{-1}$  above the singlet ground state. The influence of this small effect on the  $\chi$  versus  $T$  plot is within the experimental uncertainties. Any zero-field splitting effect is obviously without influence on the magnetic susceptibility curve when  $-J$  is of the order of  $200 \text{ cm}^{-1}$ . To fit the magnetic data it was also assumed that the low-lying states rigorously respect the Lande interval rule:

$$E(S - 1) - E(S) = JS$$

This assumption has pitfalls for its strict usage in few compounds. This discrepancy can be dealt with the addition of biquadratic term to form the following equation:

$$H = -J S_A \cdot S_B + j (S_A \cdot S_B)^2$$

It has been proved that small value of  $j$  cannot be deduced from magnetic susceptibility data, even if they are very accurately measured.

### §15.5 Asymmetrical dinuclear complexes.

This case arises for heterodinuclear compounds possessing different  $S_A$  and  $S_B$  local spins and for either bimetallic compounds containing metal ions of the similar nature but in different environments or in species containing both a transition ion and an organic radical. It is noteworthy that, spin  $S$  changes monotonically versus the energy of the pair states with the system known as regular spin state structure. This regularity has further invoked the observation of correspondence between the nature of interaction and the shape of the  $\chi T$  vs  $T$  plot. In the absence of interaction ( $J = 0$ ),  $\chi T$  remains constant over the whole temperature range with a value (Curie Law) and if the interaction is antiferromagnetic ( $J < 0$ ), then the ground state has the smallest spin  $|S_A - S_B|$  and the most excited state possesses the highest spin  $|S_A + S_B|$ . Between these two limits  $S$  increases with the enhancement in energy.

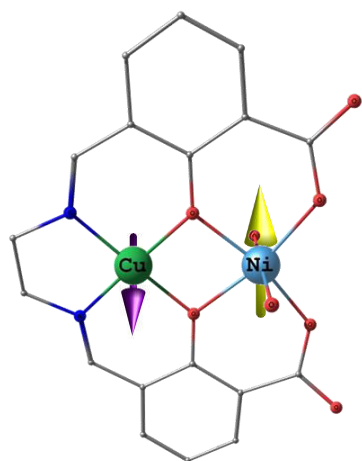


Figure 104. Crystal structure of  $\text{CuNi}(\text{fsa})_2\text{en}(\text{H}_2\text{O})_2$  with the aim to investigate magnetic properties.

Furthermore,  $\chi T$  consistently gets reduced upon cooling and approaches towards the low-temperature limit. Only in the  $S_A = S_B$  case, is the ground state diamagnetic, and the  $\chi$  versus  $T$  plot exhibits the characteristic maximum. Otherwise, although  $\chi T$  decreases on cooling,  $\chi$  continuously increases. If the interaction is ferromagnetic, the spectrum of the low-lying states is reversed.  $\chi T$  continuously increases on cooling and tends toward the low-temperature limit. It seems worthwhile to consider Cu(II)Ni(II) pair with  $S_{\text{Cu}}=1/2$  and  $S_{\text{Ni}}=1$  local spins in which  $g_{\text{Cu}}$  and  $g_{\text{Ni}}$  are isotropic with  $g_{\text{Cu}}$  and  $g_{\text{Ni}}$

principal values. We can easily procure the spin functions  $|S, M_S\rangle$  for the doublet and quartet pair states. This is noteworthy that,

for the aforementioned system  $M_S = \pm 1/2$  components arising from the doublet and quartet pair states couple through the Zeeman perturbation. For Cu(II)Ni(II) compounds, isotropic interaction leads to only two pair states owing to the local doublet nature of one of the interacting ions in the aforementioned complex. When the interaction becomes antiferromagnetic in nature, the ground state does not split in zero-field such that within the temperature range where solely this ground doublet is thermally populated the magnetic susceptibility should follow the Curie Law enabling accurate determination of average magnitude of  $g$ .

Example: Cu(II)Ni(II) and  $[\text{CuNi}(\text{fsa})_2\text{en}(\text{H}_2\text{O})_2]$

Cu(II)  $d^9$ ,  $S_A = 1/2$     Ni(II)  $d^8$ ,  $S_B = 1 \Rightarrow S' = 3/2, 1/2$

$$(\chi T)_{HT} = \frac{N\beta^2}{3k} [g_A^2 S_A (S_A + 1) + g_B^2 S_B (S_B + 1)]$$

for  $kT \gg |J|$

If  $J$  is anti-ferro then

$$(\chi T)_{LT} = \frac{Ng_s^2\beta^2}{3k} [(S_A - S_B)^2 + |S_A - S_B|]$$

Where  $g_s^2$  is the g-tensor of the GS. **AF exchange with  $J = -142 \text{ cm}^{-1}$**

$$(\chi T)_{LT} = \frac{Ng_s^2\beta^2}{3k} [(S_A + S_B)(S_A + S_B + 1)]$$

Exchange Hamiltonian ...

$$\hat{H} = - \sum_{i,j} J_{CuNi} \hat{S}_{Cu} \cdot \hat{S}_{Ni}$$

If  $J$  is ferromagnetic then,

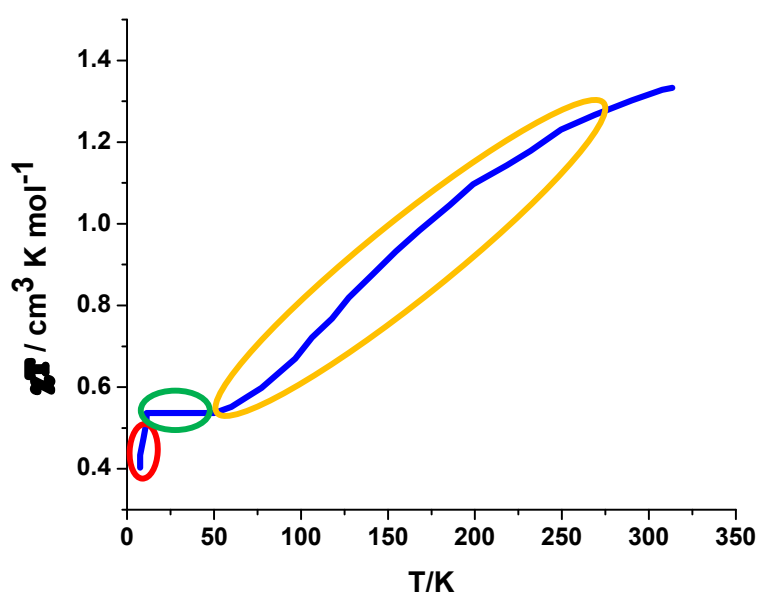


Figure 105. Product of Magnetic susceptibility and temperature vs Temperature plot for  $[\text{CuNi}(\text{fsa})_2\text{en}(\text{H}_2\text{O})_2]$

When  $\text{CuNi}(\text{fsa})_2\text{en}(\text{H}_2\text{O})_2$  complex is cooled down from 300K to about 60K,  $\chi T$  decreases, then reaches a plateau represented by  $\chi T = 0.52 \text{ cm}^3 \text{ mol}^{-1} \text{ K}$  which eventually decreases again below 16K. This observation can be explained as: the  $^2A_1$  state can be considered as ground level. Below 60K, the  $^4A_1$  excited energy level is totally depopulated in order to comply with the Curie law as expected for a spin Kramers doublet induced by zero-field splitting.

Calculate the  $(\chi T)_{LT}$  ....

Use  $S_A = 1/2$   $S_B = 1$  and  $g_A = 2.25$  and  $g_B = 2.25$   $N\beta^2/3k = 0.125$

$$\begin{array}{l}
 \text{AF} \quad (\chi T)_{HT} = \frac{N\beta^2}{3k} [g_A^2 S_A(S_A + 1) + g_B^2 S_B(S_B + 1)] \quad \chi T = 1.740 \\
 \text{Ferromagnetic} \\
 (\chi T)_{LT} = \frac{Ng_S^2 \beta^2}{3k} [(S_A - S_B)^2 + |S_A - S_B|] \quad \chi T = 0.47 \\
 (\chi T)_{LT} = \frac{Ng_S^2 \beta^2}{3k} [(S_A + S_B)(S_A + S_B + 1)] \quad \chi T = 2.373
 \end{array}$$

### §15.6 Influence of local anisotropy on the interacting ions.

For a system containing the local spin  $S_A$  (or  $S_B$ )  $> 1/2$ ; anisotropy presence will be felt. With predominant  $J$  values within a system, the pair states are well separated in energy from each other and zero-field splitting ( $D$ ) within the excited states could not play vital role in dictating the magnetic properties. Henceforth, consideration of ground state zero-field splitting is ample enough to affect the magnetic data in the low-temperature range. We can neglect the local anisotropy for singlet/doublet ground state given the large value of  $|J|$ . In order to illustrate the importance we can discuss one example: An antiferromagnetically coupled Cu(II)Fe(II) dinuclear compound possesses spins  $S_{Cu} = 1/2$  and  $S_{Fe} = 5/2$ . We can consider  $\text{FeCu}(\text{fsa})_2\text{en}(\text{CH}_3\text{OH})(\text{Cl})\cdot\text{CH}_3\text{OH}^{36}$  complex (structure shown below left hand side picture); The  $\chi T$  vs  $T$  curve for the complex (below right hand side figure) clearly describes the negative exchange interaction ( $J$ ) which gives rise to  $S=2$  ground state.

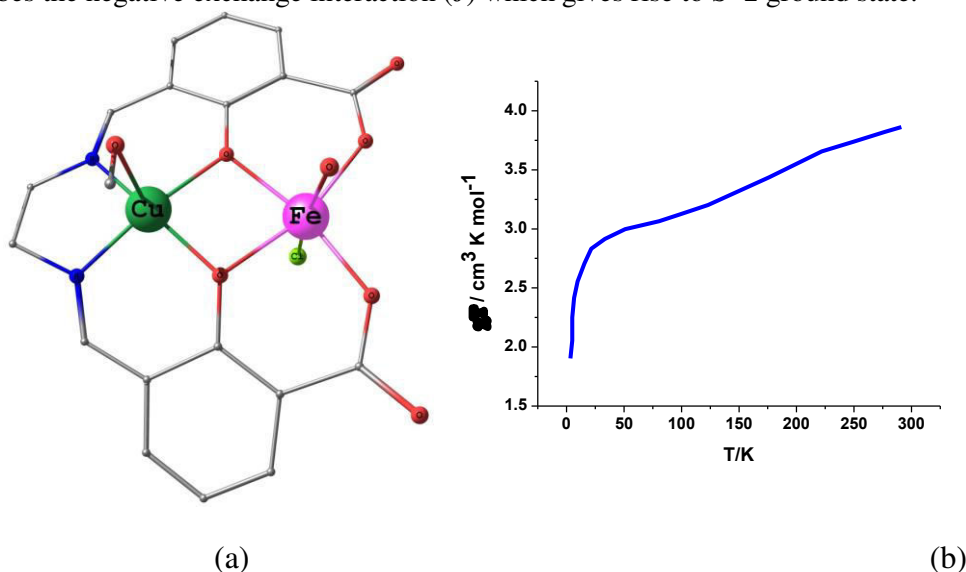
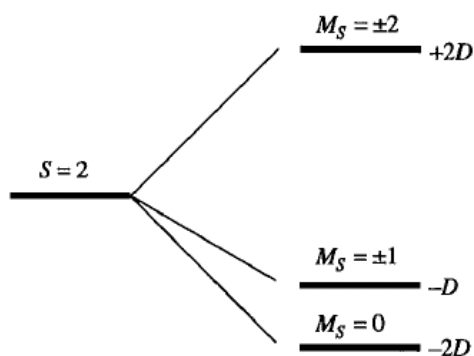


Figure 106. (a) Crystal structure of complex  $\text{FeCu}(\text{fsa})_2\text{en}(\text{CH}_3\text{OH})(\text{Cl})\cdot\text{CH}_3\text{OH}$  and (b)  $\chi T$  vs  $T$  curve for the same complex.

The  $S=2$  (GS is of quintet type) stable ground state will subsequently splits in zero field arising from the intrinsic zero-field splitting ( $D$ ) tensor contribution.



The principal magnetic susceptibilities in the system with zero-field splitting contribution can be calculated by adding the susceptibilities arising from the thermal population of the

Fig. 106. Energy level in absence of any magnetic field.

excited septet state to the parallel and perpendicular magnetic susceptibilities for the ground quintet state that axially splits in zero field. The  $\chi T$  vs  $T$  curve shows characteristic reduction of  $\chi T$  on cooling from room temperature which is an indicative of the depopulation of the septet excited state in favour of the quintet ground state. Abrupt decrease of  $\chi T$  below 30K can be explained by the zero-field splitting within the  $S=2$  state. The fitting of magnetic data gives rise to a zero-field splitting value ( $D$ ) of  $8 \text{ cm}^{-1}$  along with the quintet-septet separation of  $3J = -240 \text{ cm}^{-1}$ . If  $J$  is negative and sufficiently large with respect to the local anisotropies, only the zero-field splitting within the quartet ground state influences the magnetic properties. It is worth mentioning that, zero-field splitting pattern within the ground state can be confirmed by Mössbauer spectra analysis while the value of  $J$  in those system could be further corroborated by the temperature dependence of  $g$  anisotropy (Lande factor, dependence of spin-orbit coupling) observed in the EPR spectrum.

### §15.7 Biological Relevance.

Hemerythrin is a binuclear Fe containing respiratory protein which binds oxygen reversibly in the oxy form and has its corresponding most stable form as met. Met form possesses two Fe(III) centres bridged by an  $\mu$ -oxo group and two carboxyl bridges. The peripheral coordination in this form has been constituted by three histidine and an aspartate. This met form shows very strong antiferromagnetic coupling of  $-268 \text{ cm}^{-1}$ .

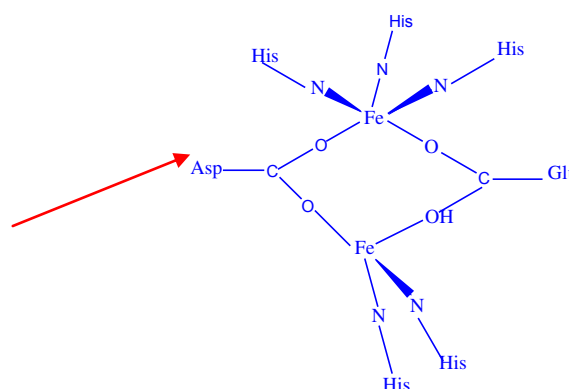
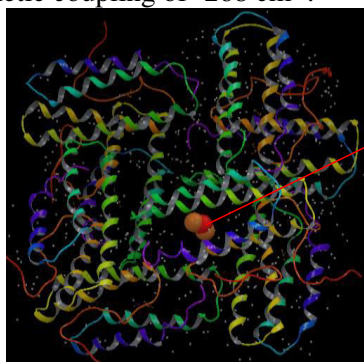
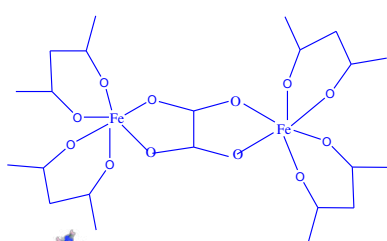
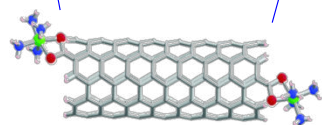


Figure 108. Exploring magnetic interaction in hemerythrin-dinuclear Fe containing protein

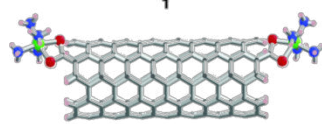
### §15.7 Longer Fe.....Fe distances.



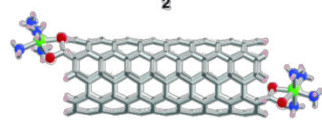
Fe.....Fe distance is  $5 \text{ \AA}$ , which shows relatively weak magnetic exchange of  $-7.2 \text{ cm}^{-1}$  .....In the quest of exploring dependence of  $J$  upon metal-metal distance we have investigated several other complexes which leads to the following tabular results:



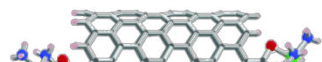
Fe...Fe distances	$J(\text{cm}^{-1})$	
24.7 Å	-208.9	metallic nanotubes



24.3	-204.1	metallic nanotubes
------	--------	--------------------



25.2	-255.6	metallic nanotubes
------	--------	--------------------

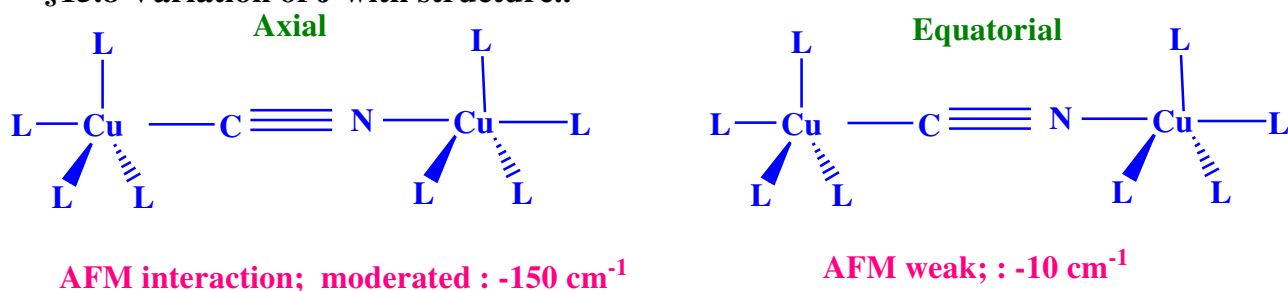


21.31	-115.7	
-------	--------	--

Figure 109. Variation of  $J$  with respect to the metal-metal (Fe-Fe) distance in the above shown Fe-Fe dimeric molecule.

We can conclude that  $|J|$  is not directly proportional/correlated to the Fe---Fe distances. Instead it is affected by the extent of well-organised propagation of unpaired electron by the bridge ( $\pi$  electrons, aromatic groups, diffuse orbitals tend to delocalise electrons to a long M...M distances..)

### §15.8 Variation of $J$ with structure..



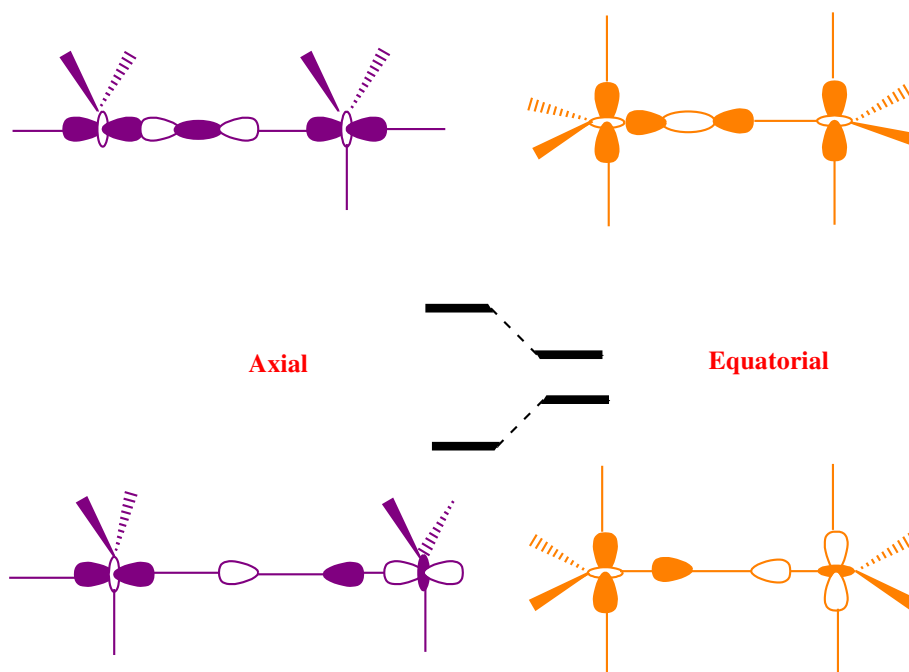
Computed (models)

(i) Equatorial : AFM;  $-19 \text{ cm}^{-1}$

(ii) Axial : AFM;  $-103 \text{ cm}^{-1}$

**Experimental**

**Orbital Interpretation:**



### §15.9 Mechanism of exchange interaction.

There exists two different kind of mechanisms:

(i) Direct exchange: It occurs via direct overlap of the atomic orbitals containing the unpaired electron. This exchange arises owing to the direct bonding leading to pairing of electrons on same orbital subsequently giving rise to antiferromagnetic exchange interaction. For direct exchange the interaction proceeds without the requirement for an intermediate atom. It is worth mentioning that, this type of exchange cannot be very important due to insufficient overlap between the neighbouring magnetic orbitals. For lanthanide containing complexes, observation of direct exchange is rare due to close proximity of 4f electrons to the nucleus. This entails the consideration of another type of exchange interaction.

Example:

$[\text{MO}_2\text{L}^6]^{n+}$ ,  $M = \text{Mo(V)}, \text{V(IV)}$   $\{\text{M}=\text{O}\}$  Square pyramidal about metal,  $d^1$  with single unpaired electron in  $d_{xy}$

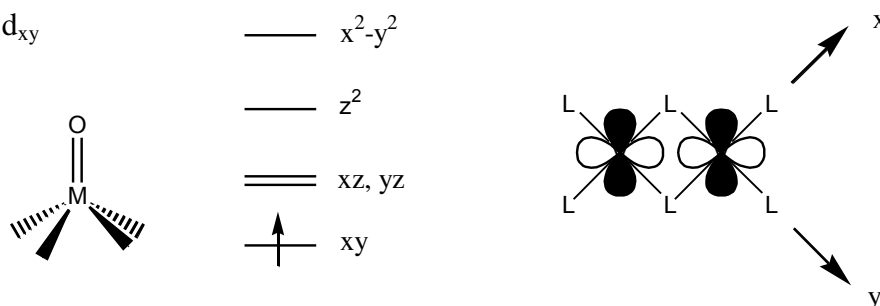


Figure 110. d-orbital splitting in a square-pyramidal complex with metal possessing one unpaired electron(3d transition metal).

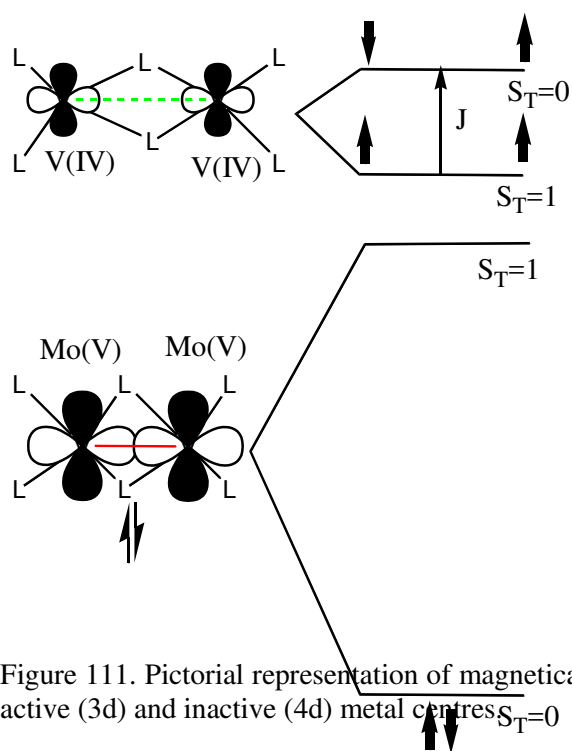


Figure 111. Pictorial representation of magnetically active (3d) and inactive (4d) metal centres  $S_T=0$

When  $M = \text{V}$ :  $\text{V} \dots \text{V}$  distance ca.  $3\text{\AA}$ , too large for large direct  $xy/xy$  overlap, therefore  $S = 0$  ground state with thermally accessible  $S=1$  excited state.  $\chi$  vs.  $T$  goes through maximum. When  $M = \text{Mo}$ : 4d orbitals much bigger than 3d, therefore much greater  $xy/xy$  overlap and  $J$  much bigger than for V and  $\gg kT$ . No thermal population and diamagnetic at room temperature. The super exchange dominates whenever a 3d metal ion is involved.

Even a mixture of 3d-4d or 3d-5d or 3d-4f often exhibit super-exchange type interactions and are therefore magnetically **ACTIVE**. On the other hand, due to diffuse nature of 4d and 5d orbitals (second and third row TM metals). 4d and 5d transition metals form metal-metal

bond via direct exchange and are in general diamagnetic and magnetically **INACTIVE**.



(ii) **Superexchange**: This is an interaction between non-neighbouring magnetic ions being mediated by a non-magnetic ion placed between the magnetic ions.

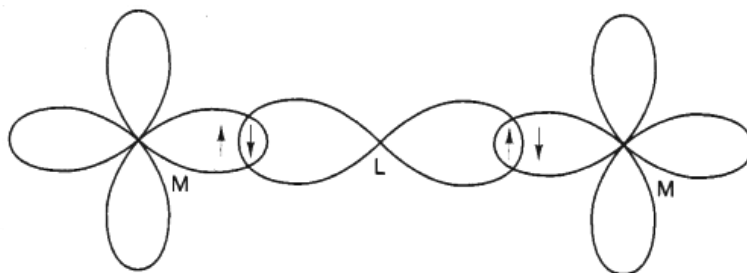


Figure 112. Pictorial representation of superexchange interaction.

This interaction is dependent on the degree of overlap of orbitals which induces strong dependence of superexchange on the angle of the M-L-M bond (eg. M-O-M) and the bridging ligand to metal distance.

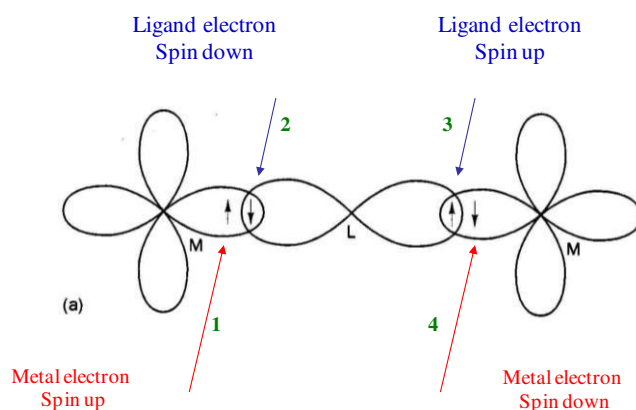


Figure 113. The above schematic diagram denotes superexchange interaction between two identical metal sites with orbitals lying at  $180^\circ$  with respect to each other (M-O-M bond angle =  $180^\circ$ ). This arrangement has resulted antiferromagnetic coupling between the two metal sites.

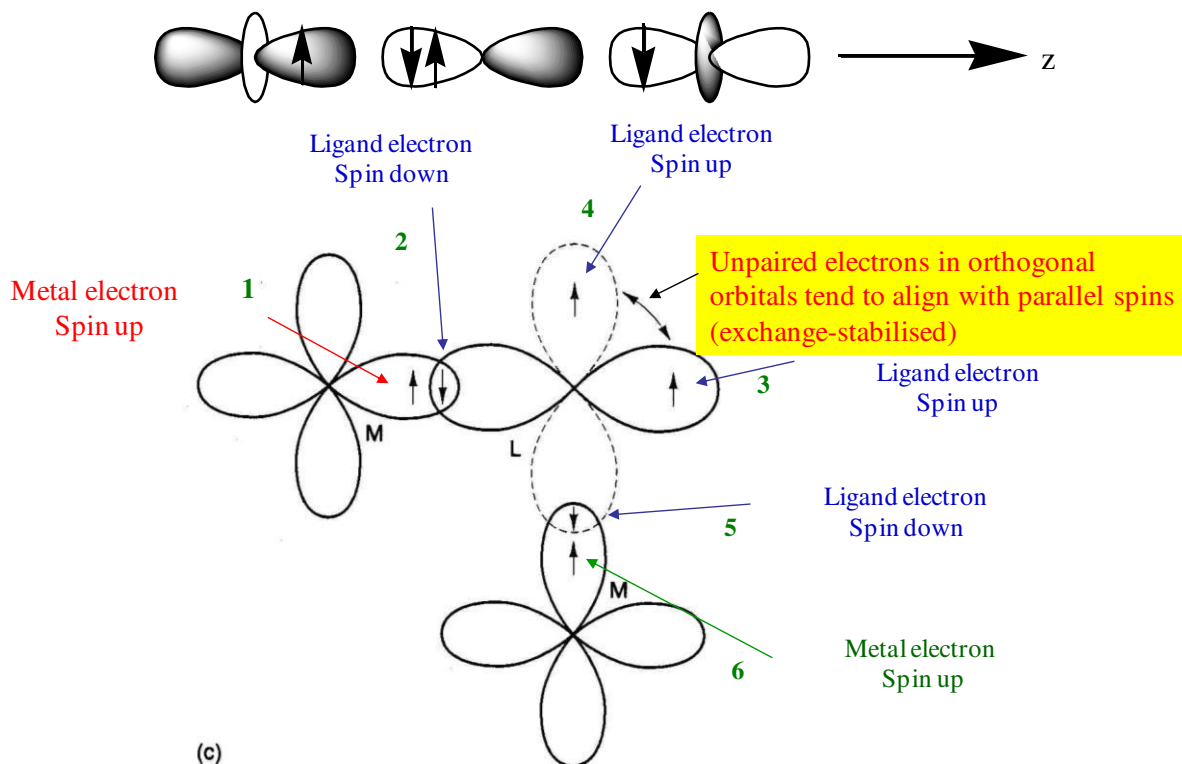
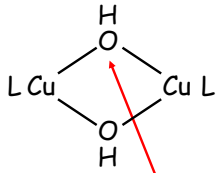


Figure 114. The above schematic diagram denotes superexchange interaction between two identical metal sites with orbitals lying at  $180^\circ$  with respect to each other ( $M-O-M$  bond angle =  $90^\circ$ ). This arrangement has resulted ferromagnetic coupling between the two metal sites. This pathway incorporates two p orbitals on the same atom.

Table. Elucidating variation in magnetic interaction on M-O-M angle:



Complex	$\phi_{\text{Cu-O-Cu}}$ , deg	$2J$ , $\text{cm}^{-1}$
$[\text{Cu}(\text{bpy})\text{OH}]_2(\text{NO}_3)_2$	95.6 (1)	+172
$[\text{Cu}(\text{bpy})\text{OH}]_2(\text{ClO}_4)_2$	96.6 (2)	+93
$[\text{Cu}(\text{bpy})\text{OH}]_2\text{SO}_4 \cdot 5\text{H}_2\text{O}$	97.0 (2)	+49
$[\text{Cu}(\text{eaep})\text{OH}]_2(\text{ClO}_4)_2$	98.8-99.5 (3)	-130
$\beta$ - $[\text{Cu}(\text{dmaep})\text{OH}]_2(\text{ClO}_4)_2$	100.4 (1)	-200
$[\text{Cu}(\text{tmen})\text{OH}]_2(\text{ClO}_4)_2$	102.3 (4)	-360
$[\text{Cu}(\text{teen})\text{OH}]_2(\text{ClO}_4)_2$	103.0 (3)	-410
$[\text{Cu}(\text{tmen})\text{OH}]_2\text{Br}_2$	104.1 (2)	-509

The above figure describes superexchange interaction between two interacting metal sites given the M-O-M bond angle to be larger than  $90^\circ$  for di-hydroxo bridged Cu(II) dimeric complexes and also we have shown in the tabular form dependence of magnetic exchange upon M-O-M angle. This to some extent enables us to conclude our previous statement that exchange interaction becomes antiferromagnetic with the enhancement of M-O-M bond angle i.e. lower angle prefers the occurrence of ferromagnetic exchange.

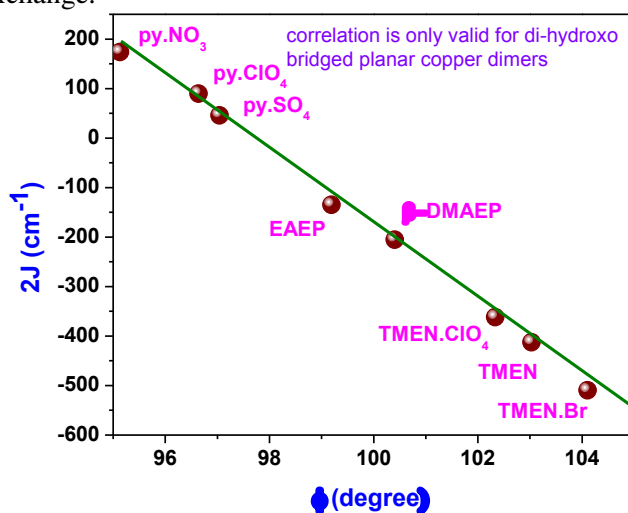


Figure 115. Figure showing variation strength of magnetic exchange upon change in the bond angle for different di-hydroxo bridged planar copper dimeric complexes.

Superexchange interaction between two different metal centres: unpaired electrons in orthogonal orbitals tend to align with parallel spins leading to exchange stabilised system.

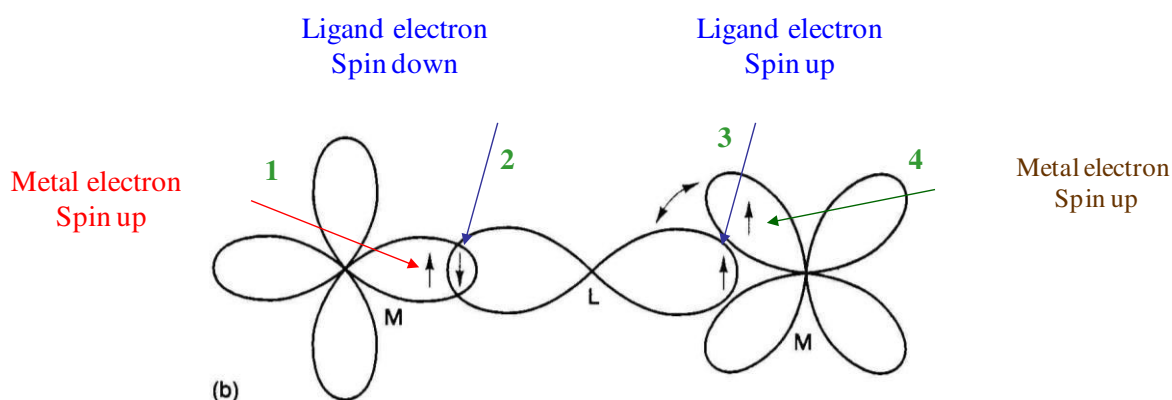


Figure 116. The above arrangement generates ferromagnetic coupling between the two metal ions. Superexchange interaction arises from the orthogonality between the  $d^9$   $\text{Cu}^{2+}$  unpaired electron of an  $e_g$  orbital  $d_{x^2-y^2}$  and  $d^1$   $\text{VO}^{2+}$  unpaired electron in a  $t_{2g}$  orbital in a binuclear compound containing  $\text{Cu}(\text{II})$  and  $\text{V}(\text{IV})$  metal centres .

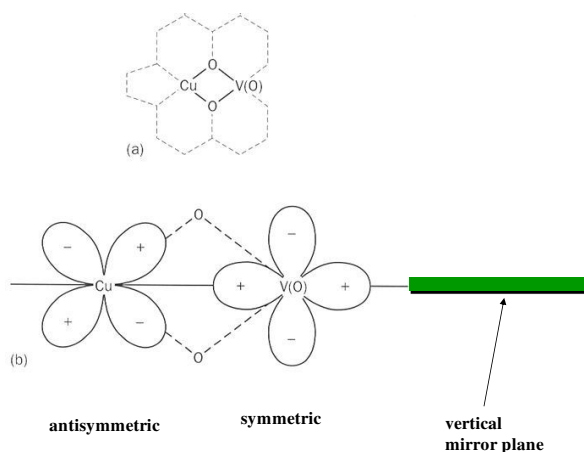


Figure 117. Schematic illustration of superexchange interaction between  $\text{Cu}(\text{II})$  and  $\text{V}(\text{IV})$  metal sites in the dimeric complex through orbital diagram.

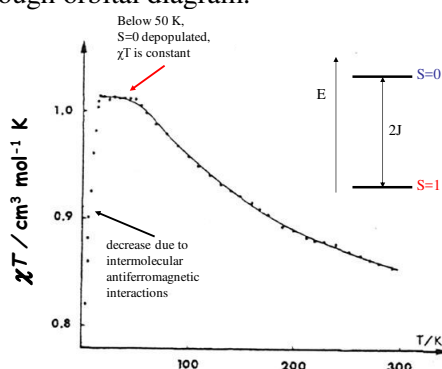


Figure 118. Explanation of the observed  $\chi T$  vs T plot for the compound  $[\text{Cu}(\text{VO})\text{L}.\text{MeOH}]$

Now, if we consider homometallic binuclear system i.e.  $\text{Cu}_2\text{L}.\text{MeOH}$ , we will discuss about the observed antiferromagnetic exchange interaction.

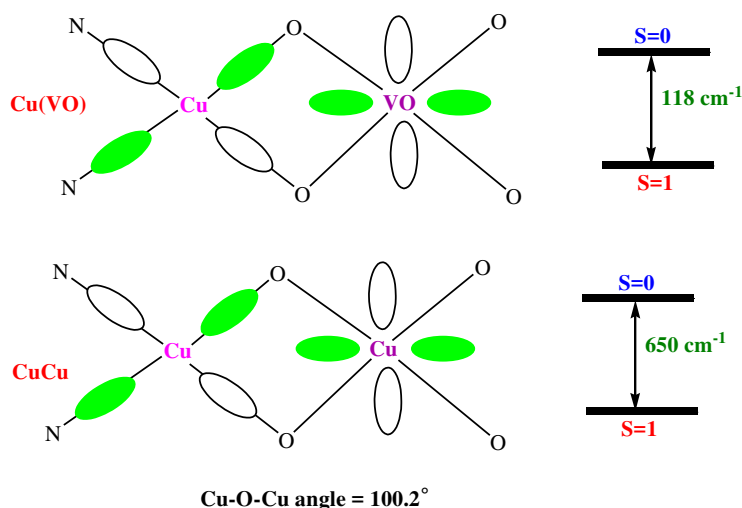


Figure 119. Antiferromagnetic exchange interaction in Cu-Cu dinuclear complex ( $S=0$  is the ground state) as compared to Cu-V analogue where ferromagnetic interaction is corroborated by stabilised  $S=1$  energy state.

Orthogonality condition between the involved metal centres is the pivotal part to induce superexchange interaction between the respective sites. Attentive selection of metal ion and bridging ligands can instigate orthogonal step which subsequently leads to the occurrence of ferromagnetic coupling between the two metal centres. However, in most cases the coupling between two linked metal atoms, each with unpaired electrons, will contain at least one antiferromagnetic coupling pathway – a pathway involving non-orthogonal orbitals, and perhaps a ferromagnetic coupling pathway through another orbital sequence...In such cases the antiferromagnetic coupling often dominates, making the design of large molecules which display purely ferro-magnetic exchange difficult.

We need to consider magnetic exchange for system where overall  $S > 1/2$  and in relevance to this we consider a reference axis and assume  $C_{2v}$  point group.

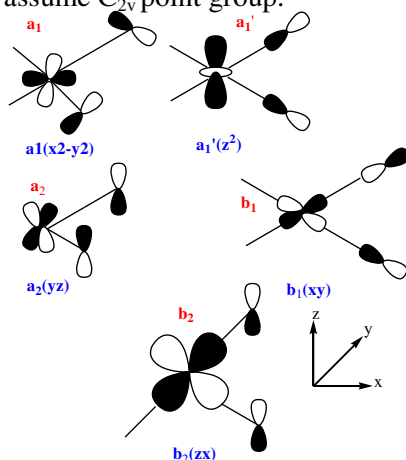


Figure 120. Schematic description of the symmetry representation labels for the five d orbitals of a transition metal ion.

Based on the above symmetry label representation of the five d orbitals, we need to gain further insights into the exchange interaction between different combination of such symmetry orbitals. i.e.

i)  $a_1 \dots a_1$  interaction:

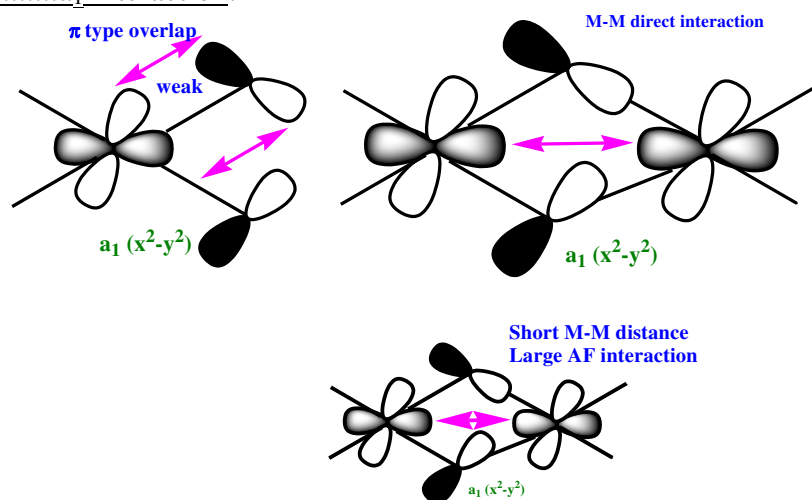


Figure 121. From above figure, we can comment that, net  $J_{a_1 a_1}$  is always AF in nature independent of the bridge composing the molecule.

ii)  $a_1 \dots a_1$  interaction:

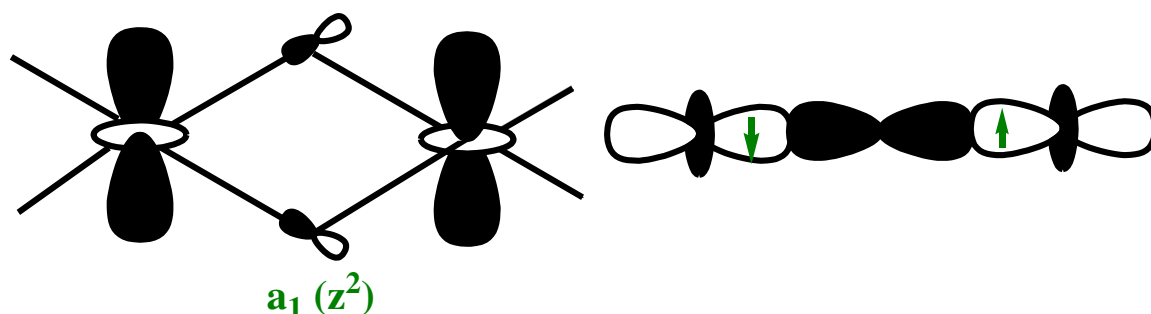
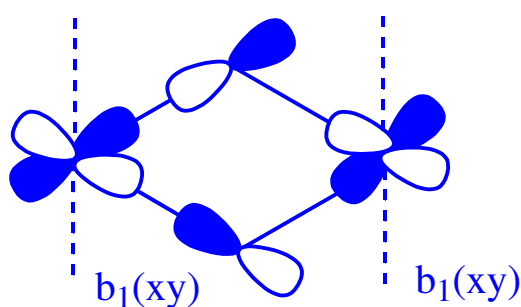


Figure 122. Effect of M-X-M bridging angle upon magnetic exchange interaction.

This interaction is very weak and contribution can be ignored. This is actually  $\sigma$ -type interaction occurs through the metal-metal bridges. This is typically ferromagnetic when M-X-M bridging angle is  $90^\circ$  while it changes to AFM nature for  $M-X-M > 90^\circ$ . So, we can conclude that this interaction is weak F/AF independent of the bridging angle.



iii)  $b_1 \dots b_1$  interaction:

This is not direct interaction and string  $\sigma$ -type through M-X-M bridges. This type of interaction is strongly FM when M-X-M is  $90^\circ$  while it is strongly AF in nature when angle  $> 90^\circ$ . So, we can conclude that this interaction is strongly

Figure 123. Significant strong  $\sigma$  type interaction between two metal sites.

F/AF independent of the bridging angle.

iv)  $b_2 \dots b_2$  and  $a_2 \dots a_2$  interaction:

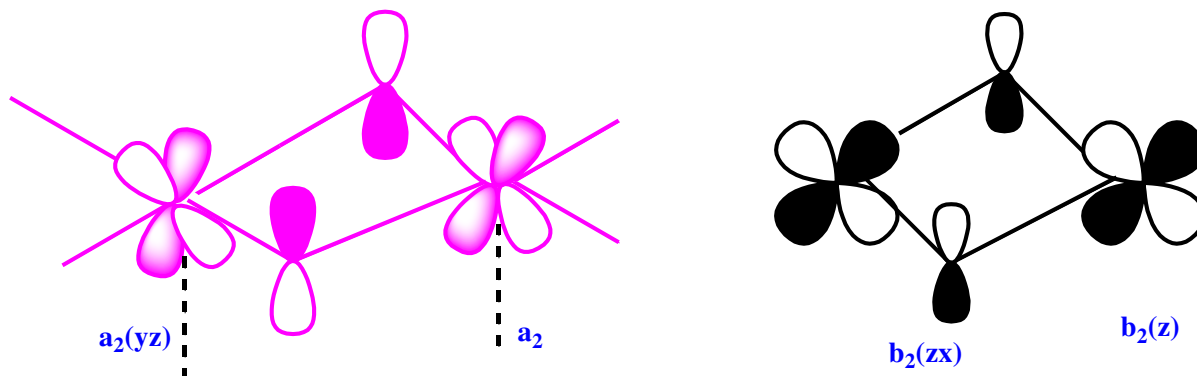


Figure 124. Pictorial depiction of weak  $\pi$  type interaction.

This is weak  $\pi$ -type interaction through M-X-M bridges. These two type of interactions are always weakly AF and no ferromagnetic contribution towards these type of interactions.

Table. Prediction of the nature and of the order of magnitude for contributions  $J_{\mu\nu}$  involving pairs of magnetic orbital:

$J_{\mu\nu}$	$a_1$	$a_1'$	$a_2$	$b_1$	$b_2$
$a_1$	AFm	AFm	Fw	Fs	Fw
$a_1'$		From Fw o AFw	Fw	Fw	Fw
$a_2$			AFw	Fw	Fw
$b_1$				From Fs to AFs	Fw
$b_2$					AFw

F : ferromagnetic ; AF:antiferromagnetic. The subscripts are w:weak; m:medium; s:strong

### §15.10 Examples.

a)  $d^3 - d^3$  in octahedral environment: ( $t_{2g}^3$ )-( $t_{2g}^3$ ) interaction:  $a_1, a_2$  and  $b_2$  orbitals are involved.

$$J = 1/9(J_{a_1 a_1} + J_{a_2 a_2} + J_{b_2 b_2} + 2J_{a_1 a_2} + 2J_{a_1 b_2} + 2J_{a_2 b_2})$$

Where  $J_{a_1 a_1}$  signifies medium AFM interaction;  $J_{a_2 a_2}$  and  $J_{b_2 b_2}$  symbolizes weak AFM interaction while notably,  $2J_{a_1 b_2} + 2J_{a_2 b_2}$  terms illustrate very weak FM interaction. In presence of prevalent  $J_{a_1 a_1}$  contribution magnetic exchange can be considered to be as AF in nature and will be governed by angle .i.e. many  $Cr_2O_2$  complexes are known to exhibit AFM interaction.

$J_{\mu\nu}$	$a_1$	$a_1'$	$a_2$	$b_1$	$b_2$
$a_1$	AFm	AFm	Fw	Fs	Fw
$a_1'$		From Fw o AFw	Fw	Fw	Fw
$a_2$			AFw	Fw	Fw
$b_1$				From Fs to AFs	Fw
$b_2$					AFw

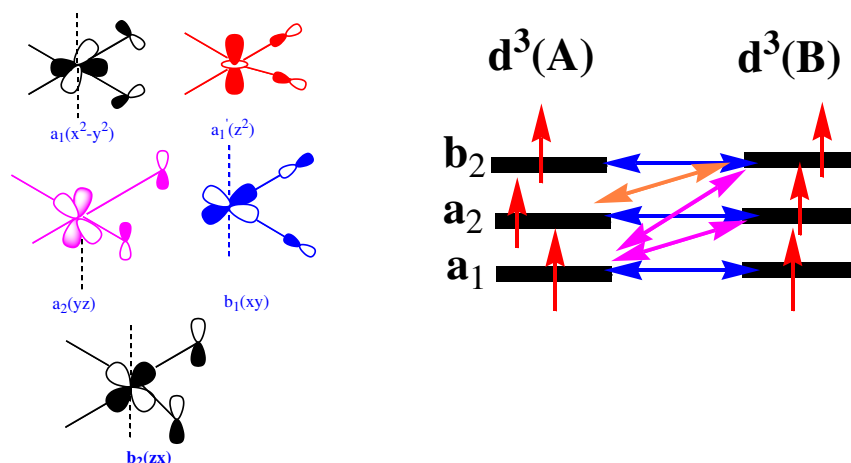


Figure 125. pictorial representation of the weak F/AF magnetic interaction using orbital diagram.

b)  $d^5-d^5$  in octahedral environment:

In this scenario,  $(t_{2g}^3)(e_g^2)-(t_{2g}^3)(e_g^2)$  interaction:  $a_1, a_1', a_2$  and  $b_2$  orbitals are involved.

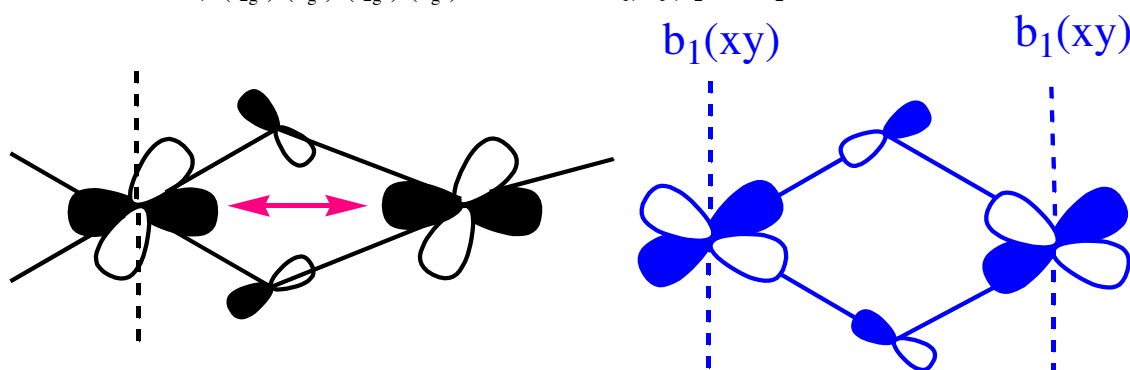


Figure 126. Orbital diagram explaining the involvement of interaction in  $d^5-d^5$  octahedral ligand field environment.

Among all the magnetic interactions mentioned before,  $J_{a_1a_1}$  will be considered as AFM for bridging angle  $90^\circ$  while  $J_{b_1b_1}$  will remain as FM. For magnetic interactions between two metals with electronic configuration of  $d^5$ , preponderant interaction is AFM in nature owing to its competing nature. Short metal-metal bond distance and larger M-X-M bond angle strongly favours the presence of AFM exchange interaction.

c)  $d^8-d^8$  in octahedral environment:

$$J = 1/4(J_{a_1'a_1'} + J_{b_1b_1} + 2J_{a_1'b_1})$$

Both  $J_{a_1'a_1'}$ ,  $J_{b_1b_1}$  depending on the M-X-M angle. Third term is weakly Ferro.

**At angle close to  $90^\circ$ , Ni(II) compounds thus exhibit Ferromagnetic interaction**

d)  $d^9-d^9$  in octahedral environment:

$$J=J_{b_1b_1} \quad \text{Depending on the M-X-M angle } \theta \text{ or } \phi \text{ or } \alpha.$$

e)  $d^3-d^4$  in octahedral...pseudo-octahedral environment:

There are 12 interactions possible.

Dominant terms will be  $J_{a_1a_1}$  and  $J_{a_1a_1'}$  .... Both AF so generally  $J$  is AF.

f)  $d^3-d^8$  in octahedral environment:

$(t_{2g})^3-(t_{2g})^6(e_g)^2$  ORBITALS:  $a_1, a_2, b_2$  for  $d^3$  and  $a_1, b_1$  for  $d^8$ .

So

$$J=1/6(J_{a_1'a_1'} + J_{a_1b_1} + J_{a_2a_1'} + J_{a_2b_1} + J_{b_2a_1'} + J_{b_2b_1})$$

Except  $J_{a_1a_1'}$  all terms are strictly positive So dominant **Ferromagnetic** interaction.

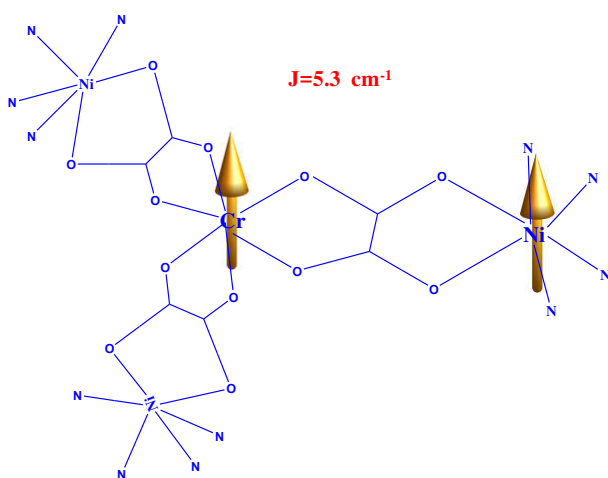


Figure 127. Crystal structure of  $\{Cr[ox]Ni(Me_6-[14]ane-N_4)\}_3^{3+}$

The magnetic susceptibility performed on tetranuclear cation [see adjacent figure 127,  $Cr[ox]Ni(Me_6-[14]ane-N_4)_3^{3+}$  [where Ox= oxalate and  $Me_6-[14]ane-N_4 = \pm 5,7,7,12,14,14$ -hexamethyl-1,4,8,11-tetraazacyclotetradecane]<sup>37</sup> clearly reveals the presence of Cr(III)-Ni(II) ferromagnetic interactions which gives rise to the ground spin state of  $S=9/2$ . In this complex, three unpaired electrons in Cr(III) lies in  $t_{2g}$  orbitals while the two unpaired electrons of Ni(II) is located in the  $e_g$  orbital having octahedral symmetry. In the  $C_{2v}$  symmetry of each Cr-Ni bridging, the  $t_{2g}$  and  $e_g$  orbitals lie at orthogonal<sup>38</sup>

position which leads to the ferromagnetic interaction between the ions.

g)  $d^3-d^9$  in octahedral environment:

$$J=1/3(J_{a_1b_1} + J_{a_2b_1} + J_{b_2b_1})$$

All terms are positive, leading to Ferromagnetic  $J$ . The dominant contribution arises from  $J_{a_1b_1}$ . Beside

is the molecular structure of  $[Cr(Me_6-[14]ane-N_4)(OH)_2Cu(bpy(MeOH))]^{3+}$  which shows strong ferromagnetic interaction ( $J=200 \text{ cm}^{-1}$ ) between its two metal sites owing to the orthogonality of the magnetic orbital centred on the Cr(III) and Cu(II) ions.

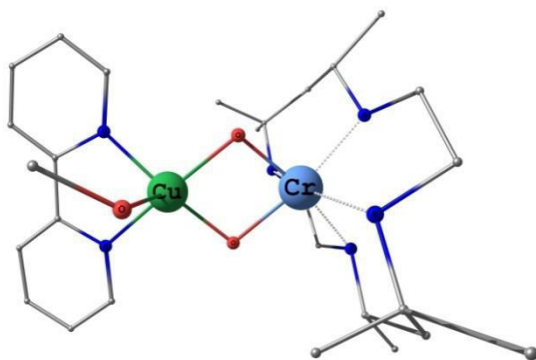


Figure 128. Crystal structure of  $[Cr(Me_6-[14]ane-N_4)(OH)_2Cu(bpy(MeOH))]^{3+}$

h)  $d^4-d^5$  in octahedral environment: possesses competing FM and AFM interaction and sign of the



magnetic exchange is directly correlated to M-X-M bridging angle.

i)  $d^4$ -  $d^9$  in octahedral environment: In this combination, FM exchange predominates along with orthogonality of the concomitant orbitals. Following is a table describing dependence of F/AF interaction on number of unpaired electrons in d orbital.

	$d^3$	$d^4$ elongated	$d^5$	$d^8$	$d^8$ elongated
$d^3$	AF ← AF	AF	AF	F	F
$d^4$ elongated	AF	AF ← AF	F	F	F
$d^5$			AF/F → AF	F → AF	F → AF
$d^5$				F → AF	F → AF
$d^9$ elongated				F → AF	

j)  $d^3$ -  $d^3$  in octahedral environment: Under this situation, interaction becomes more AFM upon enhancement of M-X-M bridging angle from  $90^\circ$ .

k)  $d^8$ -  $d^8$  in octahedral environment: Under this situation, interaction becomes more AFM upon enhancement of M-X-M bridging angle from  $90^\circ$ . It seems worthwhile to mention that, FM contribution arises from cross interaction between singly occupied orbital and empty orbital.

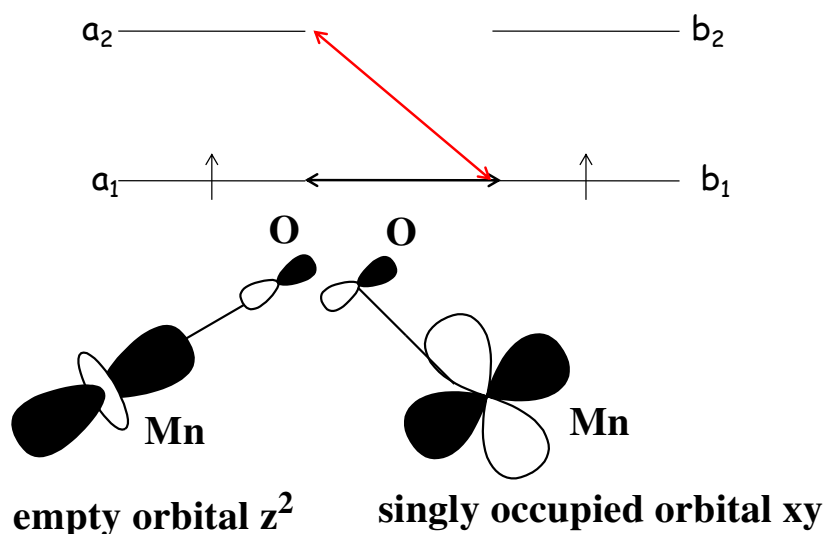


Figure 129. Above diagram represents singly occupied and empty orbitals in  $[LMnO(CH_3O_2)MnL]^{2+}$  whose interaction invoke the explanation of weak ferromagnetic interaction.

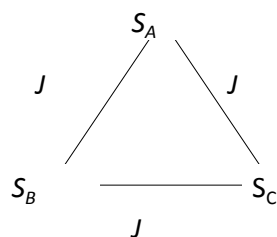
### §15.11 Magnetic interaction in trinuclear and higher clusters.

HVV Hamiltonian is still valid but need to consider interactions between each pair of interacting paramagnetic ions. where  $J_{ij}$  is the exchange integral between the two centres

$$H = \sum -J_{ij} \hat{S}_i \cdot \hat{S}_j \quad i \text{ and } j \text{ and } E \text{ represents relative energies between states as before.}$$

$$E(S') = -\frac{J}{2} S'(S'+1)$$

Trinuclear complexes: e.g.  $[\text{Cu}_3(\text{pao})_3(\text{OH})]^{2+}$ ;  $^{39}\text{C}_3$  symmetry



For the aforementioned complex, the twofold orbitally degenerate term  $2E$  is found to be thermally populated. The excited triplet level lies at  $1000\text{ cm}^{-1}$  above the ground state.

We can consider this as an additive problem: combine  $S_B$  and  $S_C$  to give “intermediate” spin states  $S^*$ :  
 $S^* = (S_B + S_C), (S_B + S_C - 1), \dots, |S_B - S_C| = 1, 0$

Then combine  $S_A$  with all possible values of  $S^*$  to give the total spin states  $S'$ :

$$S' = |S_A + S^*|, \dots, |S_A - S^*| \quad = 1/2 \text{ for } S^* = 0 \\ = 3/2, 1/2 \text{ for } S^* = 1$$

*i.e.* we have two  $S' = 1/2$  and one  $S' = 3/2$  states. The two spin doublet states arise from different values of  $S^*$ . Each energy level is defined by its two quantum numbers  $(S', S^*)$ . The relative energies are:

$$E(1/2, 0) = E(1/2, 1) = -3J/8 \quad [\text{or } 0 \text{ if set } (S' = 1/2) \text{ as reference level } (E = 0)] \\ E(3/2, 1) = -15J/8 \quad [\text{or } (-15 + 3)J/8 = -3J/2]$$

It is to be mentioned that, ground state is degenerate if  $J < 0$  *i.e.* magnetic exchange in the system is AFM in nature.

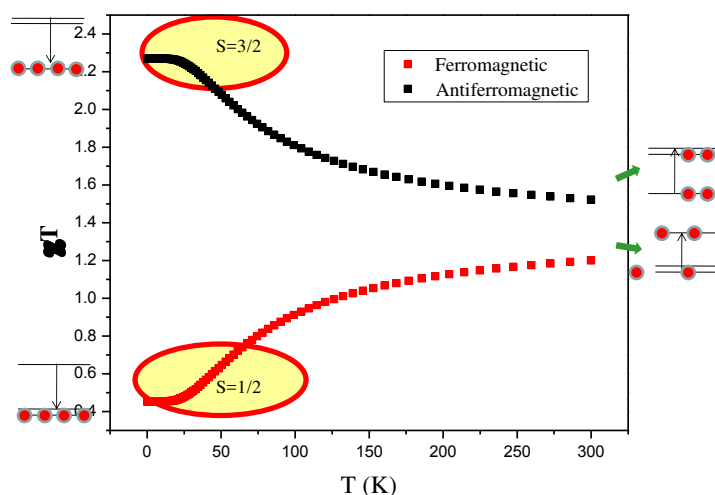
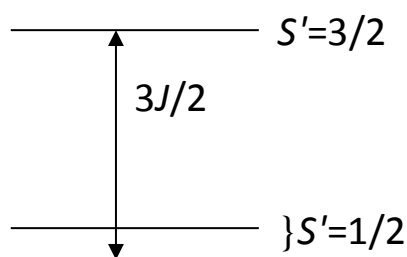
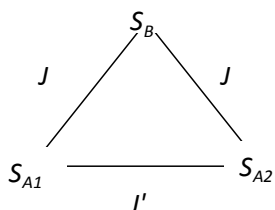


Figure 130. The above figure describes the transition of magnetic exchange upon variation of spin state of the molecule.

E.g. Isosceles triangle of  $S = 1/2$  centres (*i.e.* lower symmetry).



invoke two exchange constants ( $J, J'$ ), and a new spin-Hamiltonian:

$$H = -J(\hat{S}_{A1} \cdot \hat{S}_B + \hat{S}_{A2} \cdot \hat{S}_B) - J'(\hat{S}_{A1} \cdot \hat{S}_{A2})$$

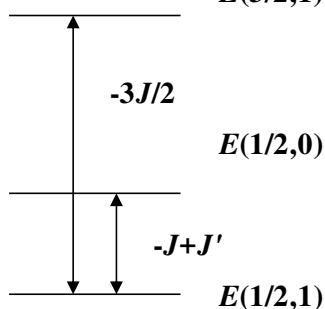
$$E(S', S^*) = -\frac{J}{2} S'(S'+1) - \frac{(J'-J)}{2} S^*(S^*+1)$$

E. levels  $(S', S^*)$   $E(1/2, 0) = -3J/8$  or  $-J + J'$  If we take  $E(1/2, 0)$

$$E(1/2, 1) = +5J/8 - J' \quad \text{or} \quad 0 \quad \text{as our reference}$$

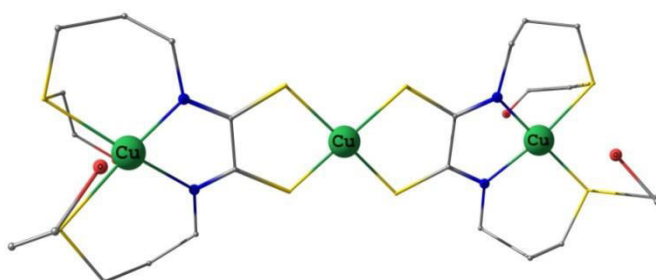
$$E(3/2, 1) = -7J/8 - J' \quad \text{or} \quad -3J/2 \quad \text{level (i.e. Subtract } 5J/8 - J' \text{ from } E).$$

$$E(3/2, 1)$$



Lowering of the symmetry has splitted the degeneracy of two  $S' = 1/2$  states. If  $J' = J$  the two  $S' = 1/2$  states are degenerate and we have the equilateral triangle case. If  $J' = 0$  this effectively uncouples  $S_{A1}$  and  $S_{A2}$ . This would be the case for a linear trinuclear species.

Linear trinuclear species:



Energy levels will be ...

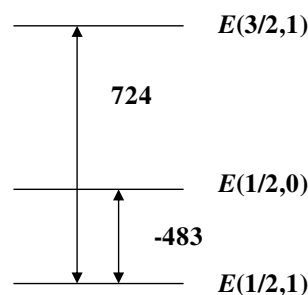


Figure 131. The above figure represents crystal structure of the linear trinuclear cation  $\{\text{Cu}_3[\text{C}_2\text{S}_2(\text{NCH}_2\text{CH}_2\text{SCH}_2\text{OH})_2]_2\}^{2+}$

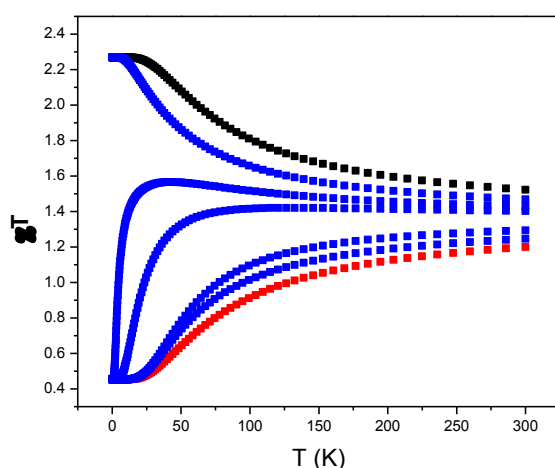


Figure 132. The above figure clearly indicates that shape of the graph becomes increasingly unpredictable owing to the different strength of  $J$  and  $J'$  with possible FM and AFM coupling.

The linear trinuclear  $[\{\text{Cu}_3[\text{C}_2\text{S}_2(\text{NCH}_2\text{CH}_2\text{SCH}_2\text{OH})_2\}_2]^{2+}$ <sup>40</sup> complex exhibits strong antiferromagnetic interaction between the nearest neighbour Cu(II) ions owing to the underlying bridging ligands.

E.g. Nonsymmetrical trinuclear compounds  $S=1/2$  centres

$$H = -J_{AB}S_A \cdot S_B - J_{BC}S_B \cdot S_C - J_{AC}S_A \cdot S_C$$

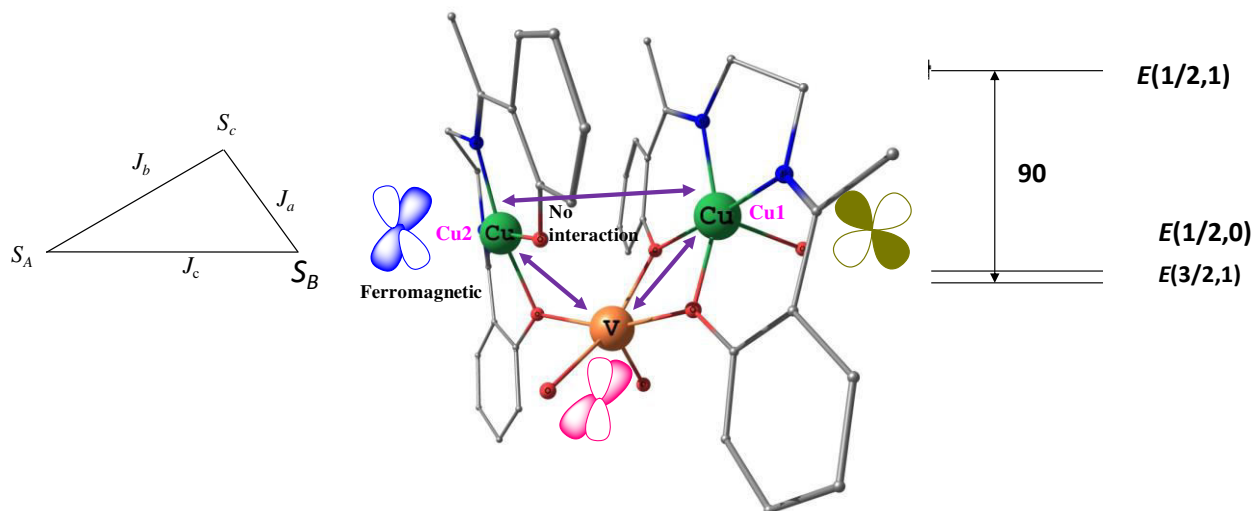


Figure 133. The above figure denotes the molecular crystal structure of the cation  $[\{\text{Cu}(\text{Mesalen})\}_2\text{VO}]^{2+}$ .<sup>41</sup> The participating orbitals for all the three metal ions and lying exchange interaction between the metal pairs are given below. We have also analysed the splitted energy level for this trinuclear complex below. The aforementioned complex exemplifies a spin cluster  $S \neq 0$  using AFM interactions.

Analysing the energy spectrum and fitting of magnetic susceptibility data gives  $J_{\text{Cu1V}}=0 \text{ cm}^{-1}$ ,  $J_{\text{Cu2V}}=+90 \text{ cm}^{-1}$  and  $J_{\text{CuCu}}=0 \text{ cm}^{-1}$ .

## §20. Conclusions:

Everything above concerns the “classical”, macroscopic, magnetism, at our scale, with various potential applications. Generally, not all the molecules are in this “magnetic” category. Nevertheless, the air that we breathe all the day long, consists essentially of a mixture of molecules of nitrogen,  $\text{N}_2$  and oxygen,  $\text{O}_2$  (each molecule is made of two atoms of nitrogen N or oxygen, O). The two molecules are “magnetic”, each of its kind. The molecules of nitrogen are diamagnetic: placed in an intense magnetic field they are very weakly repelled. Everywhere, in solid/liquid/gases, magnetism finds its origin in the magnetic properties of the electron. Magnetic properties in complexes can be fine tuned by varying the ligands, coordination number around the metal ion, geometry around the metal ion and variations in spin. It is possible to get a ligand field of medium strength, due to the wide range of

ligands available from organic chemistry. Orientation of the electronic spins should be accurately regulated in order to gain control over the magnetic exchange coupling constant (J). Extending the strategy used for the molecule, it should be possible to obtain solids showing magnetic order at a temperature as high as possible (highest Curie temperature).

We have crossed the quantum world towards transition to the macroscopic one, have seen the application of the theory, and taken the rigorous formula to the dream. It is a field persistently under development which is of essential interest not only in small, with “nano” but also with the complex. At a time when a Japanese Nobel laureate in Chemistry asserted that the synthesis of any molecule is now within reach of the chemist, the challenge was to conceive and synthesise increasingly complex systems in order to reach the requirements. These systems are not required to have only one property or function, but several functions: it is the world of multipurpose materials. These functions can exist alongside each other (magnetism and transparency) or they can interact with each other in order to create and highlight new properties.

## §16. References:

1. I. Morgenstern-Badarau, M. Rerat, O. Kahn, J. Jaud and J. Galy, *Inorganic Chemistry*, 1982, **21**, 3050-3059.
2. O. Kahn, VCH Publishers, France, 1993.
3. M. Verdaguer, French-Japanese Advanced School on Chemistry and Physics of Molecular Materials, Paris, France, 2006.
4. R. Ruamps, L. J. Batchelor, R. Guillot, G. Zakhia, A.-L. Barra, W. Wernsdorfer, N. Guihery and T. Mallah, *Chemical Science*, 2014, **5**, 3418-3424.
5. A. Santoro, A. D. Mighell and C. W. Reimann, *Acta Crystallographica Section B*, 1970, **26**, 979-984.
6. W. E. Hatfield and J. F. Villa, *Journal of the American Chemical Society*, 1971, **93**, 4081-4082.
7. D. B. Losee, H. W. Richardson and W. E. Hatfield, *The Journal of Chemical Physics*, 1973, **59**, 3600-3603.
8. S.-Y. Lin, W. Wernsdorfer, L. Ungur, A. K. Powell, Y.-N. Guo, J. Tang, L. Zhao, L. F. Chibotaru and H.-J. Zhang, *Angewandte Chemie International Edition*, 2012, **51**, 12767-12771.
9. Y.-Q. Zhang and C.-L. Luo, *New Journal of Chemistry*, 2015.
10. D. M. Halepoto, D. G. L. Holt, L. F. Larkworthy, G. J. Leigh, D. C. Povey and G. W. Smith, *Journal of the Chemical Society, Chemical Communications*, 1989, 1322-1323.
11. V. Ksenofontov, A. B. Gaspar, G. Levchenko, B. Fitzsimmons and P. Gütllich, *The Journal of Physical Chemistry B*, 2004, **108**, 7723-7727.
12. O. J. Scherer, J. Schwalb, G. Wolmershäuser, W. Kaim and R. Gross, *Angewandte Chemie International Edition in English*, 1986, **25**, 363-364.
13. J.-P. Sutter, M. Fettouhi, L. Li, C. Michaut, L. Ouahab and O. Kahn, *Angewandte Chemie International Edition in English*, 1996, **35**, 2113-2116.
14. P. Gütllich, A. Hauser and H. Spiering, *Angewandte Chemie International Edition in English*, 1994, **33**, 2024-2054.
15. E. W. Müller, H. Spiering and P. Gütllich, *Chemical Physics Letters*, **93**, 567-571.
16. B. Gallois, J. A. Real, C. Hauw and J. Zarembowitch, *Inorganic Chemistry*, 1990, **29**, 1152-1158.
17. P. Gütllich, A. B. Gaspar and Y. Garcia, *Beilstein Journal of Organic Chemistry*, 2013, **9**, 342-391.
18. S. Decurtins, P. Gutlich, C. P. Kohler and H. Spiering, *Journal of the Chemical Society, Chemical Communications*, 1985, 430-432.
19. T. Nakamoto, Z.-C. Tan and M. Sorai, *Inorganic Chemistry*, 2001, **40**, 3805-3809.
20. L. Salmon, G. Molnar, S. Cobo, P. Oulie, M. Etienne, T. Mahfoud, P. Demont, A. Eguchi, H. Watanabe, K. Tanaka and A. Bousseksou, *New Journal of Chemistry*, 2009, **33**, 1283-1289.

21. P. Gutlich and H.A. Goodwin, in *Spin Crossover in Transition Metal Compounds*, Springer-Verlag Berlin Heidelberg New York, Heidelberg, Germany, 2004.
22. J. D. Oliver, D. F. Mullica, B. B. Hutchinson and W. O. Milligan, *Inorganic Chemistry*, 1980, **19**, 165-169.
23. D. L. Reger, J. R. Gardinier, J. D. Elgin, M. D. Smith, D. Hautot, G. J. Long and F. Grandjean, *Inorganic Chemistry*, 2006, **45**, 8862-8875.
24. S. L. Holt, R. DeFasi and B. Post, *Inorganic Chemistry*, 1971, **10**, 1498-1500.
25. E. N. Maslen, C. L. Raston and A. H. White, *Journal of the Chemical Society, Dalton Transactions*, 1974, 1803-1807.
26. S. Kremer, W. Henke and D. Reinen, *Inorganic Chemistry*, 1982, **21**, 3013-3022.
27. in *Spin-Crossover Materials : Properties and Applications*, ed. M. A. Halcrow, Wiley (John Wiley & Sons Ltd.), University of Leeds, UK, 2013.
28. R. Clérac, F. A. Cotton, L. M. Daniels, K. R. Dunbar, K. Kirschbaum, C. A. Murillo, A. A. Pinkerton, A. J. Schultz and X. Wang, *Journal of the American Chemical Society*, 2000, **122**, 6226-6236.
29. D. Reinen, C. Friebel and V. Propach, *Zeitschrift für anorganische und allgemeine Chemie*, 1974, **408**, 187-204.
30. D. Chiruta, C.-M. Jureschi, J. Linares, Y. Garcia and A. Rotaru, *Journal of Applied Physics*, 2014, **115**, 053523.
31. O. Kahn, S. Sikorav, J. Gouteron, S. Jeannin and Y. Jeannin, *Inorganic Chemistry*, 1983, **22**, 2877-2883.
32. S. Sikorav, I. Bkouche-Waksman and O. Kahn, *Inorganic Chemistry*, 1984, **23**, 490-495.
33. J. Comarmond, P. Plumere, J. M. Lehn, Y. Agnus, R. Louis, R. Weiss, O. Kahn and I. Morgenstern-Badarau, *Journal of the American Chemical Society*, 1982, **104**, 6330-6340.
34. O. Kahn, in *Molecular Magnetism*, VCH Publishers, INC., Orsay, France, 1993.
35. J. Hjortas, *Acta Crystallographica Section B*, 1973, **29**, 1916-1922.
36. Y. Journaux, O. Kahn, J. Zarembowitch, J. Galy and J. Jaud, *Journal of the American Chemical Society*, 1983, **105**, 7585-7591.
37. Y. Pei, Y. Journaux and O. Kahn, *Inorganic Chemistry*, 1989, **28**, 100-103.
38. J.-P. Farges, in *Organic Conductors: Fundamentals and Applications*, Marcel Dekker, Inc., New York, USA.
39. R. Beckett, R. Colton, B. F. Hoskins, R. L. Martin and D. G. Vince, *Australian Journal of Chemistry*, 1969, **22**, 2527-2533.
40. R. Veit, J. J. Girerd, O. Kahn, F. Robert and Y. Jeannin, *Inorganic Chemistry*, 1986, **25**, 4175-4180.
41. A. Bencini, C. Benelli, A. Dei and D. Gatteschi, *Inorganic Chemistry*, 1985, **24**, 695-699.